uOttawa

L'Université canadienne
Canada's university

FACULTÉ DES ÉTUDES SUPÉRIEURES ET POSTOCTORALES

u Ottawa

L'Université canadienne
Canada's university

FACULTY OF GRADUATE AND POSDOCTORAL STUDIES

Pierre-Yves Gougeon
AUTEUR DE LA THÈSE / AUTHOR OF THESIS

Ph.D. (Neuroscience)
GRADE / DEGREE

Department of Cellular and Molecular Medicine
FACULTÉ, ÉCOLE, DÉPARTEMENT / FACULTY, SCHOOL, DEPARTMENT

Characterization of PRA2 and VAP-A, Two Regulators of Protein Trafficking Between the Endoplasmic Reticulum and Golgi Compartments

TITRE DE LA THÈSE / TITLE OF THESIS

Johnny Ngsee
DIRECTEUR (DIRECTRICE) DE LA THÈSE / THESIS SUPERVISOR

CO-DIRECTEUR (CO-DIRECTRICE) DE LA THÈSE / THESIS CO-SUPERVISOR

EXAMINATEURS (EXAMINATRICES) DE LA THÈSE / THESIS EXAMINERS

M-A. Akimenko (absent)

X. Zha

J. Dimitroulakos

N. Ridgway

Gary W. Slater
Le Doyen de la Faculté des études supérieures et postdoctorales / Dean of the Faculty of Graduate and Postdoctoral Studies

Characterization of PRA2 and VAP-A, Two Regulators of Protein Trafficking Between the Endoplasmic Reticulum and Golgi Compartments

Pierre-Yves Gougeon

This thesis is submitted as a partial fulfillment

of the Ph.D. program in Neuroscience

Department of Cellular and Molecular Medicine

Faculty of Medicine

University of Ottawa

Thesis supervisor: Dr. Johnny K. Ngsee

This thesis was submitted on the 21st of September 2006

to the School of Graduate Studies and Research

University of Ottawa

Your file Votre référence
ISBN: 978-0-494-32401-1
Our file Notre référence
ISBN: 978-0-494-32401-1

Thesis Format

The format of this thesis follows the classical thesis guidelines set by the School of Graduate Studies of the University of Ottawa. A general introduction is presented in Chapter 1, and following the results in Chapters 2 and 3 is a discussion in Chapter 4. Chapter 2 and 3 each include methods, results, figures and tables. References are inserted (Author, Year) in the text and listed in alphabetical order in the reference section in Chapter 5.

The results from Chapter 2 relate to the characterization of PRAs and their interaction with Rabs and VAMP2, and were taken from three publications and modified to follow the classical thesis format. The results from Chapter 3 have not been published, but should eventually be submitted for publication as a single article. Mohammad Abdul-Ghani performed the immunocytochemistry in Figure 1.7 (Abdul-Ghani et al., 2001), which was included in the introduction to demonstrate the difference in localization of PRA isoforms. Also, Derek Prosser performed the cellular localization of the PRA1 mutants included in Table I (Gougeon et al., 2002). Permission from the publishers to insert in the thesis elements of the published articles is included on the next pages.

Authorizations

The Journal of Biological Chemistry

American Society for Biochemistry and Molecular Biology

Two articles:

1. Gougeon, P.Y., Prosser, D.C., Da-Silva, L.F. & Ngsee, J.K. **Disruption of Golgi Morphology and Trafficking in Cells Expressing Mutant Prenylated Rab Acceptor-1.** *J. Biol. Chem.* **277**, 36408-14 (2002)

2. Abdul-Ghani, M., Gougeon, P.Y., Prosser, D.C., Da-Silva, L.F. & Ngsee, J.K. **PRA Isoforms Are Targeted to Distinct Membrane Compartments**. *J. Biol. Chem.* **276**, 6225-33 (2001)

The ASBMB provides copyright permission for not-for-profit uses of the manuscript such as inclusion in the author's thesis.

The following statement is found on the website of the society.

ASBMB Journals - Copyright Permission Policy

Copyright Permission Policy

ASBMB Journals

Journal of Biological Chemistry

Molecular and Cellular Proteomics

Journal of Lipid Research

Biochemistry and Molecular Biology Education

ASBMB Today

ASBMB does not charge for and grants use without requiring your copyright permission request for:

Original authors wanting to reproduce portions of their own work; or to republish their material in not-for-profit formats or venues.

Students wanting to reproduce or republish their work for educational purposes.

Students using other authors' material for their theses.

Reproduction or republication of abstracts only.

Photocopying up to 5 copies for personal use.

Non-profit educational institutions making multiple photocopies of articles for classroom use; all such reproduction must utilize institutionally owned equipment for this purpose.

Use of copyrighted material requires proper citation.

For all other uses, contact Copyright Clearance Center.

All ASBMB Journals Molecular and Cellular Proteomics

Journal of Lipid Research Biochemistry and Molecular Biology Education

Methods in Enzymology

Elsevier

One Article:

1.Gougeon, P.Y. & Ngsee, J.K. **Purification and functional properties of prenylated Rab acceptor 2.** *Methods Enzymol.* **403**, 799-807 (2005)

After requesting the authorization to use the aforementioned publication, I received the following e-mail granting me permission to use the publication in my thesis.

Dear Mr Gougeon

We hereby grant you permission to reproduce the material detailed below at no charge in your thesis subject to the following conditions:

1. If any part of the material to be used (for example, figures) has appeared in our publication with credit or acknowledgement to another source, permission must also be sought from that source. If such permission is not obtained then that material may not be included in your publication/copies.

2. Suitable acknowledgement to the source must be made, either as a footnote or in a reference list at the end of your publication, as follows:

"Reprinted from Publication title, Vol number, Author(s), Title of article, Pages No., Copyright (Year), with permission from Elsevier".

3. Reproduction of this material is confined to the purpose for which permission is hereby given.

4. This permission is granted for non-exclusive English rights only. For other languages please reapply separately for each one required. Permission excludes use in an electronic form. Should you have a specific electronic project in mind please reapply for permission.

5.This includes permission for the Library and Archives of Canada to supply single copies, on demand, of the complete thesis. Should your thesis be published commercially, please reapply for permission.

Yours sincerely

Marion Moss

Senior Rights Assistant

Elsevier Ltd

The Boulevard

Langford Lane

Kidlington

Oxford

OX5 1GB

Tel : +44 1865 843280

Fax : +44 1865 853333

Abstract

Regulation of vesicle trafficking is required to maintain the specific make-up of each membrane compartment. Prenylated Rab acceptor 1 (PRA1) is known to interact with Rab GTPases and VAMP2, proteins involved in vesicle trafficking, suggesting PRA isoforms could regulate vesicle trafficking. The first aim was to characterize PRA's interaction with Rabs and VAMP2. Using point mutations and *in vitro* binding assays, I discovered that PRAs interact with multiple Rabs independent of their guanine nucleotide-bound state and identified three residues (N70, S76, H166), whose mutation induced a strong modification to PRA1's interaction with both Rab3A and VAMP2. These results suggest PRA might employ the same binding site to interact with multiple proteins. The second aim was to identify novel PRA-interacting proteins and clarify the function of PRAs. I initiated a yeast two-hybrid screen with PRA1 as bait, and identified VAMP-associated protein A (VAP-A), a protein also believed to be involved in vesicle trafficking. In CHO cells, VAP-A extensively co-localized with the ER-localized PRA2 rather than the predominantly Golgi-localized PRA1, and co-immunoprecipitation confirmed the *in vivo* PRA2-VAP-A interaction. In immunofluorescence and biochemical assays, overexpression of VAP-A or PRA2 delayed the ER-to-Golgi trafficking of the secretory pathway marker $VSVG^{ts045}$. Also, FRAP assays demonstrated that unlike PRA2, VAP-A achieved this by inhibiting the ER-lateral movement of $VSVG^{ts045}$, thereby delaying the protein's exit from the ER. ER budding assays confirmed that VAP-A overexpression reduced $VSVG^{ts045}$ sequestration onto vesicles. The addition of the microtubule-depolymerizing agent nocodazole rescued the VAP-A-induced reduction in $VSVG^{ts045}$ budding. This suggests

that VAP-A creates static subcompartments of the ER via its interaction with microtubules preventing the lateral movement of $VSVG^{ts045}$. Overexpression of PRA2 also reduced the levels of $VSVG^{ts045}$ found on vesicles collected in the budding assay, and unexpectedly, microtubule depolymerization resulted in a doubling of $VSVG^{ts045}$ release from the ER. This suggests PRA2 overexpression has two effects: PRA2 can increase vesicle formation from the ER, but only when it's dominant microtubule-dependant inhibitory effect is alleviated by microtubule depolymerization. The results I obtained suggest that both PRA2 and VAP-A delay the ER-to-Golgi trafficking of $VSVG^{ts045}$, but achieve this through different mechanisms.

Table of Contents

List of Tables and Annex

List of Figures

List of Abbreviations

ΔTMD, deletion of the transmembrane domain

Δcc, deletion of the coil-coiled domain

ΔN, deletion of the N-terminus

α-SNAP, soluble *N*-ethylmaleimide-sensitive factor attachment protein alpha

ALS, amyotrophic lateral sclerosis

ARL, ARF-like

CFTR, cystic fibrosis transmembrane regulator

CHO, Chinese hamster ovary

COP, coatomer protein

DMSO, dimethyl sulfoxide

DSP, dithiobis(succinimidyl)propionate

DTT, dithiothreitol

EDTA, ethylenediaminetetraacetic acid

EEA1, early endosome antigen 1

Endo H, endoglycosidase H

ER, endoplasmic reticulum

ERES, endoplasmic reticulum exit site

ERGIC, ER Golgi intermediate compartment

FBS, foetal bovine serum

FFAT, two phenylalanines in an acidic tract

FRAP, fluorescent recovery after photobleaching

GAP, GTPase-activating protein

GDF, GDI-dissociating factor

GDI, GDP-dissociating inhibitor

GEF, GDP/GTP exchange factor

GFP, green fluorescent protein

GLUT4, glucose transporter-4

GPBP, Goodpasture's antigen binding protein

GST, glutathione S-transferase

HCV, hepatitis C virus

HF, homotypic fusion

IPTG, isopropyl-beta-D-thiogalactopyranoside

LTP, long-term potentiation

MAPK, mitogen-activated protein kinase

MEM, minimum essential medium

MSP, major sperm protein

NS, non-structural protein

NSF, *N*-ethylmaleimide-sensitive factor

ORP, OSBP-related protein

OSBP, oxysterol-binding protein

PBS, phosphate buffered saline

PEG, polyethylene glycol

PMSF, Phenylmethylsulphonylfluoride

PRA, prenylated Rab acceptor

RdgB, retinal degeneration type B

REP, Rab escort protein

Scs2p, suppressor of choline sensitivity 2 protein

SDS, Sodium dodecyl sulphate

SNAP-25, synaptosome-associated protein 25 kDa

SNARE, soluble *N*-ethylmaleimide-sensitive factor attachment protein (SNAP) receptor

TMD, transmembrane domain

TRAPP, transport protein particle

t-SNARE, target SNARE

UPR, unfolded protein response

VAMP, vesicle associated membrane protein

VAP, vesicle associated membrane protein (VAMP)-associated protein

v-SNARE, vesicle SNARE

$VSVG^{ts045}$, temperature-sensitive mutant form of the vesicular stomatitis virus G protein

VTC, vesicular-tubular clusters

VCS, VAP-conserved sequence

X-gal, β-D-galactopyranoside

Acknowledgements

Many people have helped me throughout the duration of my graduate studies. One of these people is my supervisor Dr. Johnny Ngsee, who has guided me and thought me so much, and for this I am very grateful. I would also like to thank all the lab members that have worked in the lab throughout the years and have made it a pleasant work environment. I would like to especially thank lab technician Lance Da-Silva and Dr. Darren Hutt, who have supported and encouraged me and have been great friends. My advisory committee members, Dr. Mario Tiberi, Dr. Stephen Gee and Dr Marie-Andrée Akimenko were encouraging, insightful and made me feel proud of my accomplishments, and for this I owe them much gratitude. I would also like to thank Dr. Douglas Lyles for the I14 antibody, Dr. William Trimble for the GST-VAP-A constructs and Dr. Jesse Hay for reagents for the ER budding assay and technical expertise.

Je désire aussi remercier ma famille pour toute l'aide, le support, la patience et les encouragements qu'elle m'a toujours offerts et qui m'ont permis d'atteindre cet objectif si important pour moi. Enfin, je suis infiniment choyé d'avoir pu compter, à chaque jour, sur l'appui d'Angela Hogan. Sa confiance en moi, son aide et surtout sa patience m'ont permis de surmonter les multiples défis rencontrés sur mon chemin. Je veux lui exprimer mes remerciements les plus sincères. Elle m'a donné le courage de me rendre jusqu'au bout.

Chapter 1

INTRODUCTION

Vesicle trafficking in cell biology

All eukaryotic cells contain a number of specialized membrane compartments whose diverse functions require they each maintain a unique protein composition. A large portion of these proteins originate in the endoplasmic reticulum (ER), and must be sorted and transported to their proper compartment. Transport between each membrane compartments employs a vesicle trafficking process that follows the same general basic steps: a vesicle is formed from the donor membrane, it is then targeted and transported to the acceptor membrane with which it undergoes fusion. In addition to assisting in the maintenance of the appropriate make-up of membrane compartments, vesicle trafficking is involved in the process of regulated exocytosis, which permits certain cell types to release hormones or neurotransmitters when stimulated. The great number of diseases that result from deficiencies in trafficking exemplifies the importance of these processes. For example, some mutations in the cystic fibrosis transmembrane regulator (CFTR), insulin receptor, growth hormone receptor and low-density lipoprotein receptor hinder the protein's exit from the ER, which results in cystic fibrosis, diabetes mellitus, Laron syndrome and familial hypercholesterolemia, respectively (Cassanelli et al., 1998; Kadowaki et al., 1991; Kopito, 1999; Pathak et al., 1988; Peters et al., 2000; Taylor, 1992; Tolleshaug et al., 1983; Wojcik et al., 1998). These are just a few of the diseases known to result from abnormalities in trafficking out of the ER and do not include the pathologies that result from a defect in Golgi, *trans*-Golgi network, lysosomes or endocytic trafficking (reviewed by Aridor and Hannan, 2000; Aridor and Hannan, 2002).

In order not only to increase our knowledge in cell biology, but also to help understand and cure a number of diseases, it is important to study the molecular details of trafficking.

Trafficking between the ER and Golgi compartments

Despite extensive research on ER-to-Golgi trafficking, a universally accepted comprehensive model describing the process, its various intermediates and the machinery involved, has not developed. However, it is clear that proteins exit the ER from specialized sites often termed ER exit sites (ERES) (Bannykh et al., 1996; Jamieson and Palade, 1967; Orci et al., 1991; Palade, 1975; Slot and Geuze, 1976). These specialized ER subdomains seem to be stable sites distributed throughout most of the ER both in periphery and centrally close to the *cis*-Golgi complex (Balch et al., 1994; Lotti et al., 1992; Palade, 1975; Saraste and Kuismanen, 1984; Saraste and Svensson, 1991; Schweizer et al., 1990). It is also clear that a dispersed intermediate often termed ER Golgi intermediate compartment (ERGIC) is present and that trafficking cargo proceeds through this structure (Aridor et al., 1995; Bannykh et al., 1996; Tang et al., 1995), but trafficking to and from the ERGIC as well as its origin, maturation and fate remain contentious issues.

Trafficking between the ERES and ERGIC

Vesicle trafficking between the ERES and the ERGIC has been shown to involve COPII coatomers (Barlowe et al., 1994), but separate hypotheses describe the process (Figure 1.1). The first suggests that once the COPII coated vesicles have shed their coat,

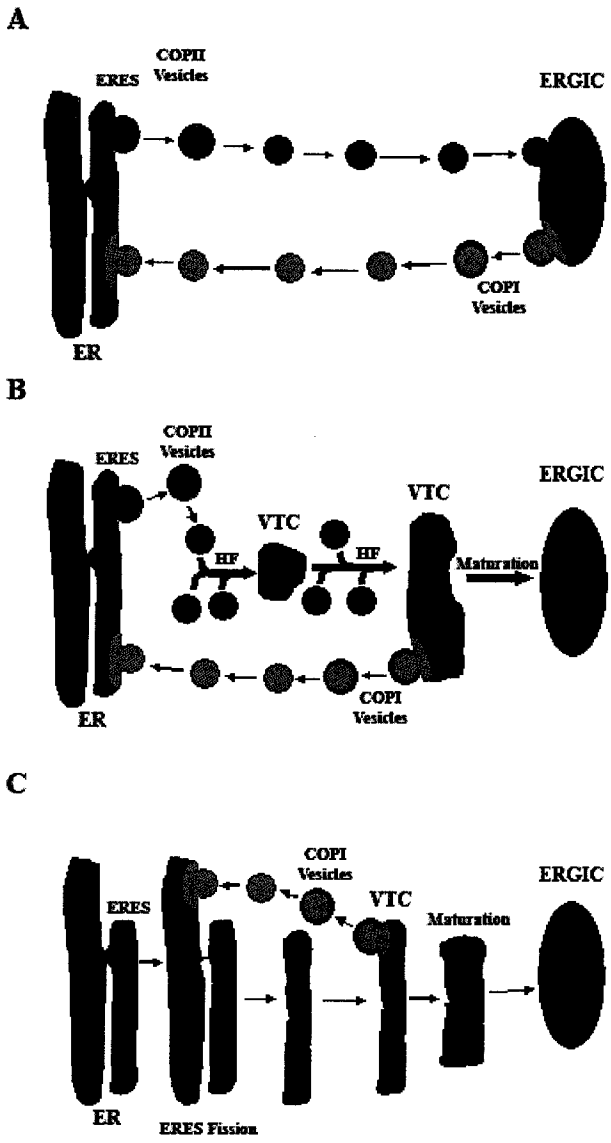

Figure 1.1. Alternative models describing trafficking between the ER and ERGIC. (A) COPII-coated vesicles (dark green) formed at the ERES move towards and fuse with the ERGIC compartment. Retrograde trafficking is achieved by COPI-coated vesicles (light green) that move back to the ER. (B) COPII-coated vesicles formed at the ERES undergo homotypic fusion (HF) to form a VTC. Retrograde trafficking allows the VTC to mature into ERGIC. (C) Fission of the ERES from the ER creates a VTC. Retrograde trafficking by COPI-coated vesicles allows the VTC to mature into ERGIC.

they traffic towards the ERGIC compartments and fuse with these somewhat non-mobile structures. The second suggests that the same vesicles traffic towards the *cis*-Golgi complex and undergo homotypic fusion along the way, creating structures termed vesicular-tubular clusters (VTC), which upon maturation become the ERGIC. An alternate view is that larger portions of the ERES undergo fission that creates VTCs, which again upon maturation become the ERGIC. At this moment it has been impossible to identify which of these hypotheses is correct, but it is conceivable that ERES-derived VTCs and COPII coated vesicles could coexist in ER-to-Golgi trafficking.

COPII and COPI coatomers in ER-to-Golgi trafficking

Nevertheless, all hypotheses share the same maturation requirement of the ERGIC and/or VTC. Vesicle formation at the ERES uses the COPII coatomer system to form vesicles and segregate certain proteins onto the vesicles. This process was first described in yeast (Barlowe, 1998), but mammalian orthologues have been identified (Aridor et al., 1998; Kuge et al., 1994; Paccaud et al., 1996; Shaywitz et al., 1995; Swaroop et al., 1994). It involves the recruitment of the small Ras-like GTPase Sar1 to the ERES and its activation by Sec12, an ER integral membrane protein whose cytoplasmic domain contains a guanine nucleotide exchange activity (Barlowe and Schekman, 1993), in order to initiate the assembling of the COPII coat (Huang et al., 2001). This activation recruits the cytosolic heterodimeric protein complexes COPII subunits Sec23-Sec24 and Sec13-Sec31 (Bi et al., 2002; Schekman and Orci, 1996), which help to create the membrane curvature necessary to form a vesicle (Bigay and Antonny, 2005; Lee et al., 2005) and are involved in segregating specific proteins to the vesicle (Aridor and Traub, 2002; Hong,

1998; Klumperman, 2000). Two competing models have been proposed to describe the export of cargo from the ER via vesicles. The first suggests that proteins are segregated onto vesicles by a selective process, while the other implies that export of cargo from the ER is non-selective and simply follows the principal of bulk flow. However, it has become evident they are not mutually exclusive, and that certain cargo will use the selective process while others exit via bulk flow. A number of studies have demonstrated that proteins like VSVG, pro-α-factor and the v-SNARE protein Sec22p, are concentrated when incorporated into COPII coated vesicles (Balch et al., 1994; Campbell and Schekman, 1997; Kuehn et al., 1998) while certain membrane proteins like the yeast ER-Golgi SNAREs Bet1p, Bos1p and sed5p, ERGIC-53 and the p23/24 family, are recruited onto ER-derived vesicles via a direct interaction with COPII components (Dominguez et al., 1998; Hauri et al., 2000; Peng et al., 1999; Springer and Schekman, 1998). Two types of ER export motifs have been identified for membrane proteins. The first comprises hydrophobic or aromatic C-terminal residues, such as the two phenylalanines (FF) residues in ERGIC-53 and the p23/24 family (Nufer et al., 2002). The other is a di-acidic motif (EXD or DXE) commonly found in membrane proteins such as VSVG and a variety of inward rectifying potassium channels (Ma et al., 2001; Ma et al., 2002; Nishimura and Balch, 1997). Both types of motifs have been shown to interact directly with COPII subunits, demonstrating that in addition to helping form the vesicles, COPII subunits may also be involved in the selection of cargo molecules. In addition, a growing number of molecules acting as cargo receptors have been identified, suggesting that complex mechanisms have evolved to control cargo sequestration onto budded vesicles. Erv14p links the membrane protein Axl2p to the COPII components to

facilitate the protein's exit from the ER (Powers and Barlowe, 2002). Also, the selective recruitment of luminal proteins requires a receptor in order to be recruited by the cytosolic COPII components. One such protein is Erv29p, which binds to the luminal glycosylated pro-α-factor thereby facilitating its incorporation into COPII coated vesicles (Belden and Barlowe, 2001). In addition, different COPII subunit homologues can alter protein selection and affect the trafficking of specific proteins. For example, the addition of the yeast protein LST1, a homologue of Sec24 allows the ER exit of Pma1p, a plasma membrane proton ATPase (Roberg et al., 1999). However, protein sorting is not perfect, especially in the case of VTCs forming directly from ERES fission, as a certain amount of proteins can traffic out of the ERES simply via bulk flow (Wieland et al., 1987). Therefore, ER resident proteins must be recycled from VTCs and the ERGIC, as well as proteins that have served their function in the trafficking and fusion of ER-derived COPII-coated vesicles. It is believed that COPI coated vesicles from these compartments and even the Golgi complex, and transport proteins back to the ER (Lee et al., 2004; Martinez-Menarguez et al., 1999). The COPI coat functions similarly to the COPII, but utilizes seven different coatomer subunits (α, β, β', δ, ε, γ, and ζ) and the small Ras-like GTPase ARF1 replaces Sar1 (reviewed by (McMahon and Mills, 2004; Rothman and Orci, 1992). Some membrane proteins such as the KDEL receptor, which recruits KDEL motif-containing luminal proteins, share a di-lysine (KKXX) motif recognized by COPI coatomers that allows for the retrograde transport of these proteins to the ER (Aoe et al., 1997; Cosson and Letourneur, 1994; Harter et al., 1996). Therefore, the effect of COPI retrograde trafficking is in part to concentrate proteins in transit, and by doing so results in what is termed as the maturation of the ERGIC compartment. It is evident that multiple

mechanisms are used for the trafficking of different classes of proteins, which provides the level of regulation required to maintain the ordered distribution of proteins between membrane compartments.

Trafficking between the ERGIC and cis-Golgi complex

Similar to ERES-to-ERGIC trafficking, there are three divergent hypotheses with respect to this trafficking step. The first implies the formation of vesicles from the ERGIC, using as of yet unidentified coatomers, which undergo fusion with the *cis*-Golgi complex. The second hypothesis involves continued maturation of the ERGIC as described earlier, which leads to the ERGIC moving closer and transforming itself into the *cis*-Golgi complex. The third hypothesis implies that the ERGIC, or a large part of it, moves towards and fuses with the *cis*-Golgi complex. Again, retrograde trafficking from the Golgi compartment to the ER or possibly the ERGIC can return ER resident proteins or proteins involved in trafficking to the Golgi apparatus back to their initial compartment. The hypothesis that requires vesicle trafficking from the ERGIC to the Golgi compartment is often dismissed due to lack of evidence, although it would provide an additional degree of selection for proteins trafficking towards the Golgi complex. However, the maturation of the ERGIC compartment through ER-directed COPI-coated vesicles, suggests that the further selection and concentration by an unidentified vesicle coat complex of proteins trafficking from the ERGIC to the Golgi is unnecessary. Although it might be simpler to transport vesicles towards the Golgi apparatus than a complete ERGIC compartment, the latter alternative eliminates the requirement for an additional vesicle-forming step.

Microtubules are involved in ER-to-Golgi trafficking

Although not absolutely necessary, most transport events employ the cytoskeleton to move more efficiently from one compartment to another. The ER's reticular structure is dependent on its interaction with microtubules (Terasaki et al., 1984), and so does its expansion towards the periphery of the cell, which involves the (+)-end directed motor kinesin (Feiguin et al., 1994; Waterman-Storer and Salmon, 1998). The ER has been shown to be very closely associated with microtubules and a number of proteins have been postulated to form a link between the two, therefore providing a stabilizing force to the large ER. One such protein is CLIMP-63, a type II integral membrane protein of the ER that binds and promotes microtubule polymerization through its cytosolic domain, and contributes to the positioning of the ER along microtubules (Klopfenstein et al., 1998; Schweizer et al., 1993). Microtubules have also been implicated in the transport of ERGIC compartments towards the Golgi compartment (Presley et al., 1997; Saraste and Svensson, 1991; Scales et al., 1997). In fact, fluorescent experiments elegantly demonstrated how the VTCs and ERGIC localize along a population of stable microtubules and follow microtubule tracts in a dynein/dynactin-dependent manner until they reach the Golgi complex (Presley et al., 1997). The extended incubation with microtubule depolymerizing agents, such as nocodazole, results in the fragmentation and dispersal of the Golgi apparatus, and the formation of multiples dispersed miniature Golgi stacks that are believed to result from the transformation of ERGICs or VTCs (Cole et al., 1996; Thyberg and Moskalewski, 1985). ERGICs also contain a kinesin involved in Golgi-to-ER retrograde trafficking, which is believed to remain inactive

during initial transport to the Golgi complex (Lippincott-Schwartz et al., 1995). Also, it has been previously shown that ERES align along microtubules in certain cell types (Ralston et al., 2001), while the plus-end-directed motor protein kinesin has been shown to localize to ERES *in vitro* (Aridor et al., 2001) and to VTC/ERGICs *in vivo* (Lippincott-Schwartz et al., 1995), and the Sec23p component of the COPII complex directly interacts with the dynactin complex pathway (Watson et al., 2005). The role of microtubules in the multiple steps of ER-to-Golgi trafficking remains unclear even though a great number of studies implicate them in various aspects.

Membrane fusion in ER-to-Golgi trafficking

As mentioned previously, the formation and transport of vesicles or larger membrane compartments are critical steps in regulated trafficking. Eventual fusion with the acceptor compartment must be specific in order to prevent promiscuous fusion with any membrane compartment. In addition, ER-to-ERGIC trafficking requires both the homotypic fusion of ER-derived vesicles and heterotypic fusion of these same vesicles with the VTCs or ERGIC, which demonstrates the level of regulation required to maintain the specificity of each distinct fusion event. Since the phospholipid make-up alone of the organelles is insufficient to fulfill the requirements of such an elaborate and regulated process, specific proteins to each trafficking step must be recruited to respect the functional demands of targeting and fusion.

The SNARE hypothesis and membrane fusion

The SNARE (soluble *N*-ethylmaleimide-sensitive factor attachment protein receptor or SNAP receptor) hypothesis has been proposed as a model to define the molecular events in vesicle docking and fusion (Figure 1.2) (DeBello et al., 1995; Rothman, 1994; Sollner et al., 1993). The model, which has undergone considerable revisions, states that specific interaction between v-SNARE (vesicular-SNARE) and its cognate t-SNARE (target-SNARE) forms the core fusion complex. The core SNARE complex of the most studied trafficking step, i.e. synaptic vesicle exocytosis, comprises the vesicle protein VAMP or synaptobrevin (Baumert et al., 1989; Trimble et al., 1990), and the two plasma membrane proteins, syntaxin and SNAP-25 (synaptosome-associated protein of 25 KDa) (Bennett et al., 1992; Oyler et al., 1989). The model is believed to apply to every other vesicle trafficking and fusion events, with VAMP, syntaxin and SNAP-25 being replaced by other compartment specific SNARE proteins or isoforms. Only cognate SNARE in the *trans* configuration constitutes a functional fusion complex, whereas non-cognate SNARE and SNARE in the *cis* configuration are non-functional. However, *in vitro* some SNAREs have demonstrated a certain promiscuity with regards to their interacting SNARE partners, but this is compensated by specific SNARE interactions with accessory proteins that facilitate the appropriate SNARE pairing (Fasshauer et al., 1999; Scales et al., 2000; Yang et al., 1999). Therefore, the resulting specificity prevents random membrane fusion events that would prevent the cell from maintaining the specific composition of each membrane compartment. The core SNARE proteins form a thermostable, *Clostridial* toxin-resistant and SDS-resistant complex (Fasshauer et al., 1999; Hayashi et al., 1994; Hunt et al., 1994; Montecucco and Schiavo,

1993; Niemann et al., 1994). Priming of the SNARE complex requires both NSF and α-SNAP to induce, by dissociating *cis*-SNARE pairings, a labile state that facilitates vesicle docking (Block et al., 1988; Clary et al., 1990; Mayer et al., 1996). Structural analyses indicate that SNARE proteins form a parallel, four-helix bundle such that the free energy derived from this bundled complex is sufficient to trigger membrane fusion (Lin and Scheller, 1997; Sutton et al., 1998; Weber et al., 1998). This concept is supported by the finding that v- and t-SNAREs reconstituted into separate artificial liposomes are sufficient to trigger fusion resulting in lipid mixing (Weber et al., 1998). Because SNARE proteins involved in ER-to-Golgi trafficking cycle between the compartments, it has been difficult to identify precisely the step in which each isoform is involved. However, two SNARE complexes have been identified in mammalian cells. The first and major SNARE complex is comprised of syntaxin5, Bet1, membrin and Sec22 (Hay et al., 1998), while the second complex is believed to be involved in the late fusion step with the Golgi compartment and contains syntaxin5, Bet1, Gos28 and Ykt6 (Zhang and Hong, 2001). As mentioned earlier, these proteins are segregated onto budding COPII vesicles via an interaction with the coatomers (Campbell and Schekman, 1997; Mossessova et al., 2003). Although the SNARE proteins previously mentioned were the equivalent to the yeast proteins, and the yeast does not seem to contain ERGIC compartments, the same requirement and recruitment process of SNARE proteins is involved in mammalian cells. In fact, experiments performed in yeast demonstrated that SNAREs are selected by the COPII coat based on their fusogenic state. Therefore, a SNARE complex in the non-fusogenic *cis* state will not be recruited, while the single v-SNARE Bet1 and the t-SNARE complex (Sed5-Sec22-Bos1) will be recruited separately by the COPII coat since

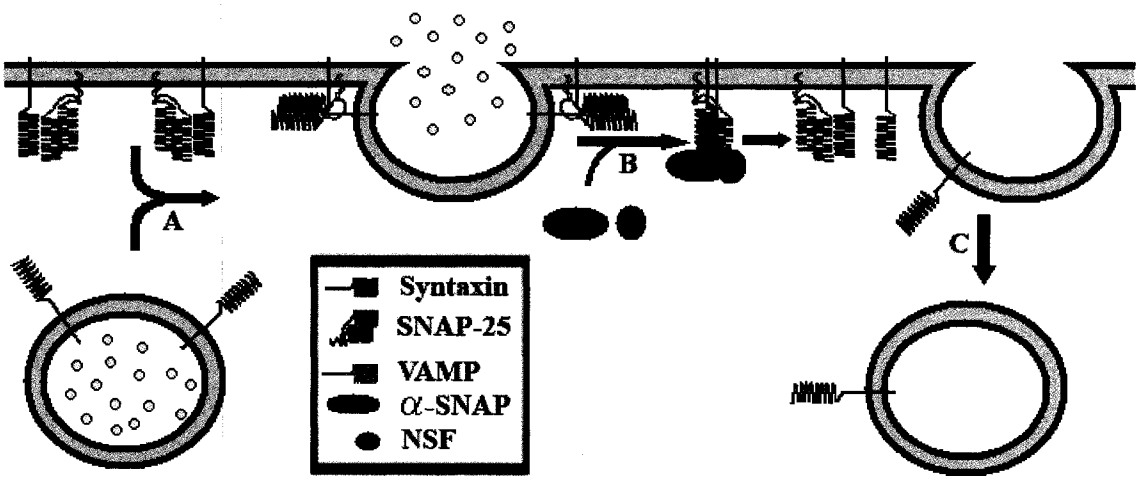

Figure 1.2. SNARE hypothesis. Description of the SNARE hypothesis using secretory vesicle fusion as an example. (A) The v-SNARE VAMP forms a *trans*–SNARE four-helical bundle with the t-SNAREs syntaxin and SNAP-25, which provides the energy necessary for vesicle fusion. (B) After fusion, α-SNAP and NSF are recruited to dissociate the *cis*-SNARE complex. (C) The free VAMP is then recycled by endocytosis.

they are ready to undergo fusion (Mossessova et al., 2003). In addition to priming the vesicles for fusion, it confers specificity that helps to ensure the vesicles will undergo fusion with the proper compartment. However, SNARE proteins are not solely responsible for the specificity of fusion.

Rab GTPases are regulators of vesicle trafficking

Although the core SNARE complex is sufficient to drive membrane fusion, other proteins facilitate effective SNARE interaction. The SNARE complex was lost in yeast carrying a mutation in the Rab GTPase Sec4p (Sogaard et al., 1994), while overexpression of the yeast t-SNARE cognate of SNAP-25 (Sec9p) can suppress the Sec4p mutations (Brennwald et al., 1994), suggesting that Rab acts upstream to facilitate SNARE pairings. Rab GTPases are a family of 20-29 kDa Ras-like GTPase with over 60 members localized to unique intracellular organelles (Figure 1.3) (Chavrier et al., 1990; Deneka et al., 2003; Elferink et al., 1992; Fischer von Mollard et al., 1990; Matteoli et al., 1991; Ngsee et al., 1990; Pfeffer and Aivazian, 2004; Stenmark and Olkkonen, 2001; Van Der Sluijs et al., 1991; Zahraoui et al., 1987). They contain a characteristic cysteine-containing motif at the C-terminus that is post-translationally modified by one or more 15-carbon farnesyl or 20-carbon geranylgeranyl residues (Andres et al., 1993; Johnston et al., 1991; Khosravi-Far et al., 1992; Khosravi-Far et al., 1991; Kinsella and Maltese, 1992; Wei et al., 1992). This modification is essential since un-modified Rab GTPases are non-functional. Rab GTPases cycle through an active membrane-bound GTP- and inactive cytosolic GDP-bound state (Bourne, 1988; Bourne et al., 1991). The number of proteins known to interact with Rab reflects the diverse role of Rab in vesicle transport as

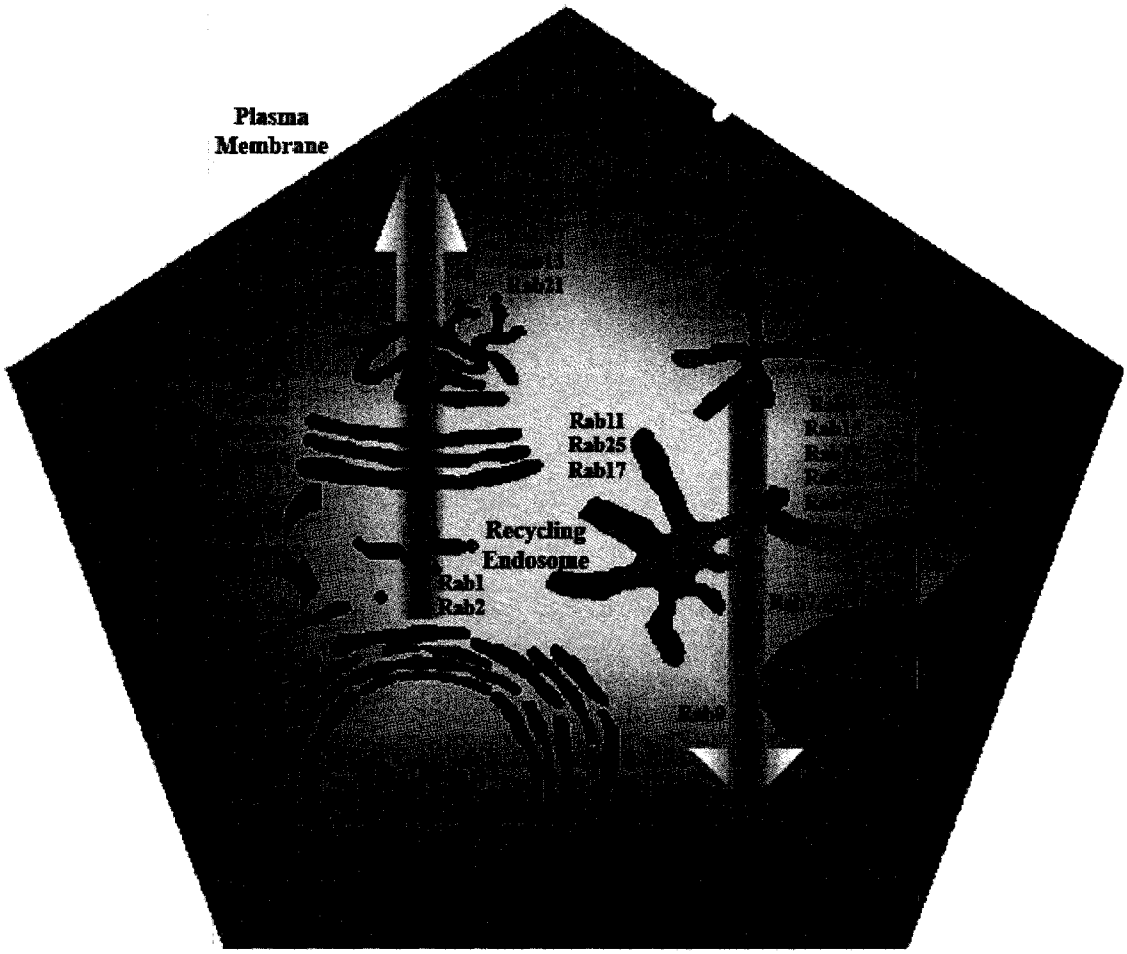

Figure 1.3. Localization of Rab isoforms. This illustration shows the localization of a number of mammalian Rab isoforms and the trafficking step they regulate.

well as proteins required for Rab recycling. All Rab GTPase isoforms follow the same GDP/GTP cycling (Figure 1.4). GDP-bound Rab is removed from the membrane by the cytosolic carrier protein GDI (GDP-dissociation inhibitor), which also maintains Rab in the inactive state (Horiuchi, 1997; Pfeffer et al., 1995; Sasaki et al., 1990). Guanine nucleotide exchange occurs at the membrane and is catalyzed by a guanine exchange factor (GEF) of which Rab3-specific and yeast Sec4p-specific forms have been identified (Elkind et al., 2000; Wada et al., 1997; Walch-Solimena et al., 1997). A GTPase activating protein (GAP), of which Rab3A-specific and yeast Ypt-specific forms have been identified, catalyzes the hydrolysis of the bound GTP to inactivate the protein and return it to its original state (Albert and Gallwitz, 1999; Fukui et al., 1997; Strom et al., 1993).

Rab GTPases tether vesicles to membranes before the docking step

The functional role of Rab is best demonstrated by a series of experiments that defined the order of events leading to vesicle docking and fusion (Brigance et al., 2000; Cao et al., 1998; Cao and Barlowe, 2000; VanRheenen et al., 1999). These studies showed that Rab recruits the cytosolic scaffolding protein Uso1p to the membranes before vesicle docking. Subsequent vesicle docking could be blocked by removal of Rab from the membrane with GDI. These two Rab-mediated steps were independent of any SNARE pairings. Once docked, however, vesicle fusion was no longer dependent on Rab (i.e. it can be removed) but required SNARE proteins. Because the initial step is a loose association of vesicles with their targets, it is now called "tethering" (as opposed to "docking"), which brings the membranes together (usually 25-30 nm). This fosters

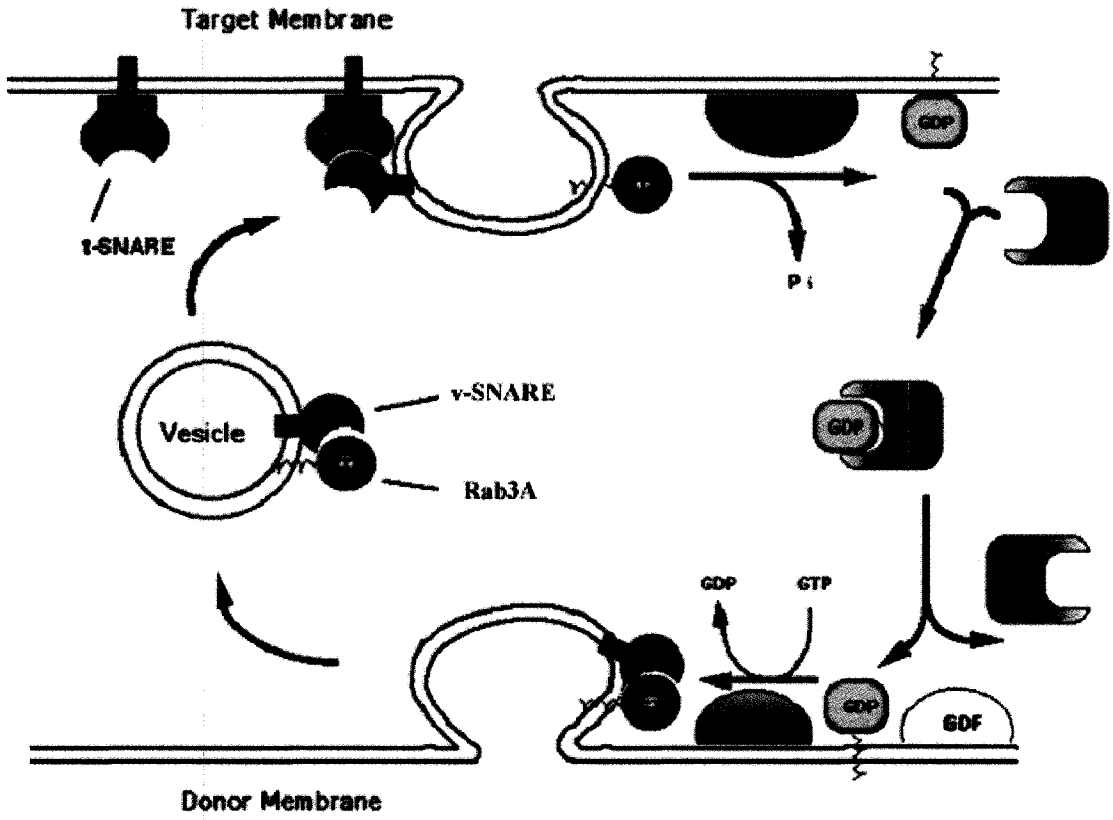

Figure 1.4. Cycling of the Rab GTPase. Illustration of Rab GTPase cycling, using Rab3A as an example. The protein is first associated with the vesicle in the GTP-bound state. After vesicle fusion with the target membrane, Rab3A hydrolyses the GTP with the help of a GTPase-activating protein (GAP). The GDP-dissociation inhibitor (GDI) can now extract the GDP-bound Rab3A from the membrane. A GDI-displacement factor (GDF) helps dissociate the complex, which allows Rab3A to associate with the donor membrane compartment. A GDP/GTP exchange occurs with the help of the GDP/GTP exchange factor (GEF), thus allowing the GTP-bound Rab3A to undergo another cycle.

subsequent "docking" of the membranes within a bilayer's distance of one another (<5-10 nm). Stability of docked vesicles may, in turn, represent a number of distinct molecular states: from molecular interactions that merely hold the two membranes in close proximity, to that needed to trigger bilayer fusion. Studies on synaptic vesicles have indicated that docked vesicles would undock about once every two minutes, a rate that is faster than spontaneous fusion (Murthy and Stevens, 1999). Thus, increasing the number of docked vesicles would have a profound effect on probability of synaptic release. This reversibility of vesicle docking also provides a time constraint on subsequent steps, allowing a point of regulation of synaptic transmission. Each transport step may contain different proteins in the tethering complexes: Uso1p/Sec34p/Sec35p and TRAPP complex in ER-to-Golgi, the giantin/p115/GM130 in Golgi, exocyst in plasma membrane, and EEA1 complex in endosomes (Barr et al., 1998; Cao et al., 1998; Cao and Barlowe, 2000; Christoforidis et al., 1999; Guo et al., 1999a; Guo et al., 1999b; McBride et al., 1999; Nakamura et al., 1997; Sacher et al., 2000; Sacher et al., 1998; VanRheenen et al., 1999). There is also a close association between Rab and cytoskeleton in vesicle transport, since Rab6 is involved in regulating the kinesin-like motor protein, rabkinesin, in intra-Golgi transport (Echard et al., 1998). In addition, recruitment of the unconventional myosin, myosin V, to synaptic vesicle is dependent on VAMP (Prekeris and Terrian, 1997).

Consequences of loss of Rab on vesicle trafficking and synaptic transmission

Rab3A is one of the Rab GTPases found on synaptic and secretory vesicle membranes (Fischer von Mollard et al., 1990). GTPase-defective and dominant negative

mutations of Rab3A decreased targeting of secretory vesicles to their normal release sites (Ngsee et al., 1993). However, the basic fusion machinery remains intact in these mistargeted secretory vesicles in that they can fuse with the plasma membrane when challenged with a depolarizing stimulus. These results were subsequently confirmed in *C. elegans*, where synaptic vesicles were redistributed in Rab3 mutants with depletion of vesicles at synapses coupled with accumulation at inter-synaptic regions of the axon (Nonet et al., 1997). In Rab3A knockout mice, synaptic transmission was apparently normal but more susceptible to fatigue upon repeated stimulation, which was attributed to elevated quantal release of neurotransmitter (Geppert et al., 1994; Geppert et al., 1997). The mice also suffered from a loss of long-term potentiation (LTP) in hippocampal mossy fiber synapses (Castillo et al., 1997). Together, these results are consistent with a decrease in readily releasable synaptic vesicles at the active zone in the knockout mice.

The Prenylated Rab Acceptor 1

Initially, the goal of my research was the characterization of the Prenylated Rab Acceptor-1 or PRA1, which was identified through a yeast two-hybrid screen as a protein that can bind the prenylated form of Rab3A (Martincic et al., 1997). PRA1 is a 185-residue protein of 21 kDa with two extensive hydrophobic domains and is broadly expressed in all tissues. These hydrophobic regions form four transmembrane domains, resulting in a membrane protein whose N- and C-termini are exposed to the cytosol (Figure 1.5) (Lin et al., 2001). PRA1 has been found to interact *in vitro* with all Rab isoforms tested so far (Abdul-Ghani et al., 2001; Bucci et al., 1999; Figueroa et al., 2001; Janoueix-Lerosey et al., 1995; Martincic et al., 1997), suggesting that *in vivo* specificity

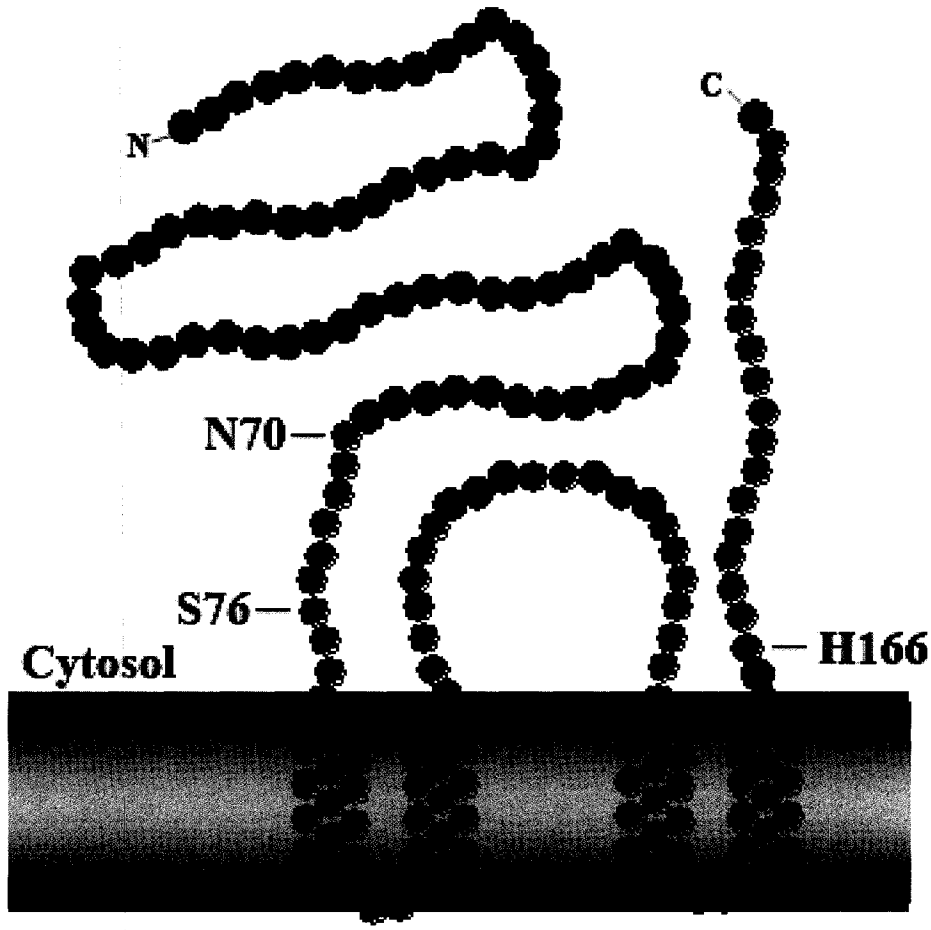

Figure 1.5. PRA1 topology. Dark blue residues represent the cytosolic N-terminus. Light green residues make up the four transmembrane domains. The light blue residues form a cytosolic loop between the 2nd and 3rd transmembrane domain. The dark green residues constitute the cytosolic C-terminus and the mutated residues N70, S76 and H166 are represented in red.

might be determined by sub-cellular localization. As with most membrane proteins, PRA1 is initially translocated in the ER membrane before it is transported to its proper compartment. A di-acidic DXE motif in the C-terminal cytosolic domain of PRA1 has been shown to facilitate its exit from the ER and trafficking to the Golgi complex (Abdul-Ghani et al., 2001). PRA1 is predominantly localized to this compartment even though it has been found to traffic further down the secretory pathway and localized to synaptic vesicles and interact with the zinc fingers of Piccolo, a presynaptic cytoskeletal matrix (scaffolding) protein found in the active zone (Fenster et al., 2000). This suggests the involvement of PRA1 in synaptic vesicle docking at the active zone. Initially, along with its interaction with Rab3A, PRA1 had been found to interact with VAMP2 (Martincic et al., 1997), as mentioned earlier a v-SNARE involved in vesicle fusion with the plasma membrane. Although this suggested that PRA1 might be a putative link between the Rab targeting/tethering function and the SNARE docking/fusion function, it could also imply that PRA1 is involved in vesicular sequestration of proteins essential for proper vesicle targeting and fusion.

PRA1 regulates Rab cycling and recruitment to membranes

Additional research demonstrated that PRA1 could inhibit GDI-mediated removal of Rab3A from the membrane (Hutt et al., 2000). Thus, recycling of Rab depends on the opposing action of PRA1 and GDI, with PRA1 favouring membrane retention and GDI favouring Rab solubilization. PRA1 was then shown to catalyze the release of Rab9 from a purified Rab9-GDI complex using an assay that measured uptake of non-hydrolysable GTPγS after GDI release (Sivars et al., 2003). However, PRA1 did not stimulate the

intrinsic nucleotide exchange rate, demonstrating that PRA1 possesses GDI Dissociating Factor (GDF) activity, but is not a Guanine nucleotide Exchange Factor (GEF). As GDFs were predicted to target specific Rabs to the correct membrane compartment, PRA1 inserted into reconstituted liposomes was sufficient to recruit Rab9. However, PRA1's GDF activity did not apply to the ER-to-Golgi Rab isoforms Rab1 and Rab2. This would suggest that Rab selectivity is dictated by cellular localization with an ER-localized PRA serving as GDF for Rabs in the ER.

PRA isoforms localize to distinct membrane compartments

In yeast, a single PRA isoform named Yip3p is expressed and possesses the same promiscuous Rab isoform–binding property as its mammalian orthologue (Calero and Collins, 2002). The yeast counterpart is not essential for cell survival. Even though it has not been researched thoroughly, the data obtained suggests a similar function to its mammalian counterparts. However, three PRA genes have been identified in the human genome, which is considerably less complex when compared to the over 60 Rab isoforms (Figure 1.6). Despite this disparity in number, the interaction of PRA with diverse prenylated Rab isoforms suggests that each PRA isoform acts on more than one Rab trafficking pathway. In fact, its ability to interact with Rabs may be constrained by its intracellular localization. PRA1 resides in the Golgi complex/plasma membrane/endosome compartments while PRA2 is primarily localized to the endoplasmic reticulum (Figure 1.7) (Abdul-Ghani et al., 2001). PRA2 therefore is an ideal GDF candidate for Rab1 and Rab2 in that it shuttles between the ER and Golgi apparatus. The PRA3/JM4 isoform has yet to be characterized. The open reading frame

Figure 1.6. PRA sequences and comparison. The yeast Yip3p, human PRA1 and JM4 as well as mouse PRA2 sequences were compared using Clustal alignment, with identical residues (red) indicated by a *star* and similar residues (blue) with a *colon*. The predicted hydrophobic domains are underlined.

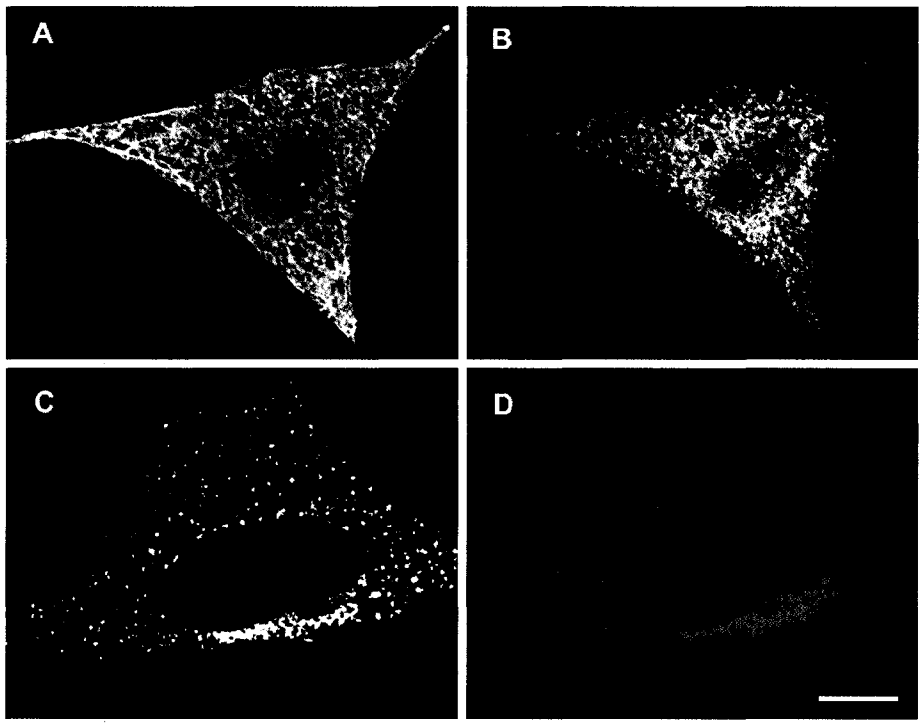

Figure 1.7. Cellular localization of PRA1 and PRA2. CHO cells were transfected with HA-tagged PRA2 (*panels A* and *B*) and PRA1 (*panels C* and *D*). The cells were stained with anti-HA (*panels A* and *C*), and with either calnexin (*panel B*) or mannosidase II (*panel D*) to highlight the ER and Golgi complex, respectively. *Scale bar,* 2.5 mm. (Abdul-Ghani et al., 2001)

of PRA2 contains 188 amino acids with a predicted molecular mass of 21.5 kDa (Abdul-Ghani et al., 2001). As with PRA1, PRA2 also contains two extensive hydrophobic domains, of 36 and 35 residues spanning amino acids 47 to 82 and 101 to 135, respectively. Comparison of the two PRA sequences reveals an overall amino acid identity of 26% and a similarity of 35%. In both cases, localization is determined by signals inherent within each PRA isoform, since a C-terminal KARE motif, similar to the previously described di-basic KKXX motif, acts as an ER retrieval signal for PRA2. Although like PRA1, PRA2 can interact with the prenylated Rab, it is not capable of binding VAMP2. PRA1 has also been shown to interact with a number of other proteins: the Epstein-Barr virus protein BHRF1 (Li et al., 2001), the gp41 protein of the simian, bovine and feline immunodeficiency virus (all part of the lentiviral family) (Evans et al., 2002) and the Rotavirus VP4 spike protein (Enouf et al., 2003), while PRA2 was found to interact with the ARF-like protein 6 (ARL6) (Ingley et al., 1999) and the excitatory amino-acid carrier 1 (EAAC1) (Butchbach et al., 2002). However, the purpose of these interactions has remained undefined. All this information demonstrates that even though both isoforms share similar properties and most likely comparable functions, there are significant differences between the two isoforms.

VAP-A is a novel PRA-binding protein

The first section of my research describes the molecular determinants of PRAs' interaction with the first identified PRA-interacting proteins Rabs and VAMP2. The second section addresses the functional role of PRAs, specifically that of PRA2. While pursuing this, I identified VAMP-associated protein of 33 kDa (VAP-33 or VAP-A) as an

additional PRA-interacting protein and also attempted to define the function of this protein. Initially, VAP-A was identified in *Aplysia californica* as a VAMP-interacting protein via a yeast two-hybrid screen (Skehel et al., 1995). Injection of specific antibodies inhibited synaptic transmission suggesting the protein was required for exocytosis. Since then, orthologues have been identified in yeast, mouse, rat, human and *Drosophila* (Kagiwada et al., 1998; Pennetta et al., 2002; Skehel et al., 2000; Soussan et al., 1999; Weir et al., 1998). The human VAP-A is a 242 amino acid protein with a molecular mass of 27.3 kDa and a similar structure to VAMP (Nishimura et al., 1999). As is the case with the SNARE protein, VAP-A is anchored in the membrane through its C-terminal transmembrane domain with the rest of the protein exposed to the cytosol. It also contains a more central coiled-coil domain, which in the case of VAMP is involved in the SNARE complex formation (Hughson, 1999) (Figure 1.8).

VAP-A contains a domain similar to the major sperm protein of the nematode

The N-terminal half of VAP-A is similar to the *Caenorhabditis elegans* isoforms of the major sperm protein (MSP) (Laurent et al., 2000). In nematode sperm, MSP has replaced actin as the basis of the motile system. In fact, similar to the pattern observed for the actin cytoskeleton in a number of other crawling cells, nematode sperm extends a lamellipodium packed with MSP filaments that assemble along the leading edge to generate movement (Stewart et al., 1994). Like actin, MSP is an abundant protein in sperm and possesses the ability to self-assemble. The similarities, however, end here because MSP shares no sequence or structural homology with actin, forms filaments with different structural and polymerization properties, its structure is based on an Ig fold that

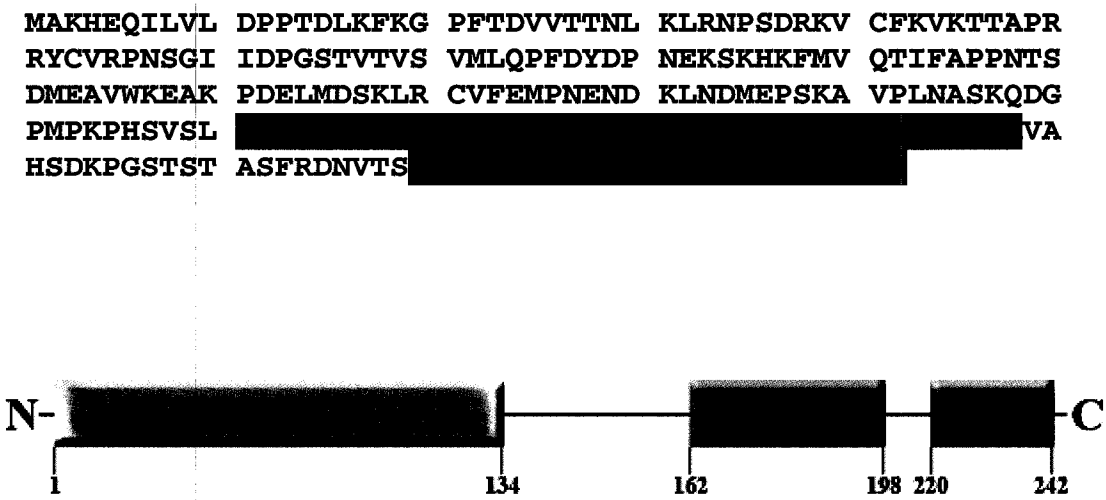

Figure 1.8. VAP-A protein sequence and domains. Representation of human VAP-A amino acid sequence and domains. The yellow box corresponds to a domain similar to the nematode major sperm protein (MSP), the green box includes the coil-coiled domain (CC), and the blue box highlights the transmembrane domain (TMD).

is different from the structure of actin, it does not bind nucleotides, and the polymerizing unit is a dimer rather than a monomer (Bullock et al., 1996; Haaf et al., 1996; Italiano et al., 1996; King et al., 1992). In addition, MSP has been found to act as a signaling molecule by activating oocyte maturation (Kosinski et al., 2005; Miller et al., 2001). Although MSP in nematodes is believed to have evolved from the original MSP domain of the ancestral VAP-A (Miller et al., 2001) and gained these unique properties, it is possible this domain in VAP-A might also possess self-assembly and cytoskeleton-binding abilities that underlie the protein's function. Following these lines VAP-A was found to homodimerize and heterodimerize with a second isoform VAP-B (Nishimura et al., 1999). VAP-B is a 243 amino acid protein that exhibits 60% amino acid sequence homology with VAP-A and contains the same basic domains. Transcripts of VAP-A and VAP-B are expressed ubiquitously and both proteins can interact with VAMPs. The P56S mutation in VAP-B has been reported to be one of the causes of familial amyotrophic lateral sclerosis (ALS8), but the effects of this mutation on the protein's function has yet to be defined (Nishimura et al., 2005; Nishimura et al., 2004). VAP-C, a third isoform also exists, but this 99 amino acid protein is the result of a splice variant of VAP-B (Nishimura et al., 1999). VAP-C consists of the first 70 residues of VAP-B's MSP domain followed by 29 unrelated amino acids resulting from a frame shift. For both proteins, the C-terminal transmembrane domain seems to be involved in dimerization, even though there is some controversy regarding its requirement (Amarilio et al., 2005; Brosig and Langosch, 1998; Nishimura et al., 2005; Nishimura et al., 2004; Nishimura et al., 1999). Interestingly, both VAP isoforms contain a GXXXG motif imbedded in their transmembrane domains, which has been identified in a number of membrane proteins

and is proposed to induce self-assembly (Amarilio et al., 2005; Brosig and Langosch, 1998; Nishimura et al., 1999; Skehel et al., 2000). There are also similar inconsistencies as to the requirement of the N-terminus for dimerization (Amarilio et al., 2005; Nishimura et al., 1999). While it has been clearly established that VAP isoforms can homo and heterodimerize, the molecular determinants remain undefined.

VAP-A is involved in vesicle trafficking

VAP-A is mostly localized to the ER (Skehel et al., 2000), although in certain cell lines it seems to traffic further down the secretory pathway where it has been found at the ERGIC (Wyles et al., 2002), and at the plasma membrane's tight junction (Lapierre et al., 1999) (where it interacts with occludin) and synaptic boutons (Pennetta et al., 2002). Two separate groups have demonstrated that VAP-A can interact with microtubules (Pennetta et al., 2002; Skehel et al., 2000), suggesting a possible functional implication for this cytoskeleton interaction. In fact, in *Drosophila* neurons, VAP-A is localized to and seems to direct the microtubule architecture of synaptic boutons (Pennetta et al., 2002). However, in the majority of cell lines, VAP-A remains in the early compartments of the secretory pathway where it is believed to be involved in vesicle trafficking. This was initially suggested to be the case because of its interaction with VAMP, and supported by the fact that a number of other molecules involved in vesicle trafficking, such as syntaxin1A, bet1, sec22, soluble *N*-ethylmaleimide-sensitive factor (NSF) and soluble *N*-ethylmaleimide-sensitive factor attachment protein alpha (α-SNAP), can interact with VAP-A (Weir et al., 2001). Overexpression of VAP-A in L6 myoblasts also reduced the insulin-induced incorporation of GLUT4 glucose transporter into the plasma membrane

(Foster et al., 2000). This effect was rescued by co-expression with VAMP2, supporting the possible function of VAP-A in protein trafficking and providing a functional relevance to its interaction with VAMP2. All these results strongly suggest a role in vesicle trafficking for VAP-A.

VAP-A interacts with a FFAT motif

Other proteins have been found to interact with VAPs. First, similar to PRA1, a number of viral proteins have been identified as VAP-interacting proteins, such as the hepatitis C virus (HCV) non-structural protein (NS) 5A and 5B (Hamamoto et al., 2005), the Norwalk virus non-structural protein p48 (Ettayebi and Hardy, 2003). The significance of these interactions has not been elucidated. Interestingly, a number of proteins involved in sterol and lipid synthesis or trafficking pathways have been shown to interact with VAP-A and VAP-B. These proteins share a motif containing two phenylalanines in an acidic tract also termed FFAT (Loewen et al., 2003). In humans, this motif is found in a number of lipid-binding proteins, such as the oxysterol-binding protein (OSBP) and seven other oxysterol-binding protein-related proteins (ORP), proteins involved in the regulation of sterol synthesis. It was also identified in the three human homologues (NIR1-3) of the *Drosophila* retinal degeneration type B (rdgB) and Goodpasture's antigen binding protein (GPBP) also known as CERT (ceramide transporter), a protein involved in ceramide transport from the ER to the Golgi compartment (Hanada et al., 2003). This FFAT motif, which seems to interact with a VAP conserved sequence (VCS) in the MSP domain of the cytosolic portion of VAP-A, is involved in the targeting of these proteins to the ER (Loewen et al., 2003). In yeast, the

same motif was identified in the three orthologues of OSBP (Osh1-3p) and in Opi1p, a transcriptional repressor of phospholipid synthesis (White et al., 1991). Targeting of these proteins to the ER involves its interaction through the FFAT motif with the suppressor of choline sensitivity (scs2p), the yeast VAP-A orthologue (Kagiwada et al., 1998). We can extract from this data that VAP-A has a role in vesicle trafficking, as well as in lipid and sterol synthesis and transport.

$VSVG^{ts045}$ and trafficking through the secretory pathway

In my research, to study the effect of PRA2 and VAP-A on trafficking in the secretory pathway, I made use of a temperature-sensitive mutant form of the vesicular stomatitis virus G protein ($VSVG^{ts045}$). This protein is often used as a marker for protein trafficking in the secretory pathway and here will also be used as an example of a membrane protein that functions at the plasma membrane (Figure 1.9). $VSVG^{ts045}$ is a protein of 55 kDa that undergoes post-translational modification through glycosylation (Hunt et al., 1978). Like all transmembrane proteins, the nascent protein is first translocated to the ER membrane, where it is held via a transmembrane domain proximal to the C-terminal. For all the membrane proteins translocated to the ER, interactions with chaperones are required to promote proper protein folding. In the case of $VSVG^{ts045}$, it also involves the formation of a non-covalently associated homotrimer containing two N-linked glycosyl modifications (de Silva et al., 1993; Doms et al., 1988; Kreis and Lodish, 1986). The properly folded $VSVG^{ts045}$ can then be segregated onto nascent COPII coated

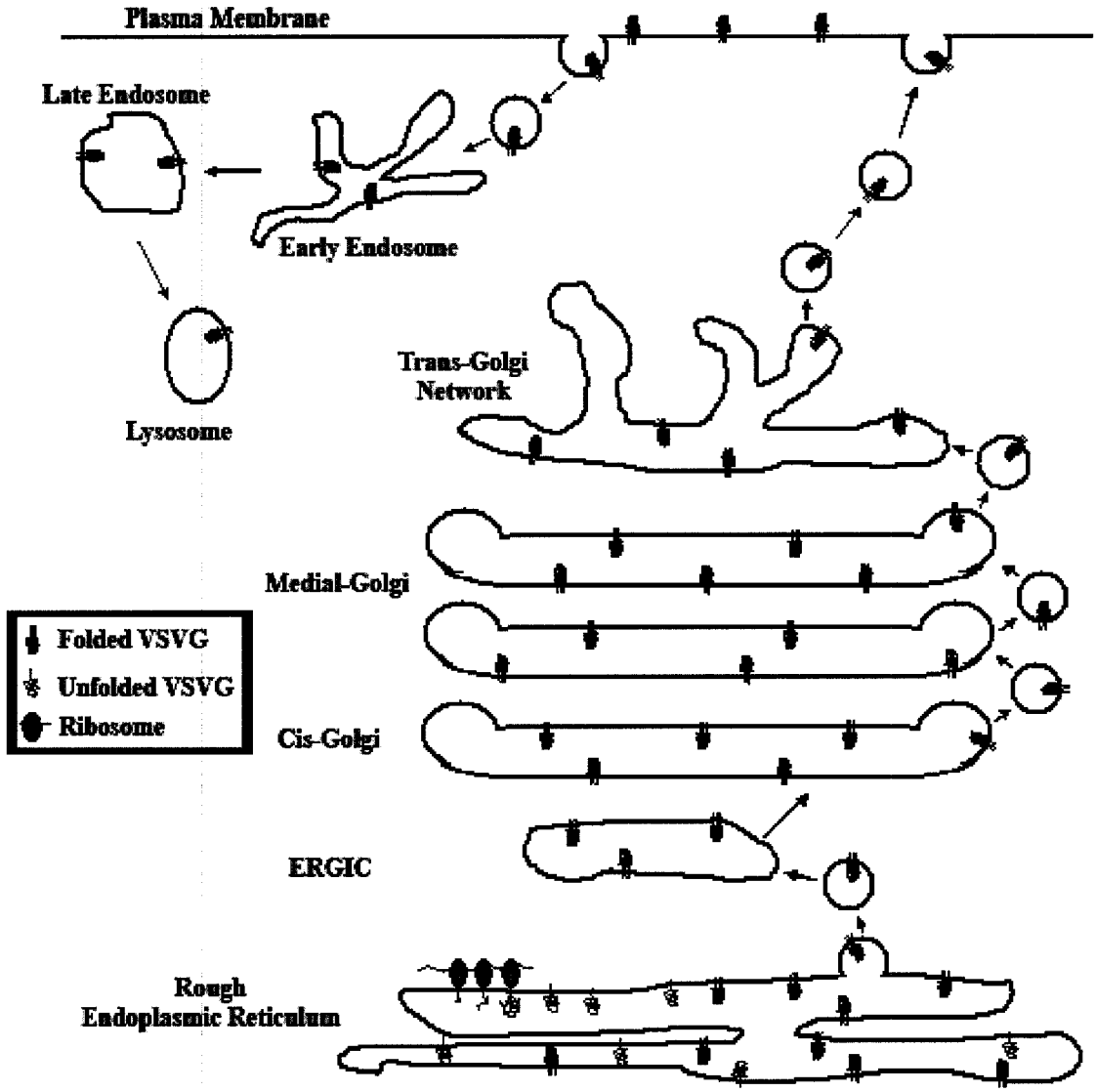

Figure 1.9. The life cycle of VSVG^{ts045}. The nascent protein is translocated in the ER membrane before folding into the proper conformation. It then traffics through the ERGIC to reach the Golgi complex. VSVG^{ts045} is then transported to the plasma membrane before being endocytosed and targeted to lysosomes for degradation.

vesicles forming at specialized ER exit sites (Zeuschner et al., 2006). The advantage of the temperature-sensitive mutant is that at elevated temperatures (above 40 °C) the protein does not fold properly preventing its sequestration into ER-derived vesicles and resulting in accumulation in the ER (Bergmann, 1989; Nehls et al., 2000). Once the cells are restored to normal temperature, $VSVG^{ts045}$ properly folds and trafficking of the protein can be followed in an *in vivo* pulse-chase manner. The majority of the protein will traffic through the ER-Golgi intermediate compartment (ERGIC) and reach the Golgi compartment in roughly 30 min. The protein progresses through the Golgi complex where the N-glycosylated carbohydrate chains are modified, before being transported by vesicles from the *trans*-Golgi network to the plasma membrane, where the majority of $VSVG^{ts045}$ can be found after 60 min (Gougeon et al., 2002; Presley et al., 1997). Eventually, the protein will be endocytosed and targeted for degradation. Because only the ER-localized $VSVG^{ts045}$ is affected by the increase in temperature, if given sufficient time, the $VSVG^{ts045}$ localized beyond the ER will traffic to the plasma membrane and eventually be targeted for degradation, thereby leaving only the accumulated unfolded ER localized $VSVG^{ts045}$. These properties of $VSVG^{ts045}$ have been widely used to study trafficking of membrane proteins in the secretory pathway and especially in ER-to-Golgi trafficking, the step more relevant in my research.

Research objectives

The overall objective of my research is to better understand how cells regulate vesicle and protein trafficking, and contains two specific aims. The first aims at characterizing the interaction between PRAs and its known interacting proteins, Rab3A

and VAMP2, in order to understand the molecular determinants of these interactions. To obtain such information, I predominantly relied on PRA1 point mutations of PRA1 and *in vitro* binding assays with recombinant proteins. The second aim consists of an attempt to elucidate the function of PRA2 and VAP-A, a protein I identified as a novel PRA-interacting protein. To achieve this, I studied the PRA-VAP-A interaction using various techniques such as *in vitro* binding assays, immunocytochemistry and co-immunoprecipitation. To study the function of PRA2 and VAP-A in ER-to-Golgi trafficking, I made use of the temperature sensitive $VSVG^{ts045}$ protein, a marker of membrane protein trafficking in the secretory pathway. I developed or adapted various biochemical and fluorescence assays to identify the PRA2- and VAP-A-mediated trafficking steps. I believe my results will help clarify our understanding of cellular biology and certain pathologies such as Familial ALS, ultimately providing clues and tools for treating diseases.

Chapter 2

Characterization of PRA and its interaction with Rab and VAMP2

Experimental procedures

Plasmid construction

pQE10/HA-PRA2: The HA-tagged PRA2 was subcloned into pQE10 (Qiagen) between the *Bam*HI and the *Hin*dIII sites after PCR amplification using the following oligonucleotides: 5'-GCG GAT CCT ATG TAC CCA TAC GAT G-3' and 5'-GAC AAG CTT ACT CCC TGG CTT TGC-3'.

PRA1 mutagenesis: PRA1 mutations were generated by PCR amplification using pQE11/HA-tagged PRA1 as template. For bacterial expression, the PCR products were inserted between the *Apa*I and *Spe*I sites of a modified pQE10* vector (Qiagen).

pQE10:* The vector was created by inserting between the *Bam*HI and *Pst*I sites of pQE10, the following annealed oligos to create additional restriction sites: 5'-GAT CCG GGC CCA GAT ATC ACT AGT CTG CA-3' and 5'-GAC TAG TGA TAT CTG GGC CCG-3'

pRS424/His$_6$-Rab3A: The His$_6$-tag was added to the Rab GTPases to facilitate purification of the recombinant proteins. The rat Rab3A was subcloned as a *Bam*HI/*Hin*dIII fragment into pRSET-A (Invitrogen) to add a His$_6$-tag. The *Nde*I to *Hin*dIII fragment was then isolated and blunt-end ligated into the *Eco*RI site of pAAR6, between the constitutive yeast ADH1 promoter and terminator. The *Bam*HI fragment was then transferred to pRS424 plasmid and transformed into yeast Y190 strain by the lithium acetate method.

Yeast transformation of pRS424/His$_6$-Rab3A: Streaked yeast Y190 (Clontech) strain on YPD (nutrient rich yeast extract, peptone and dextrose media) plate and grown for 2 days. Scraped 20-50 µl of yeast cells from plate and resuspended in 500 µl of sterile water. Cells were collected and resuspended pellet in 1 ml of 0.1 M lithium acetate (Sigma). Collected cells, removed supernatant and added to cells in order: 240 µl of 50% PEG (Sigma), 36 µl of 1 M LiAc, 25 µl of salmon testes carrier DNA 2 mg/ml (Sigma), 1 µg of Rab construct DNA and completed to 350 µl with sterile water. Vortexed to mix 2 min, incubated at 30 °C for 30 min and heat shocked at 42 °C for 20 min. Collected cells with a 6,000 x g 15 sec centrifugation, removed supernatant and resuspended gently in 100 µl of sterile water. Plated on SC –Trp (*Saccharomyces cerevisiae* minimum selection media without tryptophane) selective media and incubated at 30 °C.

pYES2/His$_6$-Rab1A: Rab1A was PCR-amplified from pQE41ΔDHFRS/Rab1A using the following oligonucleotides: 5'-TGT GGA TCC ATG TCC AGC ATG AAT CCC GAA-3' and 5'-CTA GGC ATG CTT AGC AGC AGC CTC CAC CTG-3'. The His$_6$-tagged Rab1A fragment was ligated into pYES2 (Invitrogen) between the *Eco*RI and *Sph*I sites. The plasmid was then transformed into the yeast INVSc1 (Invitrogen) strain with lithium acetate as previously described (Martincic et al., 1997) and streaked on SC -Ura plates.

pGAD424X/PRA1 mutants: The PRA1 mutants were subcloned into the modified pGAD424X (Martincic et al., 1997) prey vector at the *Eco*RI and *Xho*I sites.

Other constructs: pIRESpuro/HA-PRA2 (Abdul-Ghani et al., 2001) and pIRESpuro/HA-PRA1 (Hutt et al., 2000) were previously described.

Yeast two-hybrid binding assays

The PRA1 mutants along with the PRA1 wild type, were co-transformed as described earlier, in Y190 yeast strain with pAS2/Rab3A or pAS2/VAMP2 bait plasmids (Martincic et al., 1997) and grown on SC -Trp and -Leu drop-out media plates for 3-5 days. The cells were patched onto filter paper, lysed by brief liquid nitrogen treatment, and incubated with 1 mg/ml 5-bromo-4-chloro-3-indolyl-β-D-galactopyranoside (X-gal from Invitrogen) in Z buffer (60 mM Na_2HPO_4, 40 mM NaH_2PO_4, 10 mM KCl, 1 mM $MgSO_4$-$7H_2O$). The intensity as well as the time of onset of the blue color, resulting from the processing of x-gal by *B*-galactosidase, was used to assess the strength of the interactions.

Protein purification

His_6-HA-PRA2 and His_6-HA-PRA1 wild type, N70T, S76A and H166A mutants: For the purification of His_6-tagged HA-PRA2, His_6-tagged HA-PRA1 wild type and mutants, 1 litre cultures of LB + ampicillin (100 μg/ml) (Sigma) grown to mid-log (OD_{600} of 0.5) were induced with 1 mM of isopropyl-1-thio-β-D-galactopyranoside (IPTG) (Roche) for 5–8 h. The cells were collected at 5,000 x g for 10 min and resuspended in 10 ml of Homogenization Buffer (50 mM sodium phosphate buffer (BDH), pH 8.0, 300 mM NaCl (Sigma), 10% glycerol (Invitrogen)). Homogenates were prepared by addition of Triton X-100 (Bio-Rad) to 1% final concentration and sonication (Sonic Dismembrator Model 300, Fisher) to reduce the viscosity. The homogenates were incubated at 4 °C for 1 h and insoluble material cleared by centrifugation at 10,000 x g for 20 min (JA-17 rotor, Beckman). The homogenates were added to 1 ml of equilibrated Ni-NTA resin

(Qiagen) per litre of culture. Following a wash with 20-40 volumes of Wash Buffer (50 mM sodium phosphate, pH 6.0, 300 mM NaCl, 10% glycerol, 1% Triton X-100), the bound fusion proteins were eluted from the resin with Elution Buffer (250 mM imidazole (BDH) in 50 mM sodium phosphate, pH 6.0, 300 mM NaCl, 10% glycerol, 0.05% Triton X-100). All recombinant proteins were quantified by densitometric analysis of Coomassie Blue-stained gels using bovine serum albumin as a standard.

His_6-HA-PRA1 wild type and mutants cross-linked to CNBr-activated beads: In order to cross-link wild type and mutant His_6-HA-PRA1 to CNBr-activated Sepharose 4B (Amersham Pharmacia Biotech), the proteins were purified as described above except for their elution with 50 mM EDTA (Sigma) instead of imidazole. CNBr-activated beads were hydrated and washed with 1 mM HCl. The proteins were incubated with the beads for 1 h and washed with 5 volumes of coupling buffer (0.1 M $NaHCO_3$ (Fisher), pH 8.3, and 0.5 M NaCl). Beads were then blocked for 2 h with 0.1 M Tris-HCl (Sigma), pH 8 and washed 3 times with 5 volumes of alternating acid (0.1 M $NaHCO_3$, pH 4, 0.5 M NaCl) and basic (0.1 M Tris-HCl, pH 8, 0.5 M NaCl) buffers. The beads were finally resuspended in normal binding buffer (25 mM Tris-HCl, pH 7.5, 150 mM KCl (VWR), 10% glycerol, 0.005% Triton X-100).

His_6-Rab3A cross-linked to CNBr-activated beads: To purify the His_6-tagged Rab3A, the transformed yeast was grown to saturation in 200 ml of Trp drop-out medium. The cells were harvested at 3,000 x g for 5 min, transferred to 1 litre of YPD, and grown at 30 °C for 8 h. The cells were then collected by centrifugation at 3,000 x g for 5 min and homogenized with glass beads (0.5 mm diameter (Biospec Products)) in lysis buffer (Phosphate-Buffered Saline, pH 7, 1 mM β-mercaptoethanol (Sigma), 2 mM

PMSF (Sigma) at 1 ml/g of cell pellet. The cell debris and glass beads were removed by centrifugation at 3,000 x g for 5 min. Triton X-100 was added to the supernatant to 1% final concentration and incubated at 4 °C for 1 h. The insoluble material was then removed by centrifugation at 100,000 x g for 1 h. The supernatant was loaded onto 1 ml of Ni^{2+}-NTA beads and washed with 40 volumes of wash buffer (Phosphate-Buffered Saline, pH 7, 1 mM β-mercaptoethanol, 0.05% Triton X-100, 10% glycerol). The His_6-tagged Rab3A was eluted with 50 mM EDTA in the above wash buffer and cross-linked to CNBr-activated beads as described above.

His_6-Rab1A cross-linked to CNBr-activated beads: To purify the His_6-tagged Rab1A, the transformed yeast was grown to saturation in 500 ml of Ura dropout medium. The cells were harvested at 3,000 x g for 5 min, transferred to 1 litre of YPG (containing 2% galactose (Sigma) and 1% raffinose (Bio-Shop) instead of glucose) and grown at 30 °C for 8 h. The Rab1A was then purified and cross-linked to beads as previously described for Rab3A.

His_6-Rab3A: To verify the yeast two-hybrid results, *in vitro* binding studies were performed with recombinant GDPβS-loaded His_6-tagged Rab3A. The protein was purified as previously described, except that it was eluted from the resin with 0.3 M imidazole in wash buffer and not cross-linked to beads.

GST-VAMP2 and GST: The construct used for VAMP2 expression as a GST fusion protein was generously provided by Dr. W. S. Trimble, University of Toronto and pGEX-2T (Amersham Pharmacia Biotech) was used for GST expression. Cultures grown to mid-log were induced with 1 mM IPTG and incubated overnight. Cells were resuspended in Lysis Buffer (25 mM HEPES-KOH (Sigma), pH 7.5, 100 mM KCl, 2 mM

EDTA, 0.4 mM PMSF, 2 mM DTT (Roche), 0.3 M sucrose (GIBCO), 20% glycerol). Lysozyme (Sigma) was added to 10 mg/ml, and the suspension was incubated at 4 °C for 1 h. Cells were lysed by sonication in the presence of 1% Triton X-100. Insoluble material was cleared by centrifugation at 10,000 x g for 20 min. The GST fusion proteins were purified by affinity chromatography using glutathione-agarose beads (Sigma). The beads were washed with 20 volumes of Wash Buffer (25 mM HEPES-KOH, pH 7.5, 100 mM KCl, 2 mM EDTA, 0.4 mM PMSF, 2 mM DTT, 0.1% Triton X-100). The recombinant proteins were eluted with Elution Buffer (10 mM glutathione (Sigma), 25 mM HEPES-KOH, pH 7.5, 100 mM KCl, 2 mM EDTA, 0.4 mM PMSF, 2 mM DTT, 0.05% Triton X-100).

In vitro binding assays

PRA/Rab binding assay in various guanine nucleotide bound states: The binding of Rab1A and Rab3A to PRA1 and PRA2, in the presence of GDPβS, GTPγS or no guanine nucleotide was done using purified yeast or bacterially expressed proteins in a pull-down assay. A typical binding assay contained 20 µl of 50% bead slurry cross-linked with Rab1A or Rab3A at 2 ρmol/µl or empty control beads. This was incubated for 1 h at 4 °C with 10, 15, and 20 ρmol of recombinant PRA1 or PRA2 in a total volume of 250 µl of 25 mM Tris-HCl, pH 7.5, 150 mM KCl, 0.005% Triton X-100, 10% glycerol, 0.5 mM $MgCl_2$ (BDH), and 250 µM GDPβS, GTPγS (Roche Molecular Biochemicals) or no guanine nucleotide (EDTA). Controls were also done using inactivated Sepharose beads with no cross-linked Rab. The beads were then washed three times with 1 ml of ice-cold wash buffer (25 mM Tris-HCl, pH 7.5, 150 mM KCl, and 0.005% Triton X-100, 10%

glycerol). Denaturing loading buffer was added to the beads and proteins were subjected to Western immunoblot analysis. PRA1 and PRA2 were probed with mouse anti-HA primary antibodies (Roche) and Alexa Fluor 488-labeled goat anti-mouse IgG secondary antibodies (Molecular Probes). The signals were detected with the Typhoon 8600 imager (Amersham Biosciences).

Rab3A binding assay with PRA1 wild type and mutants N70T, S76A and H166A: A typical Rab3A binding assay with wild type or mutant PRA1 contained 10.8 ρmol of His_6-HA-PRA1 cross-linked to CNBr-activated Sepharose 4B or empty control beads and 320 nM His_6-Rab3A in 25 mM Tris-HCl, pH 7.5, 150 mM KCl, 0.5 mM $MgCl_2$, 0.25 mM GDPβS, 10% glycerol, and 0.005% Triton X-100 in a total volume of 250 μl, and incubated for 1 h at 4 °C. The beads were then washed with ice-cold binding buffer. Denaturing loading buffer was added to the beads, and proteins purified with the beads were subjected to Western immunoblot analysis using anti-Rab3A antibodies (Santa Cruz Biotechnology) with Alexa Fluor 488-labeled goat anti-rabbit IgG as secondary antibodies (Molecular Probes). The assays were done in triplicate, and the signals were quantified using the Typhoon 8600 imager and averaged for comparative analysis.

VAMP2 binding assay with PRA1 wild type and mutants N70T, S76A and H166A: A typical VAMP2 binding assay with wild type or mutant PRA1 contained 40 nM GST-VAMP2 or GST control and 30 nM His_6-HA-PRA1 in 25 mM Tris-HCl, pH 7.5, 150 mM KCl, 10% glycerol, and 0.005% Triton X-100 in a total volume of 250 μl and was incubated for 1 h at 4 °C. Glutathione-agarose was used to recover the GST-VAMP2 or GST control. The beads were washed with ice-cold binding buffer and PRA1 was

detected using anti-HA primary antibodies and Alexa Fluor 488-labeled goat anti-mouse IgG as secondary antibodies. The signals obtained were quantified as described above.

Effect of boiling on detection of PRA2 by immunoblotting

Effect of boiling on bacterial-expressed PRA2: SDS sample buffer was added to 20 ρmol of purified recombinant His_6-HA-PRA2 containing varying amounts of Triton X-100. One set was boiled for 10 min while the other was left at room temperature. The proteins were resolved by SDS-PAGE, and subjected to Western immunoblot with mouse anti-HA antibody. Bound antibodies were visualized with Alexa 488 goat anti-mouse secondary antibody on a Typhoon 8600 imager.

Effect of boiling on mammalian-expressed PRA2: I prepared extracts of Chinese hamster ovary (CHO) cells expressing either HA-PRA1 or HA-PRA2 maintained in minimum essential medium α (Invitrogen) supplemented with 5% fetal bovine serum (FBS from Invitrogen), 100 units/ml penicillin and 100 μg/ml streptomycin (PS from Invitrogen). $3x10^5$ CHO cells were seeded on a 35-mm dish overnight. The cells were transfected with 1 μg of pIRESpuro/HA-PRA1 or pIRESpuro/HA-PRA2 and 3μl of LipofectAMINE (Invitrogen). After 45 min incubation at 37 °C, the lipid-DNA mixture in 400μl Opti-MEM (Invitrogen) was added to the PBS-washed cells in 800 μl of Opti-MEM and incubated at 37 °C for 3–5 h. The medium was replaced with α-MEM (Invitrogen) supplemented with 5% FBS and 1% PS. After 24 or 48 h, the cells were washed with PBS, removed from the plate with a cell scraper in 1 ml of PBS, and collected by centrifugation at 500 x g for 5 min. The cells were immediately resuspended in 200 μl of SDS sample buffer and sonicated twice for 20 sec each to reduce the

viscosity. The samples were equally divided into two aliquot, one was boiled for 10 min while the other was left at room temperature. Equal amount (40 μl) of each was subjected to Western immunoblot analysis as described above.

Results

PRA2 binds multiple Rab isoforms in a guanine nucleotide-independent manner

I first examined and confirmed the interaction of PRA2 with Rab GTPases. In the yeast two-hybrid system, PRA2 showed a positive β-galactosidase reaction when tested against the wild type and GTPase defective Rab1A and Rab3A (Abdul-Ghani et al., 2001). As with PRA1, the interaction was abolished when the double Cys prenylation motif of Rab was deleted, suggesting that prenylation is required for interaction. To confirm this interaction also applies to PRA2, I performed an *in vitro* binding assay using recombinant Rab1A and Rab3A purified as a 6xHis-tagged fusion protein from the yeast, *Saccharomyces cerevisiae*, and covalently linked to CNBr-activated Sepharose. The proteins were pre-loaded with GDP, GTP, or maintained in the nucleotide-free state (in the presence of EDTA). Increasing amounts of recombinant HA-tagged PRA1 or PRA2 were added to the beads at 4 °C with the bound proteins recovered and analyzed by Western immunoblot. As shown in Figure 2.1A, PRA2 was recovered with the immobilized Rab1A and Rab3A but not with the control Sepharose beads. There was a slight increase in the amount of PRA2 recovered with immobilized Rab3A compared with Rab1A. PRA2 showed a slightly higher affinity for GTP-bound Rab but was clearly recovered with the GDP-bound as well as guanine nucleotide-free state of both Rab GTPases. Under the same conditions, PRA1 also showed a slight preference for Rab3A over Rab1A (Figure 2.1B). There was also a slightly higher affinity for the GTP-bound Rab followed by guanine nucleotide-free and GDP-bound forms. Thus, both PRA1 and

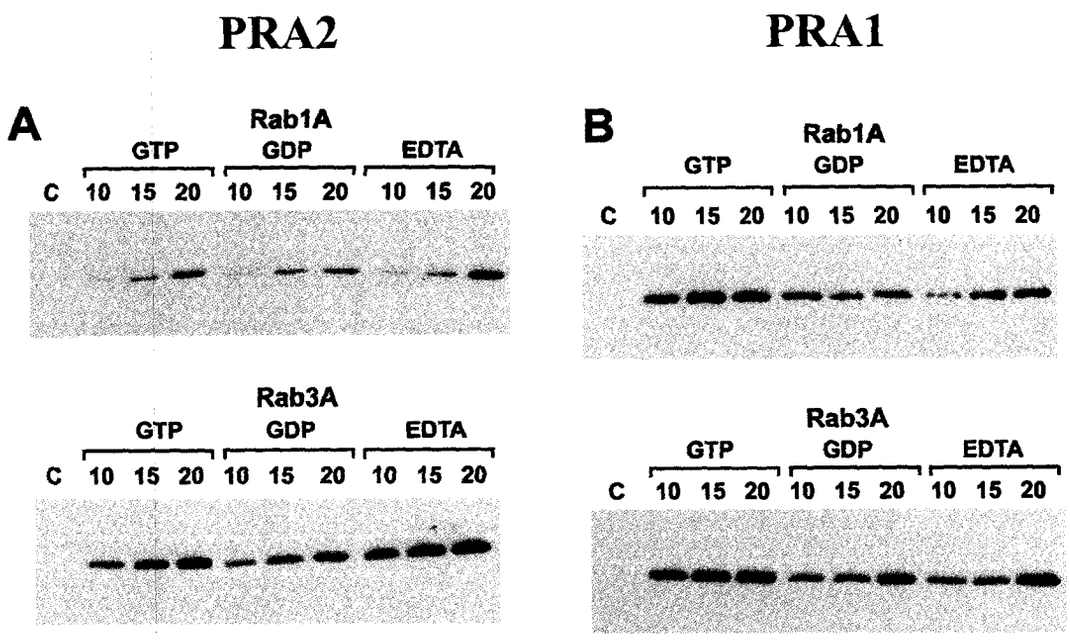

Figure 2.1. Binding of recombinant PRA1 and PRA2 to Rab1A and Rab3A. (A) 40 pmol of immobilized Rab1A (*top panel*) or Rab3A (*bottom panel*) was incubated with 10, 15, or 20 pmol of HA-tagged PRA2. The Rab GTPases were pre-incubated with GTP, GDP, or EDTA, as indicated. *Lane C* represents the control Sepharose beads incubated with 20 pmol of PRA2. (B) The same conditions were used as in panel A except recombinant HA-tagged PRA1 was added to the immobilized Rab. PRA1 and PRA2 bound to the beads were detected with anti-HA antibodies. Results were reproduced in the span of a month.

PRA2 can interact with at least Rab1A and Rab3A in the guanine nucleotide-bound and free states.

Mutation of PRA1 affects binding to Rab3A and VAMP2

To characterize PRA1's interaction with Rab3A and VAMP2, I employed a mutagenic approach by introducing point mutations to the two most highly conserved regions: one proximal to the first hydrophobic domain (residues 66-78) and a second that follows the last hydrophobic domain and spans residues 166-169 (Figure 2.2). I examined the binding properties of the PRA1 mutants to identify the molecular determinants involved in PRA's interaction with Rab3A and VAMP2, and possibly determine whether this might be an underlying cause of the altered Golgi morphology and inhibition in transport of $VSVG^{ts045}$-GFP previously observed (Gougeon et al., 2002). We and others (Abdul-Ghani et al., 2001; Bucci et al., 1999; Figueroa et al., 2001; Janoueix-Lerosey et al., 1995; Martincic et al., 1997), have shown previously that PRA1 binds to Rab GTPases and VAMP2. I first screened the binding properties of the mutant PRA1 in the yeast two-hybrid system by subcloning representatives from each into the prey vector. The resulting vectors were co-transformed into the Y190 tester strain with either Rab3A as a representative Rab GTPase or VAMP2 bait, and the transformants were scored for β-galactosidase activity. The Class A mutant N70T showed no interaction with either Rab3A or VAMP2, whereas the class B mutant S76A showed increased interaction with both Rab3A and VAMP2 (Figure 2.3 and Table I). The class C mutant H166A showed a weak interaction with VAMP2 but lost its interaction with Rab3A. I verified the binding properties of the mutant PRA1s by *in vitro* pulldown assays using purified recombinant

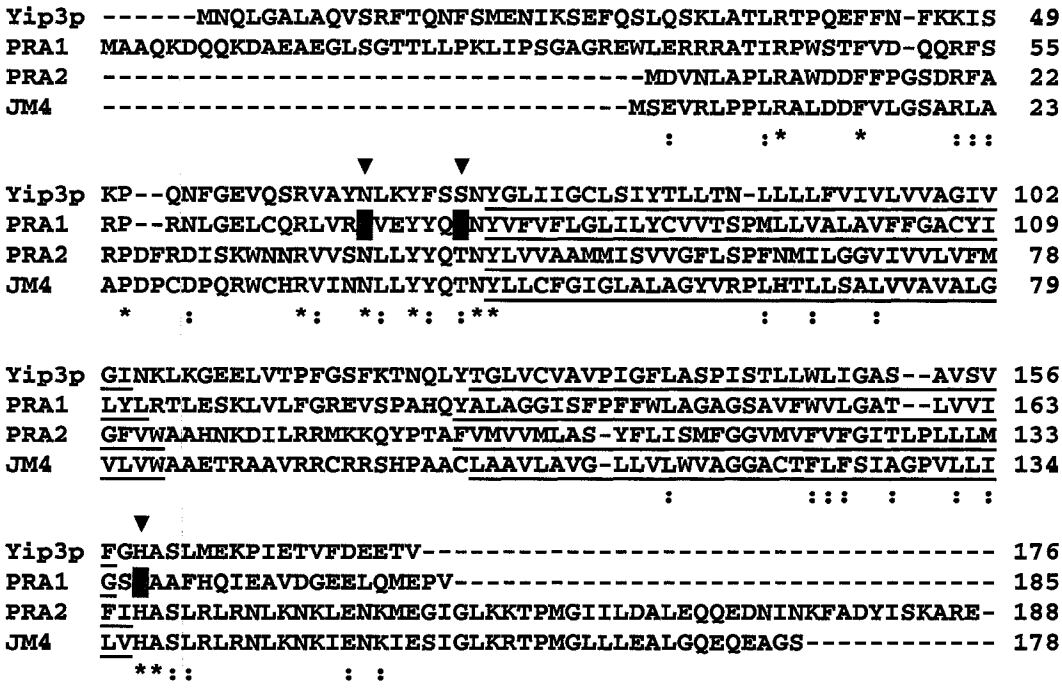

Figure 2.2. PRA2 sequence and comparison to PRA1. Duplicate of figure 1.8. The yeast Yip3p, human PRA1 and JM4, as well as mouse PRA2 sequences were compared using Clustal alignment, with identical residues (red) indicated by a *star* and similar residues (blue) with a *colon*. The predicted hydrophobic domains are underlined. Mutated PRA1 residues are identified by an arrow and framed in green.

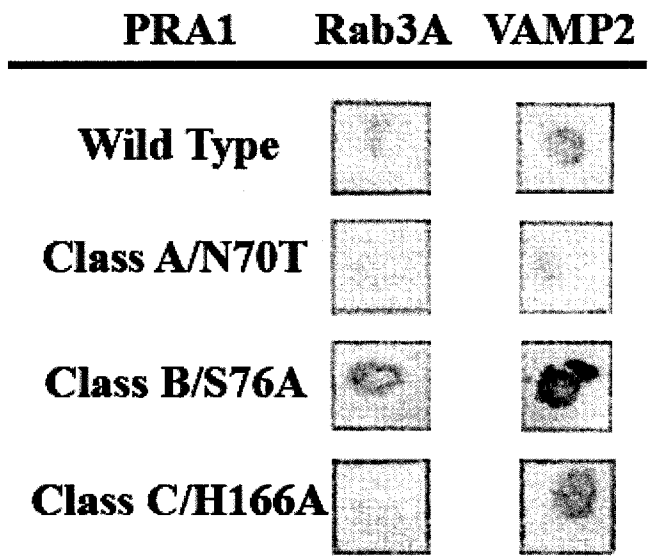

Figure 2.3. Yeast two-hybrid screen of PRA1 mutants against Rab3A or VAMP2. The bait and prey plasmids were co-transformed into Y190 tester strain and selected on Trp, Leu drop-out plates. The transformants were tested for β-galactosidase activity on X-gal filter paper and intensity as well as the time of onset of blue colour was used to assess the strength of the interactions. The results were reproduced over the span of a month.

PRA1 prey	Class	Rab3A bait	VAMP2 bait	Cellular localization
WT		++	++	Golgi
N70T	A	–	–	ER
S76A	B	+++	+++	Condensed Golgi
H166A	C	–	+	ER and Golgi

Table I. Yeast two-hybrid screen of PRA1 mutants against Rab3A or VAMP2. The bait and prey plasmids were co-transformed into Y190 tester strain and selected on Trp, Leu drop-out plates. The transformants were tested for β-galactosidase activity on X-gal filter paper and intensity as well as the time of onset of blue colour was used to assess the strength of the interactions. The last column indicates the cellular localization of the mutant when overexpressed in CHO, as observed previously by Mr. Prosser (Gougeon et al., 2002).

His_6-HA-tagged PRA1s, GST-VAMP2, and His_6-tagged Rab3A, with Rab3A expressed in yeast to ensure prenyl modification that is essential for PRA1 binding. Because both PRA1 and Rab3A were His_6-tagged, purified PRA1s were covalently attached to CNBr-Sepharose beads. I first determined the saturating amount of wild type PRA1 needed to pulldown GDP-bound Rab3A. I then used the EC_{50} value to determine the amount of Rab3A recovered with the mutant PRA1s by Western immunoblot (Figure 2.4A), and normalized this to the wild type PRA1 (Figure 2.4B). In all cases, I detected two immunoreactive Rab3A (Figure 2.4A), which probably represents mono- and di-geranylgeranylated species. A similar approach was used to determine VAMP2 binding using glutathione-agarose beads. The class A mutant N70T showed only residual binding to Rab3A and VAMP2 when compared with wild type PRA1. In contrast, there was a 3-fold increase in Rab3A and a 6-fold increase in VAMP2 binding in the class B mutant S76A. A significant reduction in Rab3A and VAMP2 binding was observed in the class C mutant H166A. Thus, there was a direct correlation between cellular distribution and ability of PRA1 to bind Rab and VAMP2. Loss of Rab and VAMP2 binding in the class A mutants correlated with retention of the mutant PRA1 in the ER, whereas enhanced binding to both in the class B mutants correlated with a highly condensed Golgi. A decrease in both Rab and VAMP2 binding in the class C mutants correlated with an intermediate phenotype. Also, the Rab3A-binding of the three mutants was mirrored by that of VAMP2. Thus, the data suggest that Rab and VAMP2 share a common binding site on PRA1 and that binding to these two proteins may underlie mislocalization of the protein, the altered Golgi morphology, and defect in $VSVG^{ts045}$-GFP transport previously observed.

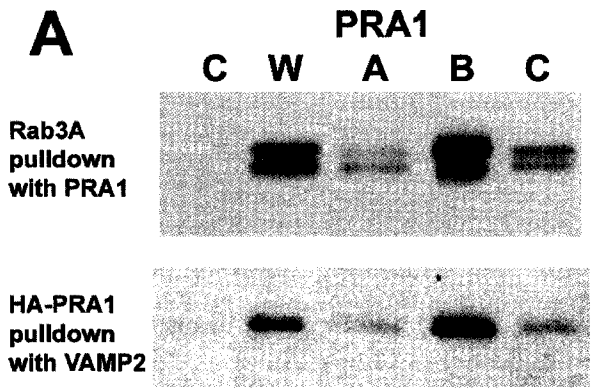

B

PRA1	Normalized Binding	
	Rab3A	VAMP2
Wild Type	1	1
Class A/N70T	0.16 ± 0.01	0.19 ± 0.09
Class B/S76A	3.39 ± 1.04	6.13 ± 1.27
Class C/H166A	0.29 ± 0.01	0.18 ± 0.10

Figure 2.4. ***In vitro*** **binding of Rab3A and VAMP2 to PRA1.** (A) Representative Western immunoblot using anti-Rab3A (upper panel) and anti-HA (lower panel). Immobilized PRA1s was used for Rab3A pulldown, and glutathione-agarose was used to recover GST-VAMP2. Control beads (*C*), wild type PRA1 (*W*), PRA1/N70T Class A mutant (*A*), PRA1/S76A Class B mutant (B), or PRA1/H166A Class C mutant (C). (B) Binding of Rab3A and VAMP2 to the mutant PRA1s normalized to that of the wild type PRA1. Values represent mean and S.E. ($n = 3$ with each performed in triplicate). Student T-test indicates the differences in binding are statistically relevant with a 95% confidence interval, except between the binding values of PRA1 N70T and H166A mutants with Rab3A and VAMP2.

Effect of boiling on bacterial- and mammalian-expressed PRA2

During purification, I noticed that boiling the samples containing recombinant His_6-HA-PRA2 prior to SDS-PAGE greatly decreased the His_6-HA-PRA2 immunoblot signal. To confirm the effect of heat denaturation, SDS sample buffer was added to 20 pmole of purified recombinant His_6-HA-PRA2 containing varying amounts of Triton X-100. One set was boiled for 10 min while the other was left at room temperature before being processed by Western immunoblot. A significant reduction in the PRA2 signal was observed in the boiled samples (Figure 2.5A). Increasing the concentration of non-ionic detergent, Triton X-100, appeared to further reduce the PRA2 signal in the boiled samples but had no effect on the samples incubated at room temperature. No detectable amount of PRA2 either as a dimer or higher oligomer was observed suggesting that heat denaturation caused formation of large SDS-insoluble aggregates leading to the loss of signal.

I next examined whether this is a property of bacterially-expressed PRA2 by expressing the protein in mammalian cells. Although transfection of HA-PRA2 into CHO cells showed a strong ER staining pattern by indirect immunocytochemistry (Abdul-Ghani et al., 2001), extracts from transfected cells showed little, if any, HA-PRA2 signal by Western immunoblot when boiled prior to SDS-PAGE. To test whether heat denaturation of PRA2 might be the underlying cause, I prepared extracts of CHO expressing either HA-PRA1 or HA-PRA2. The transfected cells were resuspended in SDS sample buffer and sonicated to reduce the viscosity. The samples were equally divided into two aliquot portions where one was boiled for 10 minutes while the other was left at room temperature. Equal amount of each was subjected to Western

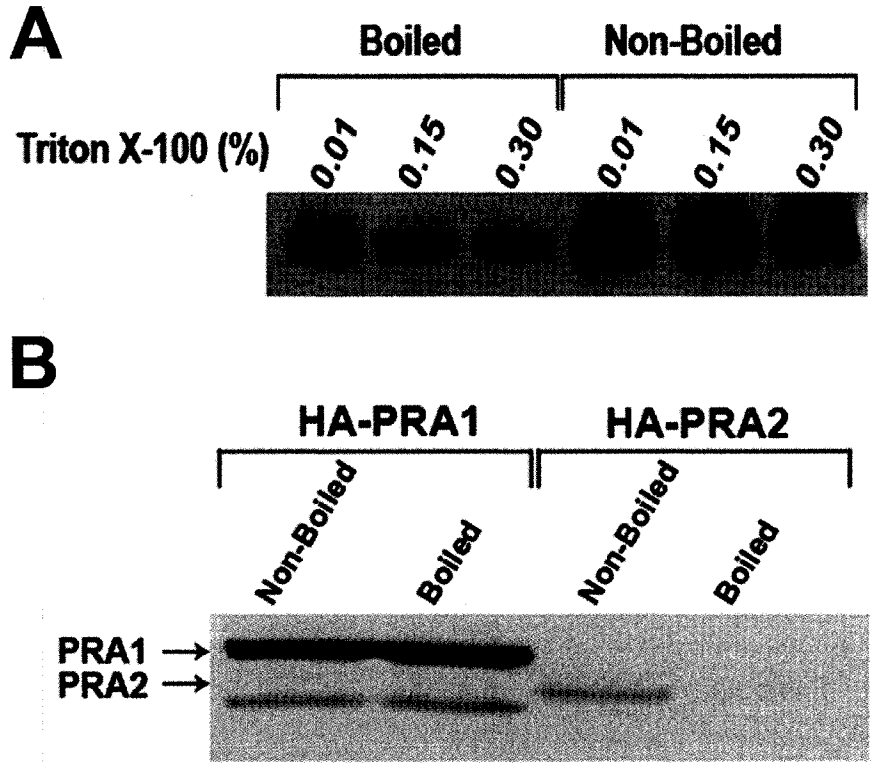

Figure 2.5. Effect of heat denaturation on PRA2 expressed in bacteria or CHO cells: (A) 20 ρmol of purified recombinant His_6-HA-PRA2 solubilized in varying amounts of Triton X-100 as indicated was added to SDS sample buffer and was either boiled or left at room temperature for 10 min before SDS-PAGE and Western immunoblot detection with anti-HA antibodies. (B) Extracts of CHO cells expressing HA-PRA1 or HA-PRA2 were either boiled or left at room temperature for 10 min before SDS-PAGE and Western immunoblot.

immunoblot analysis. As was observed previously with the bacterially-expressed recombinant protein, boiling the cell extracts also decreased the amount of detectable HA-PRA2 (Figure 2.5B). Although PRA1 and PRA2 have a similar overall structure, this sensitivity to heat denaturation is specific to HA-PRA2 as HA-PRA1 showed no loss in signal. Also, no significant protein retention was observed in the gel after electrophoretic transfer to nitrocellulose thereby suggesting the possibility that PRA2 might not transfer well is unlikely. The most likely explanation is that heat denaturation causes severe aggregation of PRA2 resulting in aberrant migration in SDS-PAGE.

Chapter 3

PRA2 and VAP-A regulate ER-to-Golgi trafficking using different mechanisms

Experimental procedures

Plasmid construction

pHyblex/rPRA1, pHyblex/rPRA2: The open reading frames were amplified from the pIRES/HA-PRA1 and pIRES/HA-PRA2 using the following oligos: for PRA1 5'-GCG AAT TCA TGG CGG CCC AGA AGG A-3' and 5'-GTC CTC GAG GAC ACT TTA CAC AGG-3', and for PRA2 5'-GGA ATT CCA TAT GGA CGT GAA CCT CGC CCC GCT-3' and 5'-CCG CTC GAG TTA CTC CCT GGC TTT GCT GAT-3'. The products were digested with *Eco*RI and *Xho*I, and inserted between the same sites in the pHyblex/zeo vector (Invitrogen).

pFLAG/VAP-A constructs: The open reading frame was amplified from the corresponding pGEX-KG/VAP-33 construct obtained from Dr. W.S. Trimble. For VAP-A wild type (amino acid 1-242) and VAP-A Δcc (deletion construct where residues 162-198 that makeup the coiled-coil domain are removed) I used oligo1: 5'-ATC AGT ATG CGG CCG CTA TGG CGA AGC ACG AGC AG-3' and oligo2: 5'-AAG AAT TCT ACA AGA TGA ATT TCC C-3', for the VAP-A ΔTMD (deletion construct where residues 220-242 that makeup the transmembrane domain are removed) I used oligo1 and oligo3: 5'-AGA ATT CAA CTG GTG ACA TTA TCT CTG AA-3' and for the VAP-A ΔN (deletion construct where residues 1-134 that contain the major sperm protein domain are removed) I used oligo2 and oligo4: 5'-GAG CGG CCG CTA TGG AAC CTA GCA

AAG CT-3'. The products were cut with *Eco*RI and *Not*I, and inserted in pFLAG-CMV2 (Sigma) using the same sites.

pCDNA3.1+/VSVG^{ts045}: The open reading frame of VSVG^{ts045} was amplified from pCDM8.1/VSVG^{ts045}-GFP using the following oligos: 5'-CGG ATC CAT GAA GTG CCT TTT GTA CTT A-3' and 5'-CGA ATT CTC ACT TTC CAA GTC GGT TC-3'. I then cut the PCR product and pCDNA3.1+ (Invitrogen) with *Bam*HI and *Eco*RI, and ligated the two digestion products.

pCS2/Myc-Sar1: The open reading frame was amplified from the pCDNA3.1/Sar1-VSVG template using the following oligos: 5'-CCG AAT TCG ATG TCT TTC ATC TTT GAG-3' and 5'-CGC TCG AGT CAG TCA ATA TAC TGG GAG AG-3'. The PCR product was cut with *Eco*RI and *Xho*I, and inserted between the same sites in the pCS2+Myc-Tag vector.

Yeast two-hybrid screen

Bait transformation: Yeast strain EGY48/pSH18-34 (Invitrogen) was streaked on SC -Ura plate and grown for 2 days. Yeast cells (20-50 µl) were scraped from the plate and resuspended in 500 µl of sterile water. The cells were collected by centrifugation and resuspended in 1 ml of 0.1 M LiAc (Sigma). After centrifugation and removal of the supernatant, the following solutions were added to the cell pellet in order: 240 µl of 50% PEG (Sigma), 36 µl of 1 M LiAc, 25 µl of salmon testes carrier DNA 2 mg/ml (Sigma), 1 µg of pHyblex/PRA1 bait plasmid and completed to 350 µl with sterile water. The content was mixed in a Vortex mixer for 2 min, and incubated at 30 °C for 30 min followed by heat shock at 42 °C for 20 min. The cells were collected with a 6,000 x g 15

sec centrifugation, resuspended gently in 100 µl of sterile water, plated on SC -Ura supplemented with Zeocin at 300 µg/ml (Z300) (Invitrogen) and incubated at 30 °C.

Library transformation: For small-scale yeast transformations, 2.5 x 10^8 yeast cells (EGY48/pSH18-34) containing the bait plasmid pHyblez/PRA1 were transferred to 50 ml of YPD medium. When the cell density has reached 2 x 10^7 cells/ml, the cells were collected by centrifugation at 3,000 x g for 5 min and washed with sterile water. To transform the cells, the following components were added in order: 2.4 ml of 50% PEG, 0.36 ml of 1 M LiAc, 250 µl of salmon sperm carrier DNA 2 mg/ml, 5 µg of human brain cDNA library prey DNA (Clontech) and sterile water to a final volume of 3.5 ml. The mixture was vortexed 2 min, incubated at 30 °C 30 min, heat shocked at 42 °C for 20 min, and chilled on ice 1 min. Cells were collected via centrifugation at 2,000 x g for 5 min, the supernatant was removed and the cells were resuspended gently in 250 ml of YC -Ura -Trp. The cells were then grown at 30 °C for 1-2 h before adding Zeocin to 200 µg/ml and incubating overnight. The culture was then plated on YC -Ura -Trp -Leu plates containing 200 µg/ml Zeocin, 2% galactose and 1% raffinose. Four colonies for each positive were tested, by patching onto selective 5-bromo-4-chloro-3-indoyl-β-D-galactopyranoside (X-gal from Invitrogen) plates. The intensity as well as the time of onset of the blue colour was used to confirm the interactions.

Rescue of positive prey DNA: DNA was isolated from the positive colonies. Each positive was grown in 5 ml of selective media overnight. The cells were collected by centrifugation and the pellet was resuspended in 0.3 ml of lysis buffer (2.5 M LiCl, 50 mM Tri-HCl, pH 8, 4% Triton X-100, 62.5 mM EDTA). One hundred and fifty microliters of 0.5 mm glass beads (Biospec Products) and 0.3 ml of phenol chloroform

were added before vortexing for 4 min in order to obtain maximum lysis. The beads and cell debris were removed by centrifugation and the DNA was collected by ethanol precipitation. The prey DNA was transformed into KC8 bacterial strain by electroporation for amplification, followed by purification.

Retransformation of prey with bait: Prey DNA was retransformed with the pHyblez/PRA1 and pHyblex/PRA2 mouse and rat in EGY48/pSH18-34 yeast strain as previously described for the bait transformation, except that the transformation was plated on YC -Ura -Trp -Leu plates containing 200 μg/ml Zeocin, 2% galactose and 1% raffinose. Four colonies for each positive were transferred to selective X-gal plates. Confirmed positives were sequenced by automated Licor sequencing (LI-COR).

Protein purification

His_6-HA-PRA2 and His_6-HA-PRA1: For the purification of His_6-tagged HA-PRA2, His_6-tagged HA-PRA1, 1 litre cultures of LB + ampicillin (100 μg/ml) (Sigma) grown to mid-log (OD_{600} of 0.5) were induced with 1 mM of isopropyl-1-thio-β-D-galactopyranoside (IPTG from Roche) for 5–8 h. The cells were collected at 5,000 x g for 10 min and resuspended in 10 ml of Homogenization Buffer (50 mM sodium phosphate buffer (BDH), pH 8.0, 300 mM NaCl (Sigma), 10% glycerol (Invitrogen)). Homogenates were prepared by addition of Triton X-100 (Bio-Rad) to 1% final concentration and sonication (Sonic Dismembrator Model 300, Fisher) to reduce the viscosity. The homogenates were incubated at 4 °C for 1 h and insoluble material cleared by centrifugation at 10,000 x g for 20 min (JA-17 rotor, Beckman). The homogenates were added to 1 ml of equilibrated Ni-NTA resin (Qiagen) per litre of culture. Following a

wash with 20-40 volumes of Wash Buffer (50 mM sodium phosphate, pH 6.0, 300 mM NaCl, 10% glycerol, 1% Triton X-100), the bound fusion proteins were eluted from the resin with Elution Buffer (250 mM imidazole (BDH) in 50 mM sodium phosphate, pH 6.0, 300 mM NaCl, 10% glycerol, 0.05% Triton X-100). All recombinant proteins were quantified by densitometric analysis of Coomassie Blue-stained gels using bovine serum albumin as a standard.

GST-VAP-A constructs and GST bound to glutathione beads: For GST, GST-VAP-A wild type, ΔTMD (a.a.1-219), Δcc (a.a.1-161+199-242) and ΔN (a.a.135-242), cultures were grown and induced with IPTG as described above. Cells were collected and resuspended in 10 ml of Lysis Buffer (25 mM HEPES-KOH, pH 7.5, 0.3 M sucrose (GIBCO), 2 mM EDTA, 2 mM DTT (Roche), 10% glycerol, 1 mM Phenylmethanesulfonyl Fluoride (PMSF from Sigma)). Lysozyme (Sigma) was added to 10 mg/ml, and the suspensions were incubated at 4 °C for 30-60 min. Cells were solubilized with 1% Triton X-100 and briefly sonicated to reduce viscosity. After a further incubation at 4 °C for 30-60 min, any insoluble material was cleared by centrifugation at 10,000 x g for 30 min. The GST fusion proteins were incubated with 1 ml of glutathione-Sepharose 4B beads (Amersham Biosciences) per litre of culture, followed by washing with 20-40 volumes of Wash Buffer (25 mM HEPES-KOH, pH 7.5, 100 mM KCl, 2 mM EDTA, 2 mM DTT, 0.1% Triton X-100, 0.5 mM PMSF). The recombinant proteins were left on the beads as a 50% bead slurry in Wash Buffer supplemented with 0.01% NaN_3 and diluted with empty beads to obtain equivalent concentrations as the binding assay is based on pre-loaded beads.

In vitro binding assay

VAP-A/PRA binding assay: I used the purified bacterially expressed recombinant proteins to confirm by *in vitro* pulldown assay the PRA-VAP-A interaction observed in the yeast two-hybrid screen. A typical pulldown assay contained 20 μl of glutathione-Sepharose beads containing 100 pmol of GST construct and 5 or 10 pmol of His_6-HA-PRA1 or His_6-HA-PRA2 in a final volume of 250 μl of Binding Buffer (25 mM Tris-HCl, pH 7.5, 150 mM KCl, 10% glycerol, and 0.01% Triton X-100). After incubation for 1 h at 4 °C, the beads were recovered by brief centrifugation and washed three times with 1 ml of ice-cold Binding Buffer. Proteins bound to the beads were eluted with SDS sample buffer and subjected to Western immunoblot analysis with mouse anti-HA primary antibodies (Roche) and Alexa Fluor 488-labeled goat anti-mouse secondary antibodies (Invitrogen-Molecular Probes). The signals were captured and analysed using the typhoon 8600 imager (Amersham Biosciences).

Cell culture and immunocytochemistry

CHO propagation: Chinese hamster ovary (CHO) cells were maintained in minimum essential medium α (Invitrogen) supplemented with 5% fetal bovine serum (FBS from Invitrogen), 100 units/ml penicillin and 100 μg/ml streptomycin (PS from Invitrogen). For transient expression, cells were transfected with LipofectAMINE (Invitrogen) and left to recover 18-48 h before assays were performed.

Co-localization studies: For VAP-A/PRA co-localization studies, CHO cells were seeded on 12 mm coverslips and transienstly transfected with pFLAG/VAP-A and pIRES/HA-PRA1 or pIRES/HA-PRA2. For Sar-1 co-localization, CHO cells were transiently

transfected with pCS2/Myc-Sar1 and pFLAG/VAP-A or pIRES/HA-PRA2. Cells were fixed 24-48 h after transfection with 4% paraformaldehyde (Electron Microscopy Science) in phosphate-buffered saline for 30 min followed by incubation in blocking buffer (1% bovine serum albumin, 2% normal goat serum and 0.4% saponin in phosphate-buffered saline) for 20 min. Mouse monoclonal anti-HA and anti-FLAG (Sigma), and rabbit anti-FLAG (Sigma) and anti-Myc (Sigma) antibodies were used as primary antibodies, and Alexa 488 and 594-labeled secondary antibodies (Invitrogen) were used. Coverslips were mounted on slides with SlowFade Light antifade (Invitrogen) and images were acquired with a Bio-Rad MRC1024 confocal microscope equipped with a 60x, 1.4-numerical aperture oil-immersion objective. For co-localization images, deconvolution was performed to optimize precision. Z-series were obtained using a 0.3 μm step and image stacks were deconvolved with computational optical sectioning microscopy software compiled for a personal computer, using an expectation maximization algorithm developed by J.-A. Conchello (Conchello et al., 1994) and coded in "C" by Keith Doolittle of Washington University, St. Louis. The point-spread function was calculated according to the method of Gibson and Lanni (Gibson and Lanni, 1992).

Effect of VAP-A and PRA2 on ER-to-Golgi trafficking of VSVG^{ts045}

Using confocal microscopy to follow VSVG^{ts045}-GFP trafficking: CHO cells were transiently transfected with pCDM8.1/VSVG^{ts045}-GFP along with the empty pFLAG-CMV2 vector control, pFLAG/VAP-A or pIRES/HA-PRA2 and 18 h after transfection were shifted to 42 °C for 6 hours. Cycloheximide (20 μg/ml from Sigma) was added 10

min before shifting back to 37 °C, cells were fixed after 0, 30 or 60 min and analysed by laser confocal microscopy. For the VSVG^{ts045}-GFP folding assay, the cells were processed identically and stained after 0 and 30 min with the mouse monoclonal folding conformation-specific I14 primary antibody (donated by Dr. Lyles) and Alexa 594-labeled secondary antibody (Invitrogen).

Using Endoglycosidase H assay to monitor glycosylation state of VSVG^{ts045}: CHO cells were transiently co-transfected with pCDNA3.1+/VSVG^{ts045} and either the empty pFLAG-CMV2 vector control, pIRES/HA-PRA2 and pFLAG/VAP-A wild type together or separately, pFLAG/VAP-A ΔN or pFLAG/VAP-A ΔTMD. After 18 h, cells were shifted to 42 °C for 6 hours. Cycloheximide (20 μg/ml) was added 10 min before shifting back to 32 °C for 0, 30, 60 or 90 min. At each time points, the cells were washed in PBS, scraped in PBS with a rubber policeman and collected by a 5 min 500 x g centrifugation. Cells were then resuspended in 200 μl of 20 mM Tris-HCl pH 7.5 and lysed by sonication. Cell debris was removed by a 5 min 500 x g centrifugation. The VSVG^{ts045}-containing membranes were collected by high-speed centrifugation (100,000 x g for 1 h) of the supernatant. The resulting pellets were resuspended by sonication in 200 μl of 50 mM sodium citrate, 0.2% SDS. The samples were then boiled and treated overnight with 5 mU Endoglycosidase H (Endo H from Roche) at 37 °C, except for the no Endo H control. Proteins in the samples were precipitated with 10% TCA, redissolved in SDS sample buffer, and subjected to Western immunoblot analysis using a rabbit anti-VSVG primary antibody (Stressgen) and an Alexa 488-labelled secondary antibody.

Co-immunoprecipitation of VAP-A with PRA2

Co-immunoprecipitation of VAP-A with PRA2 from co-expressing CHO cells: $1x10^6$ CHO cells were seeded onto a 100-mm dish, and co-transfected the next day with 2.5 μg each of pFLAG/VAP-A and pIRESpuro/HA-PRA2 or pIRESpuro/HA-PRA1 in 7 μl of LipofectAMINE. The transfected cells were maintained in α-MEM supplemented with 5% FBS and 1% PS for 48 h. The cells were then washed two times with pre-warmed PBS. After removal of residual PBS, 200 μl of ice-cold 50 mM HEPES-NaOH, pH 7.2, supplemented with 1 mM PMSF was added and the cells recovered from the plate with a cell scraper. A homogenate was prepared by brief sonication on ice, and cell debris removed by centrifugation at 1,000 x g for 5 min at 4 °C. The resulting supernatant was cross-linked at room temperature for 20 min with 2.5 mM of freshly prepared dithio-bis-succinimidyl propionate (DSP from Pierce) diluted from a 25 mM stock dissolved in dimethyl sulfoxide (DMSO from Sigma). After cross-linking, the DSP was quenched by adding Tris-HCl, pH 7.5, from a 1 M stock to 50 mM final concentration and incubated at room temperature for a further 5 min. The extract was then solubilized by adding an equal volume of 2% NP-40 (BDH), 1% deoxycholate (Sigma), 300 mM NaCl and 10 mM EDTA. After incubation at 4 °C for 1 h, insoluble materials were removed by centrifugation at 10,000 x g for 5 min, and the supernatants were equally divided into two aliquot portions. Mouse anti-HA antibody (5 μg) or control normal mouse serum was added to the samples and the volume adjusted to 0.5 ml with PBS. After overnight incubation at 4 °C, the immune complex was recovered with 20 μl of 50% protein G-agarose slurry (Roche). The beads were washed three times with Tris-buffered saline containing 1% Triton X-100 and proteins bound to the beads were reduced with DTT and

subjected to Western immunoblot analysis. Rabbit anti-FLAG primary antibody (Sigma) and Alexa 488 goat anti-rabbit secondary antibody were used to detect FLAG-VAP-A, while a polyclonal rabbit anti-HA antibody (Zymed) and Alexa 488 goat anti-rabbit secondary antibody were used to detect the HA-PRA2.

Fluorescent Recovery After Photobleaching (FRAP)

Evaluating ER lateral movement of VSVG^{ts045}-GFP: CHO cells were seeded on a 0.17 mm thick Delta T Dish (Bioptechs) and co-transfected with pCDM8.1/VSVG^{ts045}-GFP and either the empty pFLAG-CMV2 vector control, pFLAG/VAP-A wild type, pFLAG/VAP-A ΔN or pIRES/HA-PRA2. After 18 h the cells were shifted to 42 °C for 6 h. Cycloheximide (20 μg/ml) was added 10 min before shifting back to 30 °C on a Delta Vision Adaptor (Bioptechs) heating unit mounted on a laser Bio-Rad MRC 1024 confocal microscope. The 488 nm line of an argon ion laser with a 60X objective was used once a cell was selected to capture a pre-bleach image before a defined small square region of the ER was photobleached at full laser power (100%) for 5-10 sec. The recovery of fluorescence was monitored by scanning at low laser power (3-10%) and images were captured at 20 sec intervals during the recovery period. MIPAV software (McAuliffe et al., 2001) was used to quantify the signal recovery in the bleached area and correct for the general signal bleaching that occurred during the time-course. However, the extent of bleaching that occurred between the pre-bleach image and the first post-bleach image was such that signal bleach correction was inaccurate and data could not be represented as recovery compared to pre-bleach image. Therefore, the signal intensity obtained after complete recovery was used as the maximum and all values were expressed as a fraction

of this maximum. The only exception was FLAG-VAP-A wild type samples, which never reach a plateau maximum as the recovery was exceedingly slow. For this, the signal value of the last time point was used as a conservative estimate of maximum recovery. The EXDIF software (Swiss Federal Office of Public Health and the Engineering school of Fribourg) was used to take into account the corrected FRAP values (up to seven minutes due to increased variability after this time, except for VAP-A wild type where the complete 10 minute time course values were used), as well as the size and shape of the bleached areas, in order to calculate the diffusion coefficient of $VSVG^{ts045}$-GFP.

Microtubule pull-down

VAP-A binds to purified microtubules: CHO cells were seeded on a 100-mm dish and transfected with pFLAG/VAP-A wild type or pFLAG/VAP-A ΔN (two dishes each). After 24 h, the cells were washed in PBS, scraped with a rubber policeman and collected with a 500 x g centrifugation. The cell pellet was then resuspended in 250 μl of buffer (5 mM HEPES pH 7.4, 100 mM NaCl, protease inhibitor cocktail), sonicated 2 times for 30 sec, collected at 5,000 x g 20 min at 4 °C and solubilized with 0.5% Triton X-100 at 4 °C for 30 min. Cell debris was removed by a 130,000 x g 20 min 4 °C centrifugation and 15 μl of extract was added (or 5 μl of VAP-A ΔN CHO extract + 10 μl control CHO extract was added for the VAP-A ΔN sample in order to get the same amount of each construct in the sample. A strong level of expression of VAP-A WT is required to observe binding to 20 μl (equivalent to 10 μg of tubulin/sample) of commercially purified polymerized tubulin (Cytoskeleton Inc.) in polymerization buffer, according to the manufacturer. For the control samples, tubulin was replaced with equal volume of equivalent buffer without

the tubulin. The samples were incubated at room temperature for 20 min. Afterward, 50 µl of G-PEM/Taxol was added and the microtubules were collected by centrifugation with a 100,000 x g for 40 min at room temperature on a 100 µl of 20% sucrose cushion containing 10 µM taxol (Sigma). The pellets were resuspended in SDS sample buffer and processed with comparative cell extract inputs by Western immunoblot using mouse anti-FLAG and rabbit anti-tubulin primary antibodies (ABR-Affinity BioReagents) and Alexa 488-labelled secondary antibodies.

Preparation of polymerized microtubules. Briefly, 250 µg of lyophilized tubulin was dissolved in 50 µl of ice-cold G-PEM by pipetting up and down gently, resulting in a 5 mg/ml concentration of tubulin. The G-PEM solution contained 250 µl of PEM (80 mM PIPES, 1 mM EDTA, 1 mM $MgCl_2$) and 2.5 µl of 0.1M GTP. The dissolved tubulin was divided into two 25 µl fractions and snap-frozen in liquid nitrogen before transferring to –80 °C for storage. To obtain polymerized microtubules, 2.75 of polymerization buffer (G-PEM + 50% glycerol) was added to 22 µl of thawed tubulin and incubate at 37 °C for 30 min. Meanwhile, 2.2 µl of 2 mM taxol was added to 198 µl of G-PEM (kept at room temperature) to obtain a 20 µM solution and equilibrated at 37 °C. After the 30 min polymerization, 198 µl of the G-PEM/Taxol was added to the tubulin sample and mixed thoroughly but gently, and kept at room temperature before use in the pull-down assay.

ER budding assay

CHO cells seeded on a 100-mm dish were co-transfected following the Lipofectamine protocol with 1.33 µg pcDNA3.1+/VSVG^{ts045}-Myc and 1.66 µg either

control empty pFLAG-CMV2 vector, pFLAG/VAP-A or pIRES/HA-PRA2. After 18 h the cells were transferred to 42 °C for 6 h, washed with pre-warmed (42 °C) 50/90 buffer (50 mM HEPES, pH 7.2 and 90 mM potassium acetate) and collected and permeabilized by scraping with a rubber policeman in pre-warmed (42 °C) 50/90 buffer before their collection by centrifugation at 500 x g for 3 min. The cell pellets were resuspended in pre-warmed (42 °C) 50/90 buffer and passed 4 times through a 28-gauge 1cc syringe to help permeabilization, which can be monitored by staining with 0.4% trypan blue (Sigma) and counting the number of perforated cells under light microscopy. Cells were collected with a 500 x g 3 min centrifugation and resuspended in 65 µl of 50/90 buffer. The budding assay contained 25 µl of semi-intact cells, 50 µl of rat liver cytosol (dialized into 25/125 buffer (25 mM HEPES buffer, pH7.2, and 125 mM potassium acetate)), 10 µl of ATP regenerating system (0.1 M creatine phosphate (Sigma), 40 mM high grade ATP (Roche), 100 U/ml creatine phosphokinase (Sigma)), 55 µl 25/125, 32 µl water, 5 µl 0.1 M magnesium acetate (Sigma), pH 7, 3 µl 1 M HEPES-KOH, pH7.2, 20 µl of budding buffer (50 mM EGTA (Sigma), 18 mM $CaCl_2$ (BDH), 20 mM HEPES-KOH, pH 7.2). Duplicates of each sample were made with the first incubated at 32 °C for 40 min, while the second was incubated on ice 40 min as a negative control. The samples were centrifuged successively at 4,000 x g for 1 min and 15,000 x g for 1 min to remove the permeabilized cell. The budded vesicles were collected by centrifugation of the supernatant at 100,000 x g for 1 h and resuspended in SDS sample buffer. The samples were processed by Western immunoblot with a mouse monoclonal anti-Myc primary antibody ($VSVG^{ts045}$–Myc) (Stressgen) and an Alexa 488-labelled secondary antibody. The signal was quantified using ImageQuant software and the signal obtained from the

incubation on ice (very minimal) was subtracted from the sample incubated at 32 °C and this value was compared to the input in order to calculate the amount of budded $VSVG^{ts045}$–Myc as a percentage of total $VSVG^{ts045}$–Myc. For the microtubule depolymerization by chilling, the cells were washed with ice-cold 50/90 buffer, scraped on ice in ice-cold 50/90 buffer and left on ice for a total of 1 h before being collected. The cells were then resuspended in ice-cold 50/90 buffer and passed through a 28-gauge 1cc syringe. The rest of the assay was performed identically. For the microtubule depolymerization by nocodazole (Sigma), 10 μM nocodazole (in DMSO) was added after 5 h at 42 °C. 10 μM nocodazole was also present in the 50/90 buffer used to scrape and syringe permeabilize the cells, as well as in the budding reaction to prevent microtubule repolymerization. The rest of the assay was identical to normal conditions.

Results

VAP-A interacts with PRA1 and PRA2

The second goal of my research was to clarify the function of PRAs. The identification of a protein's interacting partners often yields great insight into possible function. Therefore, I used rat PRA1 as bait in the yeast two-hybrid system in a discovery-driven approach to identify PRA1-interacting proteins from a human brain cDNA library. The screen yielded a number of interesting proteins listed in Table II. VAMP Associated Protein of 33 KDa (VAP-A) was an intriguing positive due to its ability to interact with VAMPs as well as its structural similarity to the SNARE protein. Since it was also believed to be involved in vesicle trafficking, it suggested the PRA-VAP-A interaction might be functionally relevant and thus I attempted to characterize the function of this protein as well. VAP-A was represented 5 times in the 64 sequenced positive clones and also interacted with PRA2 when substituted for the PRA1 bait. The clones all expressed the C-terminal half of VAP-A (a.a. 95-242), suggesting the major PRA binding domain resides in this portion of the protein. Bacterially-purified recombinant proteins and deletion constructs were then used in binding assays to confirm the interaction *in vitro* and to identify the critical interacting domains. As shown in Figure 3.1, VAP-A interacted with both PRA1 and PRA2. Deletion of VAP-A's C-terminal transmembrane domain completely abrogated binding whereas deletion of VAP-A's coil-coiled domain or N-terminus, which contains a major sperm protein (MSP) domain, had no major effect on PRA binding. These results suggest the interaction involves the hydrophobic domains of both proteins. The fact that VAP-A is one of 11 hydrophobic proteins identified in the screen (44% of total) suggests that there might be some specificity to the hydrophobic interaction (Table II).

Y2H Positive Preys retrieved using PRA1 as bait	Y2H Interaction with PRA2 as bait	Hydrophobic Domain
Synapse-Associated Protein 1	NO	NO
Cysteine-rich with EGF-like domains 1	YES	YES
Neurotactin	Undetermined	YES
Lysosomal H+ transporter ATPase	NO	YES
Ribosomal Protein, Large, P0 (RPLP0)	NO	YES
G protein-coupled receptor, family C, group 5, member C (GPRC5C)	NO	YES
Phosphoglycerate Kinase 1 (PGK1)	NO	NO
ARL-6 interacting protein 1	YES	YES
Phosphodiesterase 6A	NO	NO
VAMP-associated protein A (VAP-A)	YES	YES
Tubulin Beta 2	NO	NO
Tubulin Beta 4	Undetermined	NO
Farnesyl diphosphate synthase	YES	NO
FXYD domain-containing ion transport regulator 6 (FXYD6)	NO	YES
Hypothetical protein KIAA0930	NO	YES
Unidentified protein BAC clone CTA-348C20	NO	N/A
Sorting Nexin 2	NO	NO
Methionine adenosyltransferase regulatory beta subunit (MAT II)	Undetermined	NO
HERPUD-2	Undetermined	YES
Tumor protein D52 (TPD52)	Undetermined	NO
Tumor protein D52-like 2 (TPD52L2)	Undetermined	NO
Ovarian cancer immunoreactive antigen domain containing 1	Undetermined	NO
Forkhead box P1 (FOXP1)	Undetermined	NO
Reticulon 1	Undetermined	YES
L-type voltage-dependant calcium channel Beta-1 subunit	Undetermined	NO

Table II. List of yeast two-hybrid positives. Positive preys retrieved from the yeast two-hybrid screen of a brain cDNA library using PRA1 as bait. Kyte-Doolittle evaluation was used with a window size of 20 to determine the presence of hydrophobic domains with a scale value ≥ 1.5.

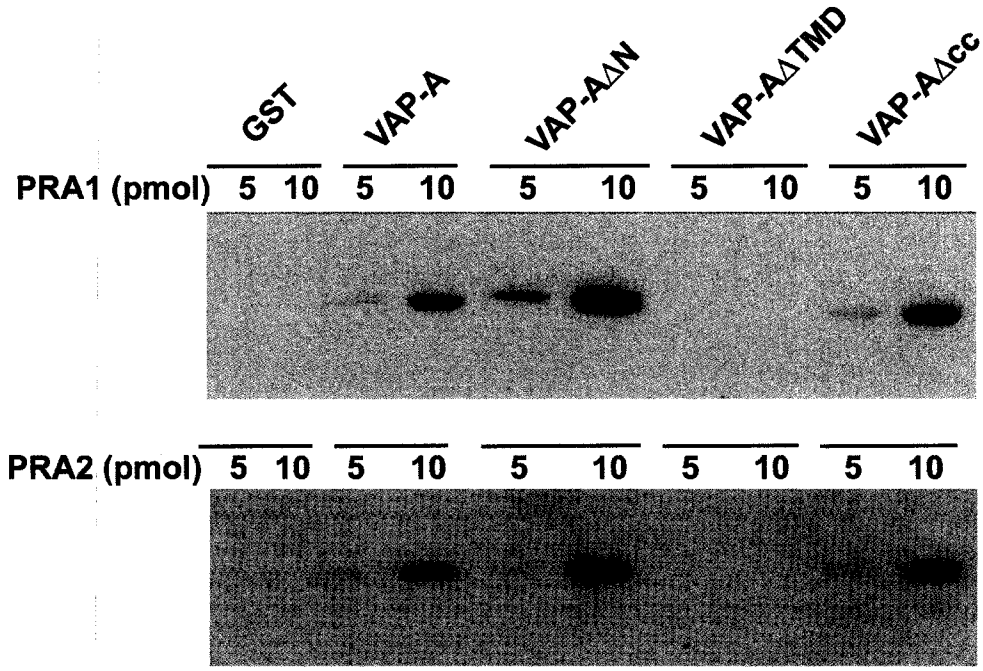

Figure 3.1. ***In vitro*** **binding assay of VAP-A with PRA1 and PRA2.** 100 pmoles of GST, GST-VAP-A Wild Type, GST-VAP-A ΔN (deletion of the N-terminal major sperm protein domain), GST-VAP-A ΔTMD (deletion of the C-terminal transmembrane domain) or GST-VAP-A Δcc (deletion of coiled-coil domain), immobilized on glutathione-Sepharose beads was incubated with 5 or 10 pmoles of HA-tagged PRA1 (upper panel) or HA-tagged PRA2 (lower panel). PRA1 and PRA2 bound to the beads were detected with anti-HA antibodies.

Since PRA1 and PRA2 are differentially localized to the Golgi complex and ER, respectively (Abdul-Ghani et al., 2001), while VAP-A is predominantly distributed in the ER (Skehel et al., 2000), I sought to determine whether expression of VAP-A might alter the cellular localization of the PRA isoforms or vice versa. Expression of FLAG-VAP-A in CHO showed a reticular staining pattern with extensive co-localization with HA-PRA2 (Figure 3.2). No obvious co-localization was observed with the Golgi localized HA-PRA1. Moreover, co-expression of VAP-A and PRA1 or PRA2 showed no detectable alteration in the cellular distribution of the proteins, suggesting that interaction between VAP-A and the PRA isoforms has minimal effect, if any, on cellular localization. Although VAP-A is capable of binding both PRA isoforms *in vitro*, its subcellular distribution would restrict its interaction to the ER-localized PRA2 in the cell. To confirm this, I performed co-immunoprecipitation experiments on DSP cross-linked, detergent solubilized cell extracts from FLAG-VAP-A and HA-PRAs co-transfected CHO cells. Since the interaction is sensitive to detergent, covalent cross-linking prior to solubilization is required to stabilize the interaction. FLAG-VAP-A was found to co-immunoprecipitate with HA-PRA2 but not HA-PRA1 (Figure 3.3), supporting intracellular interaction between VAP-A and PRA2. Ideally, it would have been preferable to perform these subcellular co-localization and co-immunoprecipitation assays with antibodies specific to the endogenous PRA and VAP-A proteins. However, I did not have access to adequate antibodies and generating them ourselves proved unsuccessful. I believe the results obtained support a real *in vivo* interaction, but the extent with which the endogenous PRA2 and VAP-A interact remains to be clarified.

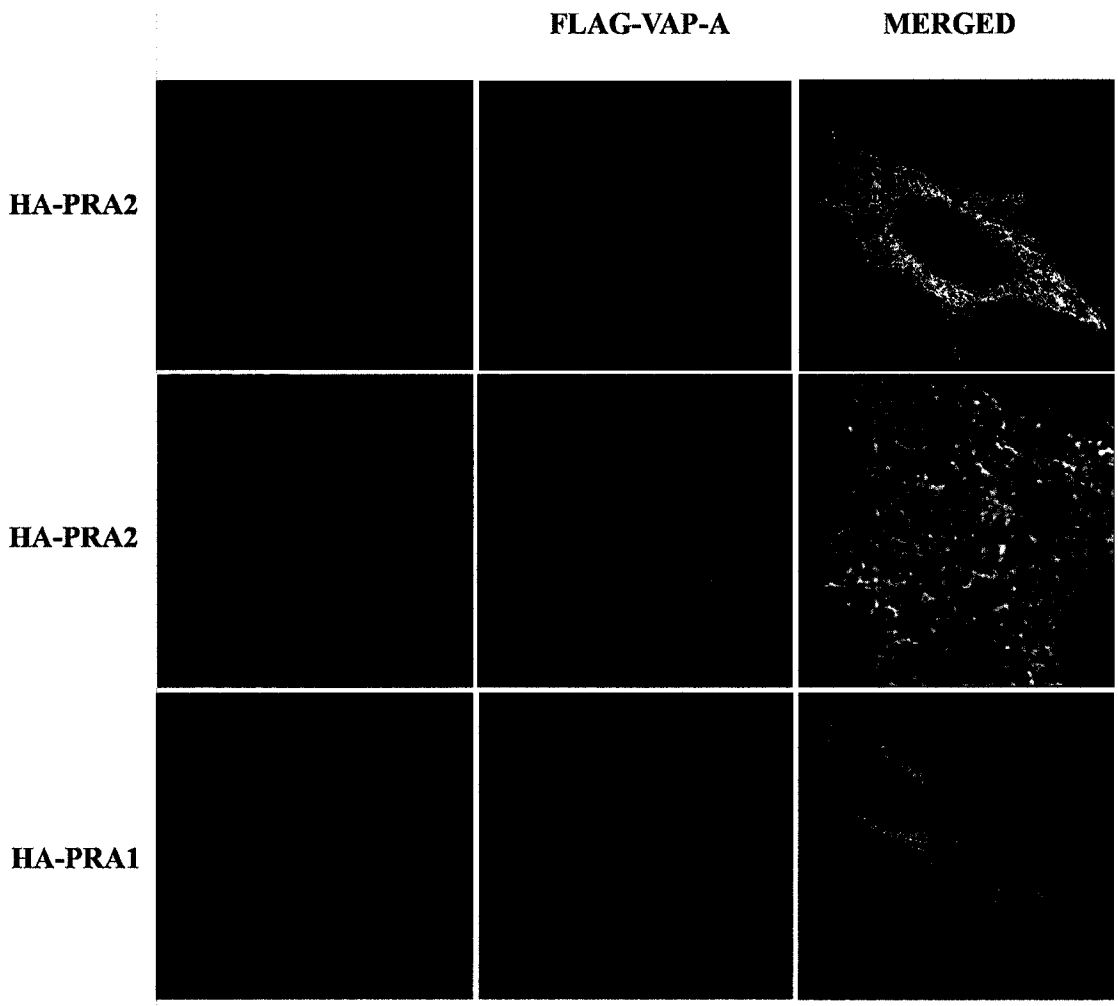

Figure 3.2. Subcellular co-localization of PRA2 with VAP-A. CHO cells were co-transfected with FLAG-VAP-A and HA-PRA2 or HA-PRA1 (as indicated in the left margin). The cells were stained with anti-HA (first column) and anti-FLAG (second column) antibodies, followed by image deconvolution. The experiment was reproduced and the images are representative of what was observed.

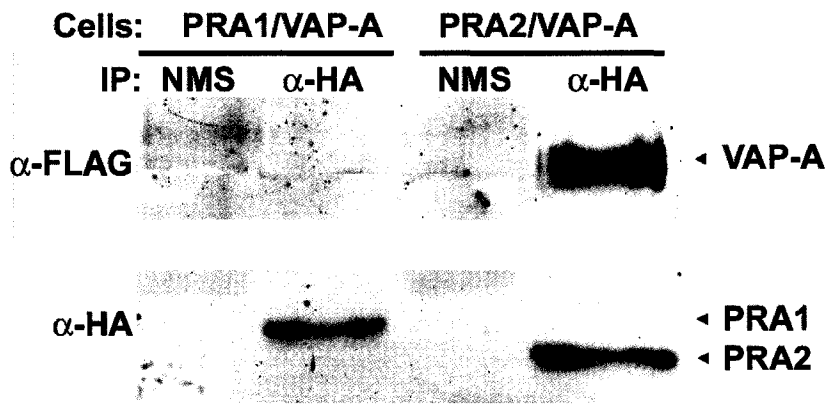

Figure 3.3. Co-immunoprecipitation of VAP-A with PRA2. Extracts of CHO cells co-expressing FLAG-VAP-A and HA-PRA2 or HA-PRA1 were cross-linked with DSP followed by solubilization with Triton X-100 and immunoprecipitation with control normal mouse serum (NMS) or mouse anti-HA antibodies (HA). The immunoprecipitated complex was processed by Western immunoblot with anti-FLAG (top panel) and anti-HA antibodies (lower panel).

Both VAP-A and PRA2 inhibit ER-to-Golgi transport of VSVG

We had previously shown that overexpression of PRA1 inhibited trafficking of the temperature sensitive mutant VSVG^{ts045}-GFP (Gougeon et al., 2002), a marker used to trace anterograde trafficking through the secretory pathway. This led me to hypothesize that overexpression of the ER localized VAP-A or PRA2 might also affect ER-to-Golgi trafficking of VSVG^{ts045}-GFP. Trafficking of the temperature sensitive VSVG^{ts045}-GFP was examined on cells co-transfected with empty pFLAG-CMV2 vector, pFLAG-VAP-A wild type or pIRESpuro/HA-PRA2. The cells were shifted to 42 °C for 6 h to trap VSVG^{ts045}-GFP in the ER. Cycloheximide was added to prevent further synthesis, before the cells were returned to the permissive temperature of 32 °C. Progression of VSVG^{ts045}-GFP through the secretory pathway was monitored by fixing cells at various time-points. VSVG^{ts045}-GFP progressed unhindered in the control samples reaching the Golgi complex in 30 min and plasma membrane in 60 min. However, overexpression of either VAP-A or PRA2 clearly inhibited ER-to-Golgi trafficking of VSVG^{ts045}-GFP with most of the VSVG^{ts045}-GFP remaining in the ER after 60 min (Figure 3.4).

I next examined whether the proteins might alter the folding of VSVG^{ts045}-GFP causing it to be retained in the ER. I repeated the trafficking assay with VSVG^{ts045}-GFP while simultaneously monitoring with the conformation-specific VSVG monoclonal antibody I14, which only recognizes properly folded VSVG (Lefrancois and Lyles, 1982). As shown in Figure 3.5, no VSVG signal was detected with the I14 antibody at the non-permissive temperature as expected. However, properly folded VSVG was detected with the I14 antibody in all transfected cells after a chase period of 30 min at the permissive temperature, indicating that overexpression of VAP-A or PRA2 had no effect on VSVG^{ts045}-GFP folding. It is interesting to note that properly folded VSVG remained in the ER in both VAP-A and PRA2 transfected cells whereas

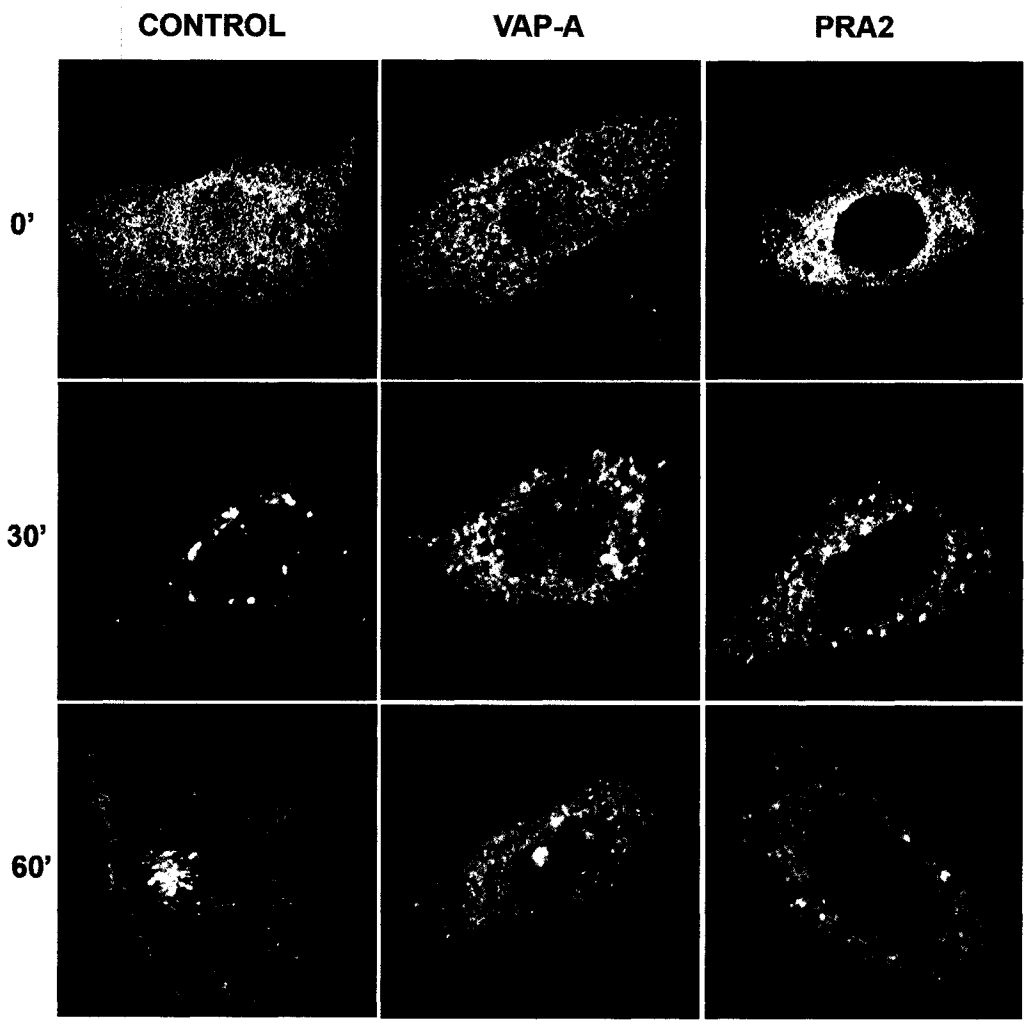

Figure 3.4. Transport of VSVG^{ts045}-GFP in CHO cells co-transfected with VAP-A or PRA2. Representative confocal images of VSVG^{ts045}-GFP in CHO cells co-transfected with control empty pFLAG-CMV2, pFLAG/VAP-A or pIRES/HA-PRA2 (as indicated at the top). Cells were incubated at the non-permissive temperature for 6 h and shifted to the permissive temperature for time intervals indicated in left margin. The experiment was reproduced and the images are representative of what was observed.

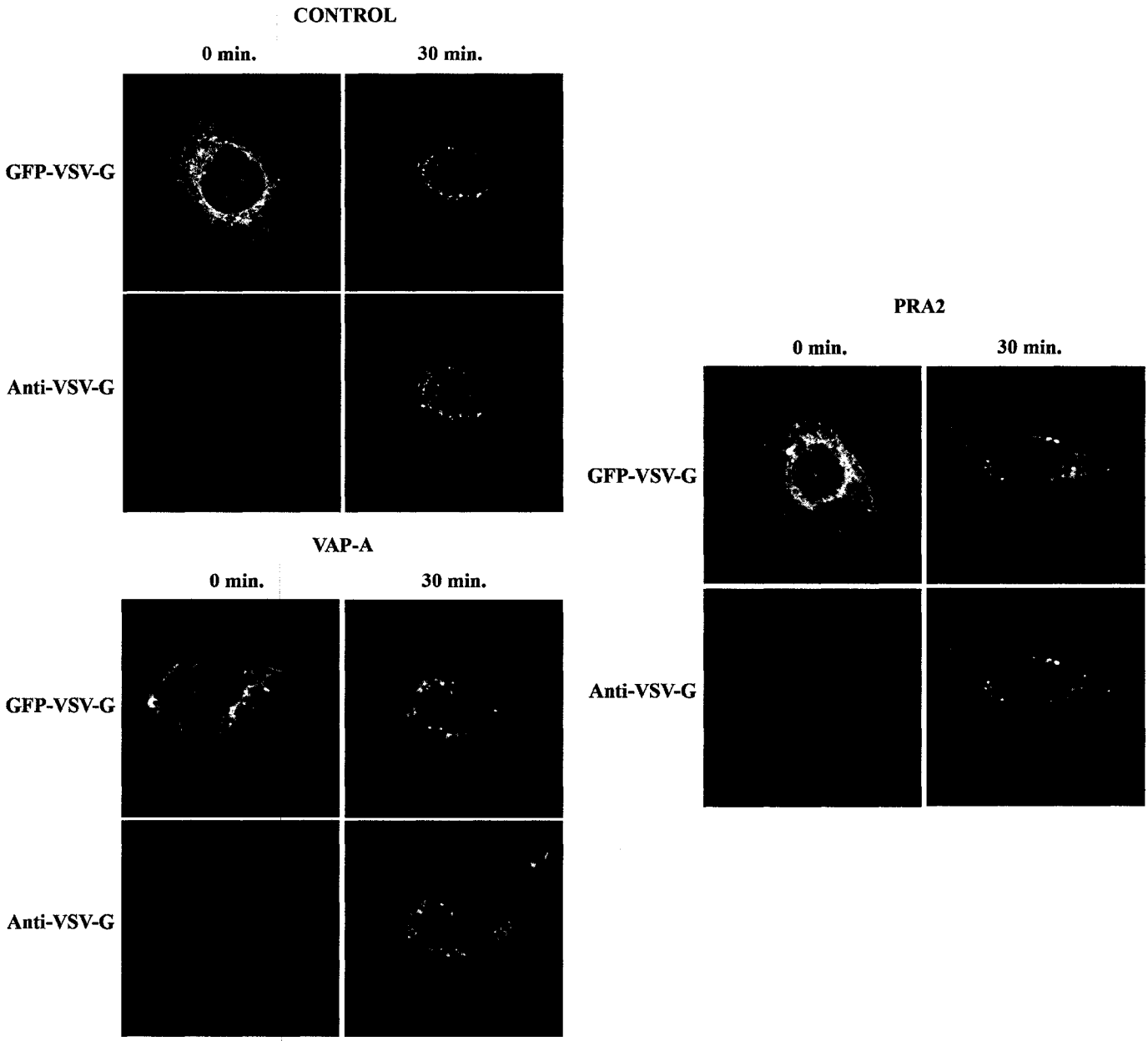

Figure 3.5. VAP-A and PRA2 do not affect VSVG^{ts045}-GFP folding. CHO cells were co-transfected with pCDM8.1/VSVG^{ts045}-GFP and pFLAG/VAP-A or pIRES/HA-PRA2 or the control empty pFLAG-CMV2 (as indicated at the top). After 24 h, the cells were incubated at the non-permissive temperature for 6 h and shifted to the permissive temperature for a time interval indicated at the top. The cells were fixed and stained with I14 to identify properly folded VSVG^{ts045}-GFP (lower panels). The experiment was reproduced and the images are representative of what was observed.

properly folded VSVG has progressed to the Golgi complex in the control sample. Thus, VAP-A and PRA2 can cause ER retention of the properly folded membrane protein cargo.

To determine the extent of ER retention and verify that none of the $VSVG^{ts045}$ had progressed to the Golgi complex, I examined the sensitivity of the glycosylated $VSVG^{ts045}$ to endoglycosidase H (Endo H) digestion. Trimming and modification of high mannose glycosyl chains occur at the Golgi complex and result in resistance to Endo H digestion (Trimble and Maley, 1984). $VSVG^{ts045}$ in extracts from cells co-transfected with empty vector, VAP-A, PRA2 or both, with ER-trapped $VSVG^{ts045}$ released at the permissive temperature for varying lengths of time, were tested for Endo H sensitivity. In control samples, the Endo H resistant VSVG was present 30 min after release at the permissive temperature, whereas no appreciable Endo H resistant VSVG was present throughout the 90 min chase period with either VAP-A or PRA2 expressing cells (Figure 3.6). Co-expression of VAP-A and PRA2 did not rescue the block in $VSVG^{ts045}$ trafficking, which differed from a previous study suggesting that the inhibitory effect of VAP-A on secretion can be alleviated by co-expressing its interacting protein VAMP2 (Foster et al., 2000). The Endo H sensitivity pattern was identical to that of singly transfected VAP-A or PRA2, suggesting the two proteins might act on separate stages of the secretory pathway. $VSVG^{ts045}$ readily exited the ER when the C-terminal transmembrane domain of VAP-A was deleted, indicating that insertion into the ER membrane is essential (Figure 3.6). Interestingly, deletion of the N-terminal major sperm protein-like domain partially rescued $VSVG^{ts045}$ ER-to-Golgi trafficking, implicating a role for this domain in VAP-A-mediated inhibition.

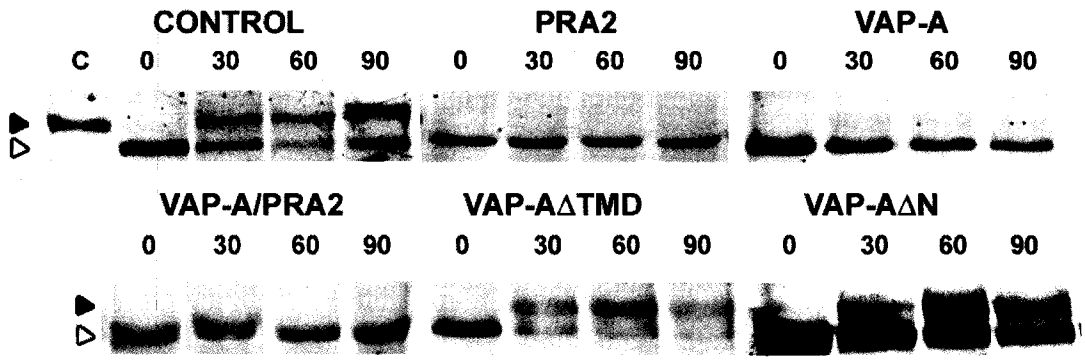

Figure 3.6. Monitoring ER-to-Golgi trafficking of VSVG^{ts045} using endoglycosidase H sensitivity. CHO cells were co-transfected with pCNA3.1+/VSVG^{ts045} and either control empty pFLAG-CMV2, pFLAG/VAP-A and pIRES/HA-PRA2 separately or together, pFLAG/VAP-A ΔTMD or pFLAG/VAP-A ΔN (as indicated above the panels). After 24 h, the cells were incubated at the non-permissive temperature for 6 h and shifted to the permissive temperature for time intervals indicated above the panels. The cells were lysed and membranes were recovered by high-speed spin before the samples were treated with Endoglycosidase H. The samples were processed by Western immunoblot with anti-VSVG antibodies. The lower band indicated by a clear arrow represents pre-Golgi endoH-sensitive VSVG, whereas the upper band indicated by a black arrow consists of endoH-resistant VSVG. The results were reproduced over the span of months.

VAP-A but not PRA2 inhibits lateral diffusion of VSVG

I next examined the possibility that VAP-A and PRA2 inhibit VSVG trafficking by affecting aspects of vesicle budding. I found that although VAP-A and PRA2 are broadly distributed throughout the ER, they did not co-localize with the ER exit site marker Sar1 (Figure 3.7). This suggests that the two proteins are predominantly excluded from ER exit sites and raises the possibility that they might affect the sequestration of membrane proteins to Sar1-containing bud sites. The current view is that membrane proteins diffuse laterally in the ER towards budding sites where they are segregated or concentrated before budding. Therefore, inhibition of $VSVG^{ts045}$ lateral movement in the ER membrane could explain the delay in transport to the Golgi complex. To test this, I used Fluorescent Recovery After Photobleaching (FRAP) to determine if overexpression of VAP-A or PRA2 affected the lateral movement of $VSVG^{ts045}$-GFP in the ER. $VSVG^{ts045}$-GFP was trapped in the ER at 42 °C as described before, and a high intensity laser light was used to photobleach the GFP signal from a small region (Figure 3.8). Recovery of the GFP signal in the photobleached area was measured, and used to determine the diffusion coefficient. The VSVG signal recovered very quickly in control cells with maximum recovery levels within 2 min (Figure 3.9). In contrast, only a marginal recovery of the GFP signal was observed in VAP-A transfected cells, indicating a significant decrease in lateral diffusion of VSVG. Deletion of the N-terminal MSP domain of VAP-A abrogated this inhibitory effect with a lateral diffusion rate comparable to that in control cells. This is consistent with its weak inhibitory effect on ER-to-Golgi transport of VSVG (Figure 3.6), and suggests that along with insertion into the ER membrane, this is an essential feature. Surprisingly, the GFP signal recovered albeit at a slightly lower kinetics in the PRA2 transfected cells despite its overall inhibitory effect on ER-to-Golgi transport (Figure 3.4 and 3.6). Under my experimental

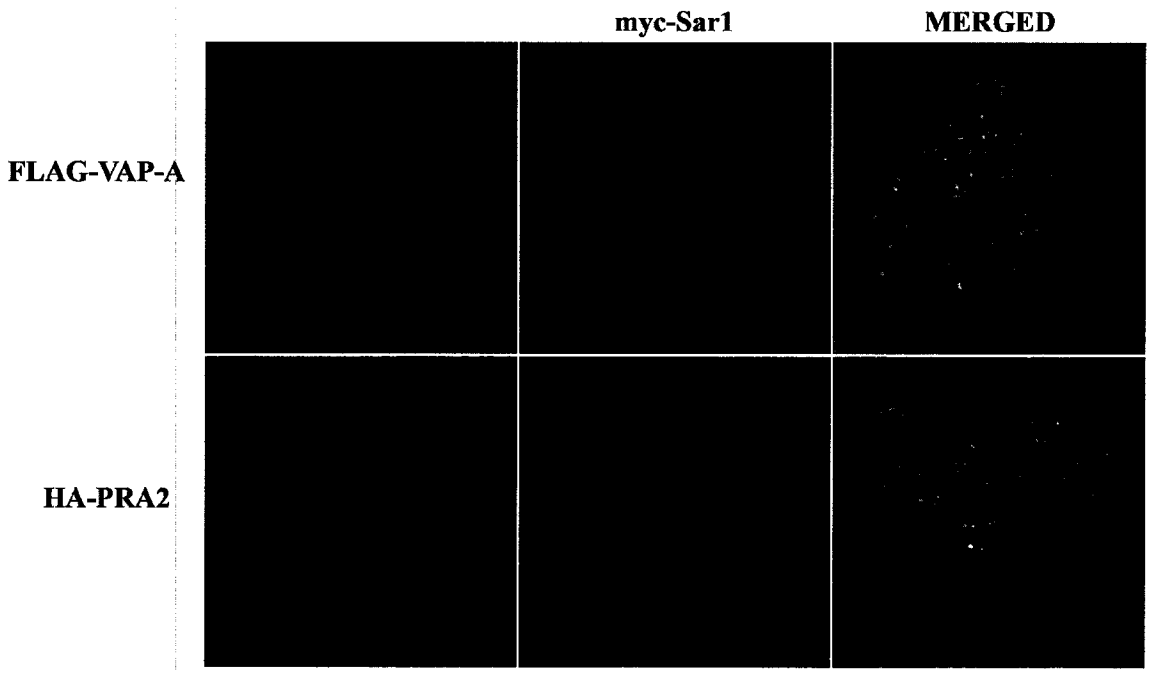

Figure 3.7. Comparing VAP-A and PRA2 localization with Sar1. CHO cells co-expressing myc-Sar1 and HA-PRA2 or FLAG-VAP-A were fixed and stained with anti-myc (Sar1) and anti-FLAG (VAP-A) or anti-HA (PRA2) antibodies, followed by image deconvolution. The experiment was reproduced and the images are representative of what was observed.

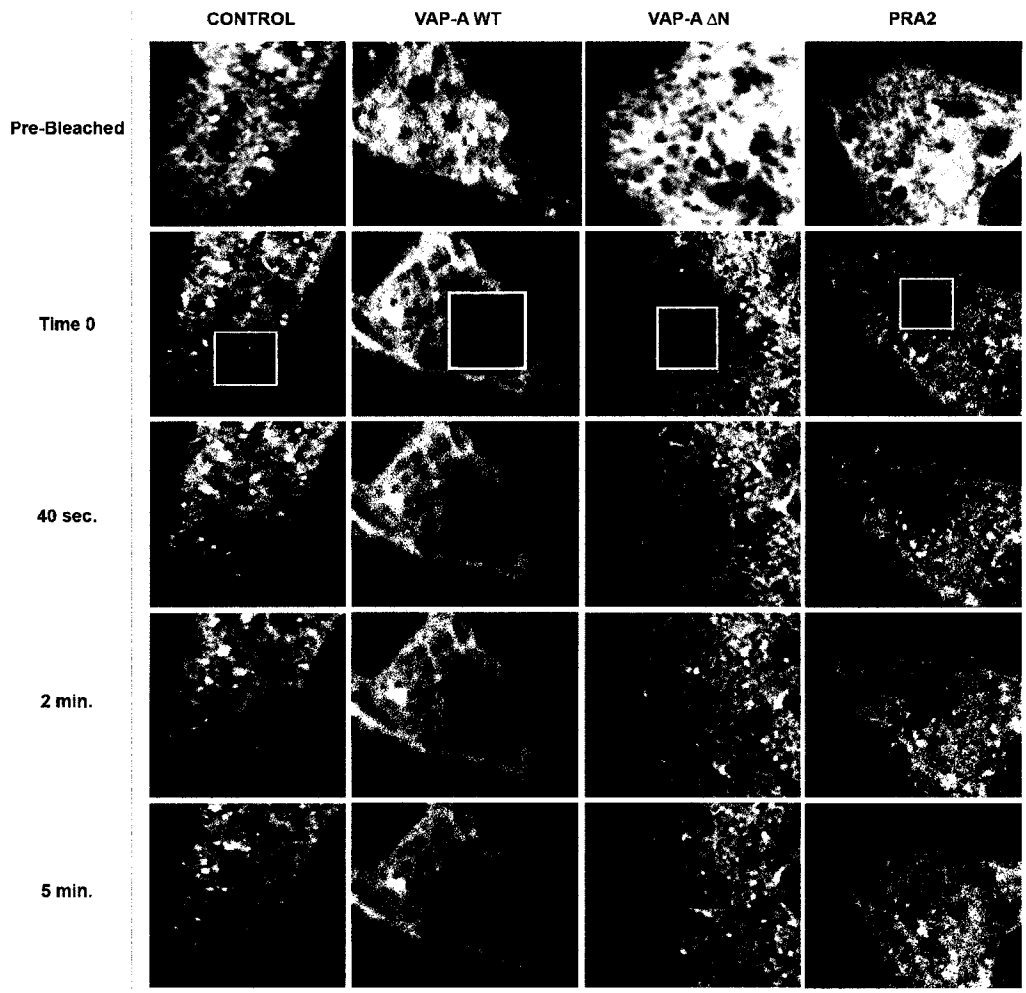

Figure 3.8. Fluorescent Recovery After Photobleaching of VSVG^{ts045}-GFP. CHO cells were transfected with pCDM8.1/VSVG^{ts045}-GFP and empty pFLAG-CMV2, pFLAG/VAP-A WT, pFLAG/VAP-A ΔN or pIRES/HA-PRA2. After 24 h the cells were incubated at the non-permissive temperature for 6 h and shifted to the permissive temperature. A laser was used to bleach a small area and images were collected at twenty seconds intervals. Images of the pre-bleached cells, as well as various time points (indicated in the left margin) are represented with the photobleached area outlined by a box. Results were reproduced a minimum of three times in the span of two months.

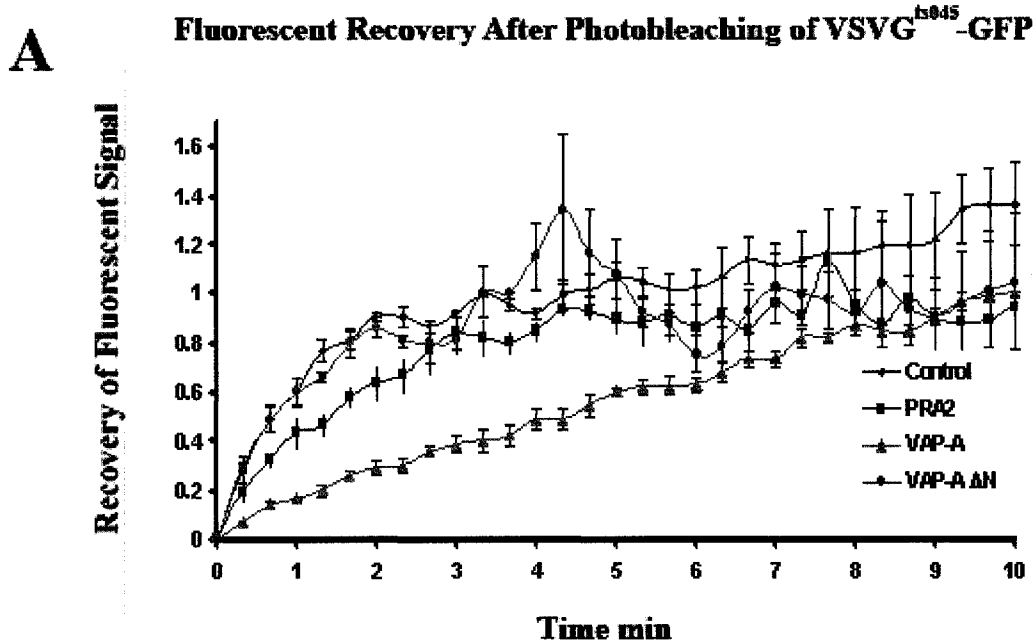

B

	Control	VAP-A WT	VAP-A ΔN	PRA2
VSVG^{ts045}-GFP Diffusion Coefficient 10^{-3} um/sec	4.72 ±0.80	0.56 * ±0.05	2.75 ±0.28	1.39 ±0.09

Figure 3.9. Quantification of Fluorescent Recovery After Photobleaching of VSVG^{ts045}-GFP. (A) The time-dependent recovery of the VSVG^{ts045}-GFP signal in the bleached area represented in Figure 3.8 was measured (and normalized to values of maximum recovery plateau) and plotted against time. (B) These quantified values for signal recovery, along with the size of the bleached area were used to calculate the diffusion coefficient of VSVG^{ts045}-GFP. * Since VAP-A samples never reach a maximum recovery plateau, the final time point was used as maximum recovery. This produces the highest possible diffusion coefficient for VSVG^{ts045}-GFP in these VAP-A expressing cells. Values represent mean and standard error (n=3 with each performed in triplicate). Student T-test indicates the differences in diffusion coefficient are statistically relevant with a 95% confidence interval, except between PRA2 and VAP-A wild type where the confidence interval is higher than 90%.

conditions, the control samples had an average diffusion coefficient of 4.72 x 10^{-2} μm^2/sec while overexpression of PRA2 reduced this three-fold to 1.39 x 10^{-2} μm^2/sec (Figure 3.9). However, overexpression of VAP-A greatly reduced fluorescent signal recovery to such an extent that recovery to pre-bleach level was not reached at the end of the 10 min time-course. Substituting the last time-point for maximal fluorescence recovery yielded a highest possible estimation of $VSVG^{ts045}$-GFP's diffusion coefficient of 0.56 x 10^{-2} μm^2/sec in VAP-A overexpressing cells. Interestingly, deletion of VAP-A's N-terminal MSP domain rescued this inhibition in ER lateral diffusion, yielding a diffusion coefficient of 2.75 x 10^{-2} μm^2/sec (Figure 3.9). Thus, the data indicate that overexpression of VAP-A inhibits the lateral movement of VSVG in the ER membrane, and that this is dependent on the presence of the C-terminal transmembrane and N-terminal MSP domains of VAP-A. Together with the lack of co-localization with Sar1, it raises the possibility that VAP-A inhibits the sequestration of VSVG to designated ER exit sites. PRA2 also caused a reduction in lateral diffusion with a value between that of VAP-A(ΔN) and full length VAP-A. Thus in this case, reduced lateral diffusion is unlikely to be the underlying mechanism for the block in ER-to-Golgi transport.

VAP-A binds polymerized microtubules

One hypothesised function of the MSP domain is its interation with the cytoskeleton based on the close association of VAP-A with microtubules in mouse cultured neurons (Skehel et al., 2000). This raises the possibility that VAP-A inhibits lateral movement of VSVG by creating immobile islands in the ER membrane through its inserted transmembrane domain, while simultaneously anchoring these membrane domains to stable microtubules through its N-terminal MSP domain. Such a condition might account for the reduced lateral diffusion and limit

sequestration of VSVG to the bud sites. To confirm that the mammalian VAP-A is capable of binding polymerized microtubules, I used commercially purified tubulin polymerized in the presence of GTP to pull-down VAP-A from detergent solubilized membranes. The wild type VAP-A associated with polymerized microtubules whereas deletion of the N-terminal MSP domain completely abolished this interaction (Figure 3.10). This indicates that the N-terminal MSP domain is essential for microtubule binding, supporting the view that inhibition of trafficking requires VAP-A's C-terminal domain to be firmly imbedded into the ER membrane with the N-terminal MSP domain anchoring that portion of the membrane to microtubules.

VAP-A and PRA2 inhibit VSVG^{ts045}-Myc budding from the ER

I then attempted to confirm that overexpression of VAP-A, by reducing lateral movement of ER VSVG^{ts045}, inhibited its recruitment to newly forming ER-derived vesicles. I performed an ER budding assay where CHO cells co-transfected with VSVG^{ts045}-Myc and a control empty vector, FLAG-VAP-A or HA-PRA2, were transferred to 42 °C for 6 h to accumulate VSVG^{ts045}-Myc in the ER. The cells were scraped, permeabilized and washed to allow the removal of the cytosol. The collected cells were then reconstituted with rat liver cytosol and an energy regenerating system at a permissive temperature to enable ER budding. In this context, COPII coated vesicles that contain VSVG^{ts045}-Myc destined for trafficking to the Golgi compartment are formed at the ER exit sites. Because of previous cell permeabilization, a portion of these vesicles is released from the cell and can be collected via centrifugation. By quantifying the amount of VSVG^{ts045}-Myc cargo found on these vesicles compared to total cellular VSVG^{ts045}-Myc, the rate of ER exit of VSVG^{ts045}-Myc can be measured. In the control samples an average of 6.4% of total cellular VSVG^{ts045}-Myc was recovered in the budded vesicles, but

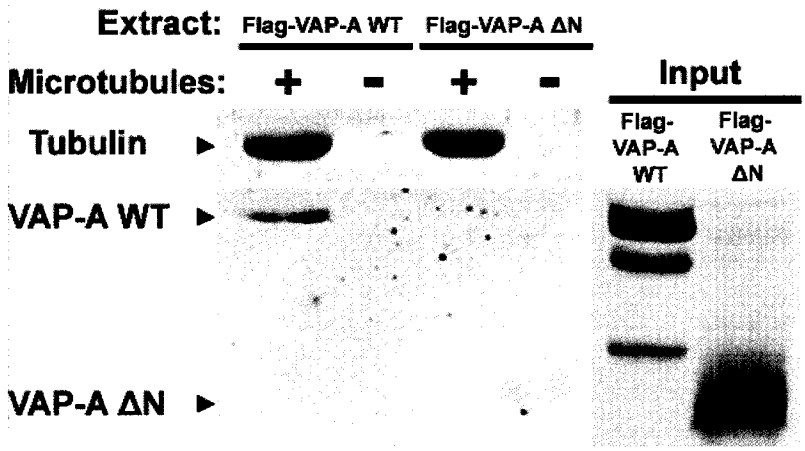

Figure 3.10. Mirotubule binding assay of CHO extracts. CHO cells expressing FLAG-VAP-A WT or FLAG-VAP-A ΔN were lysed and solubilized with 1% Triton X-100 and the extract were incubated with polymerized commercial microtubules. The microtubules were collected via centrifugation and the pellets were processed by Western immunoblot with anti-FLAG (VAP-A) and anti-tubulin antibodies. The experiment was performed in triplicates and results were reproducible.

overexpression of VAP-A reduced this to 0.9%, an 86% reduction relative to the control vector (Figure 3.11). If this reduction is due to VAP-A anchoring to the microtubules and preventing sequestration of VSVG^{ts045}-Myc onto COPII coated vesicles, then depolymerization of microtubules might rescue this inhibition. Microtubules are known to depolymerize under cold treatment. Therefore, the collected cells were kept on ice for 1 h to induce depolymerization of microtubules prior to the budding assay. The control samples showed a slightly lower level of budded VSVG^{ts045}-Myc (4.9%), suggesting that cold treatment also reduced the overall efficacy of the process. The cold treatment partially rescued VAP-A's inhibition resulting in an increase in VSVG^{ts045}-Myc ER budding to 2.3% or 47% of control samples (Figure 3.11). This rescue could be explained by an increase in VSVG^{ts045}-Myc lateral movement, resulting in improved access to COPII coated budding vesicles. Rescue was not complete probably because a 1 h ice treatment may not be sufficient to completely depolymerize microtubules, in addition to the likely partial repolymerization that occurs during the budding assay step performed at 32 °C. Therefore, smaller remaining microtubular fragments, though not part of a complete cellular network, could still be sufficient to provide anchor points for VAP-A. In addition, the specificity of cold treatment remains an issue, since it could affect multiple other cellular functions. To obtain a more thorough and specific depolymerization of microtubules, I added nocodazole after 5 h at 42 °C and kept it throughout the remainder of the assay, which aside from this was performed normally (Luduena and Roach, 1991). Under these conditions, the control levels of budded VSVG^{ts045}-Myc were reduced to 2.5%, however this treatment rescued VAP-A's inhibition and restored ER budding of VSVG^{ts045}-Myc to near control levels of 2.2% or 89% of control samples (Figure 3.11). This confirmed the role of microtubules in VAP-A's inhibition of VSVG trafficking, as well as the importance of

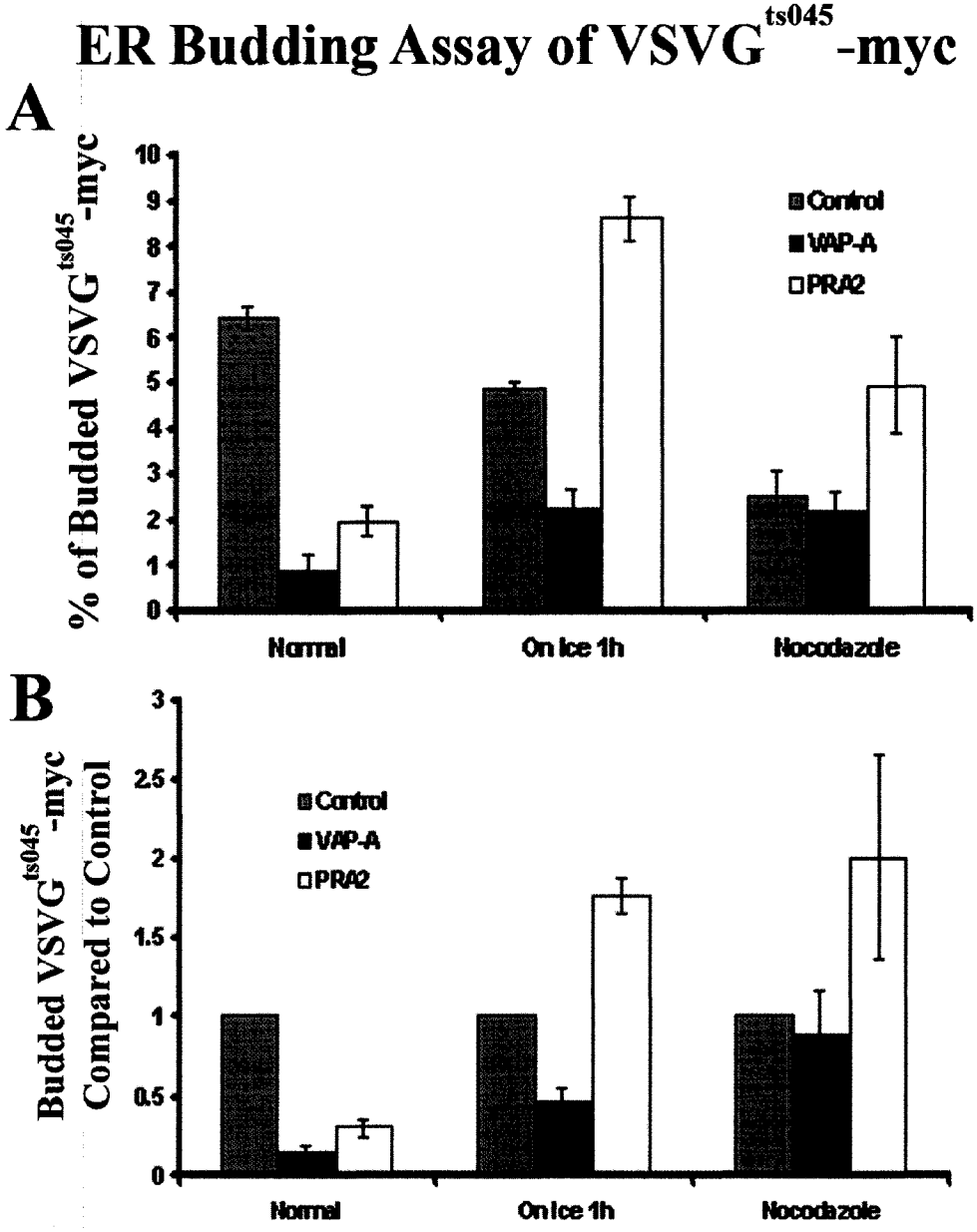

Figure 3.11. ER budding assay of VSVG^{ts045}-myc. CHO cells were co-transfected with VSVG^{ts045}-Myc and empty pFLAG-CMV2, FLAG-VAP-A WT or HA-PRA2 constructs. After 24 h, the cells were incubated at the non-permissive temperature for 6 h and then scraped, permeabilized and washed. The collected cells were resuspended in a reconstituted cytosol at permissive temperature to initiate ER budding. The budded vesicles were isolated via centrifugation and processed by Western immunoblot with

anti-myc antibodies. To depolimerize microtubules, two different techniques were utilized separately, cooling the cells on ice and adding nocodazole. A) Percentage of total cellular VSVGts045-myc measured on ER-derived vesicles, while B) represents these results compared to the untransfected control of each experimental condition. Values represent mean and standard error (n=3 with each performed in triplicate). Student T-test indicates the differences are statistically relevant with a 95% (A) and 90% (B) confidence interval, except between VAP-A and PRA2 under control conditions, as well as between control and VAP-A in the presence of nocodazole.

microtubules in the process of vesicle budding from the ER. Interestingly, PRA2 also blocked budding of $VSVG^{ts045}$-Myc to 2.0% or 31% of control samples and performing the experiment on ice not only rescue the PRA2 inhibition but resulted in an increase to 8.6% ER budding of $VSVG^{ts045}$-Myc or 176% of control samples (Figure 3.11). Similar results of 4.9% ER budding of $VSVG^{ts045}$-Myc or 200% of control samples, were obtained with nocodazole treatment, suggesting that PRA2's effect on ER budding is more complicated than previously thought.

Chapter 4

DISCUSSION

PART 1:Characterization of PRA and its interaction with Rab and VAMP2

PRA2, a novel member of the prenylated Rab acceptor family

Proteins involved in vesicle transport tend to be conserved throughout evolution, often with specific members of each protein family mediating similar functions at each step of the secretory pathway. We have previously isolated a second PRA isoform from a rat brain cDNA library based on sequence similarity to a conserved domain in PRA1 (Abdul-Ghani et al., 2001). As a basis for understanding their function, in chapter 2 I set out to characterize the structural properties of PRAs and their interaction with multiple binding proteins. Although the overall sequence similarity between the two proteins is relatively small, we concluded that they both belong to the same family based on their overall structural similarity, membrane-association properties and ability to bind Rab. In fact, I found that PRA2, like PRA1, was able to bind Rab1A and Rab3A in an *in vitro* binding assay. The binding properties were very similar in that both proteins can bind Rab1A and Rab3A in GDP-, GTP-, and guanine nucleotide-free states (Fig.2.1). This is comparable to the cytosolic protein Mss4, one of the rare proteins that can bind to the transient guanine nucleotide-free state of Rab (Nuoffer et al., 1997). Their interactions differ, however, with respect to the prenylation state of Rab. Binding of Rab to PRA1 and PRA2 is highly dependent on prenylation as deletion of the double cysteine-motif completely abrogated protein-protein interaction in the yeast two-hybrid system (Abdul-Ghani et al., 2001; Martincic et al., 1997). In contrast, Mss4 can interact with the lipid-

unmodified form of Rab (Miyazaki et al., 1994). These facts establish the shared characteristics of PRA family members: overall structure, membrane association properties and ability to bind the prenylated form of Rab regardless of the guanine nucleotide present.

Domains involved in the PRA-Rab interaction

The interaction between two proteins requires that both molecules be folded in a certain manner usually dictated by their primary sequence. In this case, we have two members of the PRA family, which can interact with multiple members of the Rab family. Domains involved in the PRA-Rab interaction must therefore be conserved in each isoform. Identifying these conserved domains is an important step in understanding the molecular characteristics of the interaction. The perceived membrane topology of PRAs supports the hypothesis by which the transmembrane domains bind through a hydrophobic interaction with the isoprene moiety of Rab (Figure 4.1). Since PRA binding is limited to the Rab subfamily and does not bind other isoprenylated small GTPases (Martincic et al., 1997), other Rab domains are most likely involved in the interaction. As mentioned earlier, because PRAs seem to interact with all Rabs, we would expect the Rab domain involved to be conserved, as is the case of the isoprene moiety. The major conserved domain in the Ras superfamily is the guanine nucleotide-binding pocket (Stenmark and Olkkonen, 2001). For the Rab subfamily, aside from the prenylation site motif, the other conserved regions are all localized in and around the two switch domains, whose three-dimensional structure varies depending on which guanine nucleotide is present (Schlichting et al., 1990). Thus, by interacting with a specific folded state of the

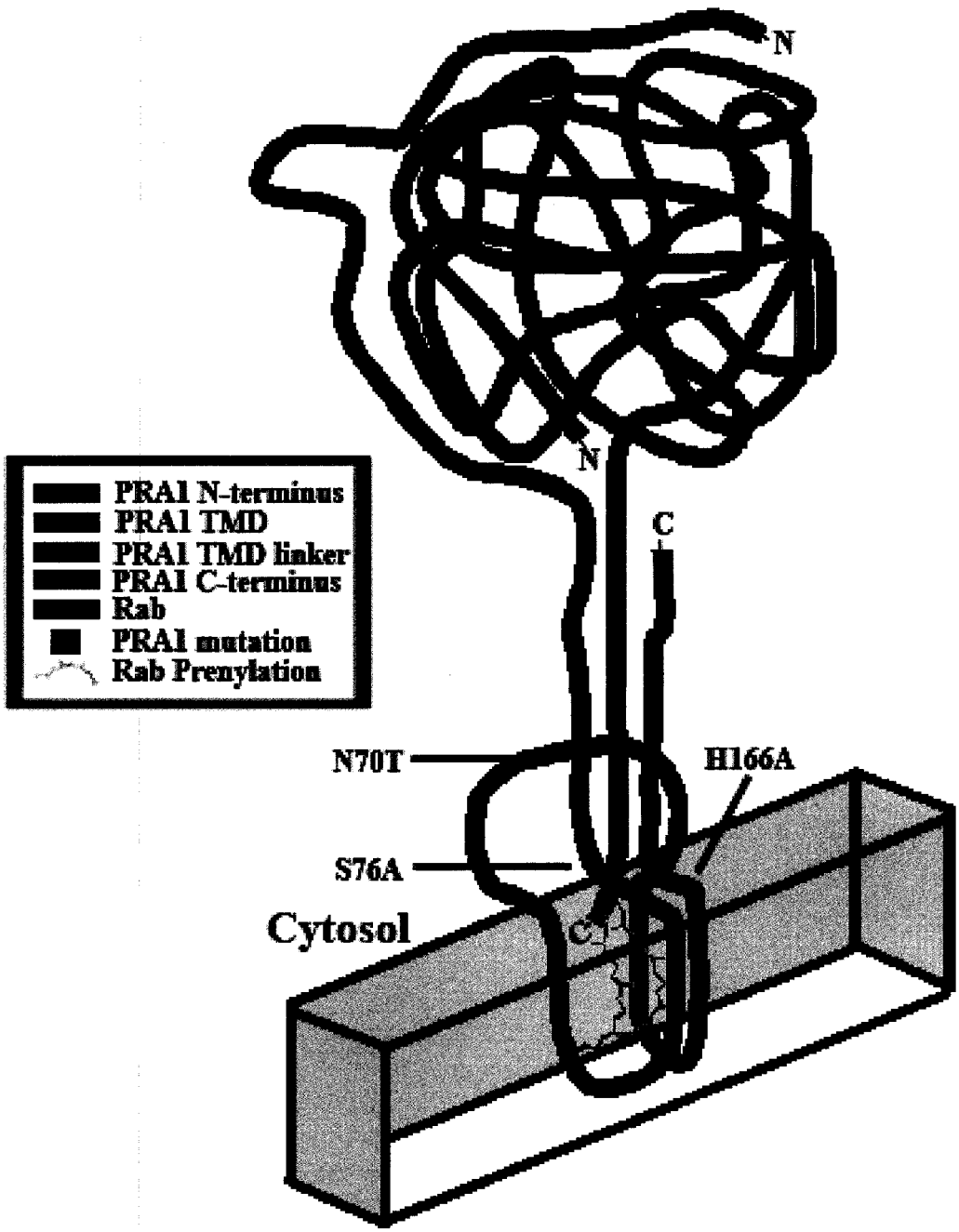

Figure 4.1. Model illustration of the PRA1 interaction with Rab. Representation of the possible orientation of PRA1 and Rab, interacting in the context of a membrane compartment. The various PRA1 domains, as well as the mutated residues are colour-coded to facilitate domain recognition.

switch domains, multiple Rab effectors can bind specifically to active GTP-bound Rabs or inactive GDP-bound Rabs (Stenmark and Olkkonen, 2001). Although PRAs could possibly interact with the GTP and GDP-bound conformations of Rab's switch domains, the fact that PRAs bind Rabs regardless of their guanine nucleotide-bound state suggests that other domain(s) might be involved. One such alternative is the C-terminal hypervariable domain of Rabs, which extends the globular shaped Rab away from the membrane (Rak et al., 2003; Rak et al., 2004). This domain has attracted a lot of interest because it is the most divergent region of Rab isoforms. This has led to the hypothesis that this domain is involved in the subcellular localization of each isoform (Chavrier et al., 1990). The hypervariable domain is of varying length, is primarily unstructured and at first appears ill-suited to provide specificity to the PRA-Rab interaction (Neu et al., 1997; Ostermeier and Brunger, 1999). However, this domain is involved in Rab's interaction with GDI, another multiple Rab isoform binding protein (Rak et al., 2003). As with PRAs, GDI's interaction with Rab requires prenyl groups, one of which inserts into a grove within GDI, while the second sits on the surface of the protein (Pylypenko et al., 2006). This interaction also involves the base of Rab's switch domains (Pylypenko et al., 2006; Rak et al., 2003), which could explain why Rab's interaction with GDI, unlike with PRAs, is specific to the GDP-bound state. The last domain involved in the interaction is the hypervariable domain that extends down the side of GDI (Pylypenko et al., 2006). Although the lack of structure and sequence homology in this region would initially suggest otherwise, two key conserved hydrophobic residues seem to be critical in the association with GDI. The same two conserved hydrophobic residues were also shown to be important in Rab's interaction with the Rab escort protein (REP), a protein which

interacts with Rab in a similar manner to GDI (Rak et al., 2004). We can see how PRAs could compete with GDI for the GDP-bound Rab as previous results have suggested, by interacting with Rab in a similar fashion to GDI (Hutt et al., 2000). As demonstrated in Figure 4.1, the extreme C-terminal prenyl modifications of Rab could interact with the hydrophobic transmembrane domains of PRA1, while the C-terminal hypervariable domain of Rab could interact with a cytosolic domain of PRA. And finally, the C- and or N-termini of PRA could interact with conserved residues located at the base of the switch domains. The next step was therefore to identify the PRA residues involved in the PRA-Rab interaction.

Mutagenic analysis of PRA1

Since the Rab binding property is not only conserved between the PRA isoforms, but also with the single yeast orthologue Yip3p, which can also interact with yeast Rab orthologues and is believed to share PRA's function, we can expect residues involved in the interaction to be conserved. When comparing PRA1 to its yeast counterpart, there are indeed two fairly well conserved regions (Figure 2.2), which are located immediately before the first transmembrane domain and after the last transmembrane domain. When viewed in the context of the predicted PRA1 topology, the conserved residues of both domains are located on the cytoplasmic side of the membrane and could be involved in the interaction with Rab's isoprene moiety or regulate PRA's possible association with the hydrophobic residues located within the hypervariable domain of Rab. I performed an alanine scanning mutagenesis of these conserved domains in order to identify the residues involved in Rab binding. Also, PRA1 was previously shown to interact with VAMP2

(Martincic et al., 1997), a protein which like Rab contains a hydrophobic region (in this case a transmembrane domain), and does not form a trimeric complex but competes with Rab for PRA1 binding (Hutt et al., 2000). Consequently, it is logical to also study the effect of mutating these conserved residues on VAMP2 binding, since both proteins might share the same binding site. In order to test their Rab3A and VAMP2 binding properties, these mutants were first inserted as baits in the yeast two-hybrid system along with Rab3A or VAMP2 as preys. Mutants that contained a single mutation and demonstrated a strong change in Rab and/or VAMP2 binding intensities, were confirmed by *in vitro* binding assays. I identified three types of PRA1 mutants. The class A is represented by the N70T mutant, which exhibited a strongly reduced binding to both Rab3A and VAMP2, while the class B, represented by the S76A mutant, caused an increase in Rab3A and VAMP2 binding. Finally the class C, represented by the H166A mutant, caused a more moderate reduction in binding to both proteins (Fig.2.4). It seems the effect induced on Rab3A binding by these PRA1 mutations is mirrored by their effect on VAMP2 binding. It suggests that these residues are important for PRA1 binding to both proteins and supports the hypothesis where both proteins share the same binding site on PRA1.

Although one could hypothesize the N70T, H166A and S76A mutations might bring about complete denaturation of the protein, the results obtained in experiments performed by Mr. Prosser suggest otherwise (Gougeon et al., 2002). In the case of the Class B mutant, in addition to increasing PRA1's affinity for Rab3A and VAMP2, which would not necessarily be expected from a denatured protein, the S76A mutant retains

both its subcellular localization to the Golgi compartment and ability to delay the trafficking of the temperature sensitive $VSVG^{ts045}$-GFP (a marker for the secretory pathway). However, in the case of the Class A and C mutants, there is a change in the subcellular distribution of the N70T and H166A mutants, which parallels the reduction in Rab3A and VAMP2 binding affinity. In fact, the level of ER localization of these mutants appears proportional to the loss of Rab3A and VAMP2 binding. Furthermore, although denatured membrane proteins often remain localized to the ER before being targeted for degradation (Bonifacino et al., 1989; Lin et al., 2001), these mutants retained an ability to delay trafficking of $VSVG^{ts045}$-GFP at the step where they are localized. This suggests that the mutants might not be completely denatured since they retain some of their functional properties and the integrity of the binding site is required for proper localization of PRA1. Therefore, the PRA1 residues N70, S76 and H166 seem to be involved in a binding site that both Rab and VAMP2 share, as well as to be involved in targeting PRA1 to the correct compartment.

PRAs possess a conserved binding site shared by multiple proteins

The results I have obtained suggest that the same binding site might be used for VAMP2 and Rab, and could explain their inability to form a trimeric complex. Interestingly, the residues I identified to be important in PRA1 binding to Rab and VAMP2, are well conserved in PRA2 and support the idea of a conserved Rab binding site on PRAs. I suspect that mutations of these residues on PRA2 would result in similar modifications of Rab binding properties. One noticeable difference in PRA2 is that, unlike PRA1, which can bind specifically to VAMP2, it appears unable to interact with

VAMP1, VAMP2, or VAMP3 (cellubrevin) (Abdul-Ghani et al., 2001; Martincic et al., 1997). This suggests that the binding site, containing the aforementioned conserved residues, is not sufficient for VAMP2 binding. This requires additional residues that are likely located in the cytosolic C- and/or N-terminal of PRA1, which are absent in PRA2. These results do not exclude the possibility that other PRA1 domains may also be required for Rab3A binding. This would imply, however, that there is similar conserved region in PRA2 as well, something that I was unable to clearly identify. Thus, even though PRA2 shares PRA1's structural characteristics and that multiple proteins with similar hydrophobic properties can interact with both PRA isoforms, the fact that PRA1 interacts with only one member of the VAMP family and that PRA2 interacts with none of them, suggests a more specific interaction than a simple hydrophobic interaction. This suggests that PRA2 possesses its own function, most likely at a different trafficking step, and is not simply an orthologue of PRA1. Identifying the proteins that interact with PRA1 and PRA2, and which ones share this same binding site will help shed some light into the details of the interaction and provide clues as to the possible function of PRAs.

Boiling of PRA2 causes aggregation of the protein

During purification of recombinant PRA2, I identified an additional property specific to this isoform. In fact, boiling the protein greatly decreased the immunoblot signal (Fig.2.5). Increasing the concentration of non-ionic detergent appeared to exacerbate the situation in the boiled sample, but had no effect on the sample incubated at room temperature. The PRA2 from transfected mammalian cell-extracts was also found to be sensitive to boiling, suggesting the property was not due to another protein present

in the extract and suggests it is not an artefact of bacterial expression. I cannot rule out however the possibility that other molecules may contribute to this aggregation. This might also explain why transfection of HA-PRA2 into CHO cells previously showed a strong ER staining pattern as seen using indirect immunofluorescence, while extracts boiled prior to SDS-PAGE showed little, if any, HA-PRA2 signal on Western immunoblot. In fact, no detectable amount of PRA2 was observed in the form of a dimer or higher oligomer, suggesting that heat denaturation causes large SDS-insoluble aggregates to form, leading to the loss of signal due to an inability to migrate into the SDS-PAGE gel. Interestingly, I found this characteristic to be specific to PRA2, even though both PRA isoforms share a similar overall structure. The two isoforms also migrated differently on SDS-PAGE. For instance, although PRA1 is three residues shorter than PRA2, the latter can be found to migrate significantly faster. Because both isoforms possess a similar structure, they would most likely become folded in a comparable manner *in vivo*. It is, however, understandable how a variation in SDS binding and protein denaturation could result in conformational differences that lead to different migration speeds. This hypothesis is supported by the PRA2-specific boiling-induced denaturation that prevents Western detection of PRA2, and is most likely due to protein aggregation. This property demonstrates an additional difference between the PRA isoforms, with as of yet unclear functional repercussions, but which will help increase PRA2 purification yields.

PART 2: PRA2 and VAP-A regulate ER-to-Golgi trafficking using different mechanisms

Screening for PRA1-interacting proteins

The second chapter revealed valuable information on the structure of PRAs and molecular details regarding their interaction with multiple proteins. With this information in hand, the objective of the third chapter was to clarify the functional role of PRAs in trafficking. The ability of PRA1 to bind VAMP2 and Rab (Martincic et al., 1997), two proteins involved in vesicle trafficking, and regulate the cycling of Rab by competing with GDI (Hutt et al., 2000; Sivars et al., 2003), suggests that PRAs have a role in vesicle trafficking. When trying to clarify the function of a protein, much can be gained from identifying its interacting partners. Using the yeast two-hybrid system with PRA1 as bait, I screened a human brain cDNA library for putative interacting proteins. A yeast two-hybrid screen, especially with a hydrophobic protein like PRA1, can produce false positives. The screen yielded a number of interesting proteins listed in Table II. Out of the 25 positives identified, 44% were proteins with at least one strong hydrophobic domain. Because the screen was not dominated by hydrophobic proteins, I expect most of them to be true PRA1-interacting proteins, and not false-positives that bind via a non-specific hydrophobic interaction. VAMP Associated Protein of 33 KDa A (VAP-A) was an intriguing positive due to its ability to interact with VAMPs as well as its structural similarity to the SNARE protein (Nishimura et al., 1999; Skehel et al., 1995). VAP-A was also believed to be involved in trafficking (Foster et al., 2000; Skehel et al., 1995; Soussan et al., 1999; Weir et al., 2001; Wyles et al., 2002). Since switching the PRA1 bait for PRA2, with VAP-A as prey, demonstrated that both PRA isoforms appear to be

able to bind VAP-A. Therefore, I decided to pursue the functional characterization of VAP-A.

PRAs interact in vitro with VAP-A

The next step was to confirm that PRAs could truly interact with VAP-A via an independent method. *In vitro* binding assays confirmed that both PRA isoforms could bind VAP-A and deletion constructs allowed me to identify which of VAP-A's major domain were involved in the interaction with PRAs (Fig.3.1). Deletion of VAP-A's coiled-coil or major sperm protein (MSP) domains did not prevent the construct from interacting with both PRA isoforms, but deletion of the C-terminal transmembrane domain completely eliminated VAP-A's PRA-binding ability. This property conforms to the hypothesis discussed previously regarding hydrophobic PRA-interacting proteins, where VAP-A's hydrophobic transmembrane domain could associate with PRA's hydrophobic domains. The fact that VAP-A can interact with both PRA isoforms suggests again that the PRA conserved regions are involved in this interaction and that VAP-A might utilize the same binding domain on PRA shared by Rab and VAMP2, although I cannot exclude the possibility that VAP-A might interact with multiple proteins, such as PRA, simply via hydrophobic interaction. Whatever the properties of this interaction, an obvious question remained: does this interaction actually happen *in vivo*?

PRA2 interacts in vivo with VAP-A

In order for two proteins to interact *in vivo*, they have to at least be localized to the same compartment. As previously mentioned, PRA1 and PRA2 are localized to distinct subcellular membrane compartments. The former is mostly localized to the Golgi apparatus and beyond, while the latter is localized to the ER compartment. VAP-A has been previously shown to localize predominantly to ER structures (Skehel et al., 2000), except for rare instances such as in *Drosophila* neuronal cells, where it can be found at the plasma membrane (Pennetta et al., 2002). Indirect immunofluorescence on transfected CHO cells demonstrated that VAP-A co-localized extensively with PRA2 at the ER, whereas minimal co-localization could be observed with PRA1, whose distribution was not significantly affected by VAP-A (Fig.3.2). I then performed a co-immunoprecipitation assay using transfected cell lysates to determine whether VAP-A could form a stable complex with PRA2, and confirm that the two proteins interact *in vivo*. Similar to what has been shown for the other interactions with PRA, I found the PRA2-VAP-A interaction to be detergent sensitive (Martincic et al., 1997; Sivars et al., 2003). To circumvent this, I cross-linked the transfected CHO extracts before detergent-solubilization, a step required in order to co-immunoprecipitate membrane proteins. As expected, VAP-A co-immunoprecipitated with PRA2, but not PRA1, demonstrating that VAP-A only interacts with PRA2 in the cell (Fig.3.3). Therefore, even though VAP-A can interact with both PRA isoforms *in vitro*, it could only interact with the one found in the same compartment *in vivo*. However, this does not exclude the possibility that PRA1 interacts with VAP-A in cells, such as *Drosophila* neurons, where VAP-A is transported further down the secretory pathway. I believe there must be an unidentified cellular signal

in certain cell types that allows VAP-A to move out of the ER and to the plasma membrane. In such a case, localization to the plasma membrane could allow VAP-A to be involved in events such as secretion or insulin-induced GLUT4 translocation, events which VAP-A has been shown to affect (Foster et al., 2000). However, in cells such as L6 myotubes and 3T3-L1 adipocytes where VAP-A localization to the plasma membrane has not been properly confirmed, I can not exclude the possibility that ER-localized VAP-A could hinder the trafficking of proteins involved in events at the plasma membrane such as VAMP2, thereby affecting the insulin-induced translocation of GLUT4 to the plasma membrane. Although I have demonstrated the *in vivo* interaction between PRA2 and VAP-A, two proteins believed to be involved in trafficking, this still does not clarify their function and the purpose of this interaction.

PRA1 affects VSVG^{ts045}-GFP trafficking from the Golgi complex

To understand the function of PRA2, I took advantage of the information we previously obtained on PRA1. Derek Prosser, a Ph.D. student our lab, has found that overexpression of PRA1 delayed the trafficking of the temperature sensitive VSVG^{ts045}-GFP construct, a marker for trafficking in the secretory pathway (Gougeon et al., 2002). In fact, overexpression of PRA1 delayed VSVG^{ts045}-GFP exit from the Golgi complex, the subcellular compartment where PRA1 is predominantly localized. In addition, overexpressing PRA1 S76A, which localizes to the Golgi complex and demonstrated increased binding to Rab3A and VAMP2, accentuated the delay of VSVG^{ts045}-GFP exit from the Golgi complex and produced a condensed Golgi complex morphology. Because PRA1 is known to interact with multiple Rab GTPases, it is likely that Golgi-localized

Rab GTPases, which in yeast are required for formation of transport vesicles out of the Golgi apparatus (Benli et al., 1996), are affected. I hypothesize that the increased binding of Rab and VAMP2 by PRA1 S76A might affect recruitment of VAMP2 to forming vesicles and either recycling of Rab or functional interaction with Rab effector molecules that ultimately leads to decreased transport out of the Golgi apparatus and amplification of the phenotype observed with wild type PRA1. This idea is supported by the fact that the condensed Golgi complex morphology observed when PRA1 S76A is expressed, is similar to that observed in cells expressing dominant negative dynamin 2, which blocks vesicle formation from the trans-Golgi network (Cao et al., 2000). It was clear from these previously obtained results that PRA1 regulates the trafficking of VSVG^{ts045}-GFP at the Golgi compartment.

PRA2 and VAP-A affect ER-to-Golgi trafficking

Due to many similarities between PRA1 and PRA2, I decided to examine if PRA1's ability to delay VSVG^{ts045}-GFP's exit from the Golgi complex was shared by PRA2, even though in this case the delay would most likely occur at the ER due to PRA2's localization to this compartment. I performed a similar time-course experiment as the one performed by Mr. Prosser and showed that overexpression of PRA2 strongly impedes the ER-to-Golgi trafficking of VSVG^{ts045}-GFP. Even after one hour, the majority of VSVG^{ts045}-GFP remained in the ER (Fig.3.4). Interestingly, similar results were obtained when VAP-A was overexpressed, suggesting that both proteins are involved in ER-to-Golgi trafficking (Fig.3.4). However, in both cases inhibition was not complete, since at steady state VSVG^{ts045}-GFP does traffic to the plasma membrane. This data

supports previously published results that overexpression of VAP-A affects the trafficking of multiple proteins and lipids, including VSVG (Foster et al., 2000; Soussan et al., 1999; Wyles et al., 2002). However, it contradicts the recently published results by Amarilio *et al.* (Feb. 2005), which showed that overexpression of VAP-B did not inhibit the ER-to-Golgi trafficking of $VSVG^{ts045}$-GFP. This is somewhat unexpected due to the similarity between the two isoforms, but may support the idea that although the isoforms are similar, they are not redundant and possess distinct functional properties. It would be interesting to evaluate which of the previously described effects of VAP-A are shared by VAP-B, such as GLUT4 translocation to the plasma membrane (Foster et al., 2000), secretion (Skehel et al., 1995), PRA binding, etc. I then confirmed the delay in ER-to-Golgi trafficking of $VSVG^{ts045}$ using a biochemical technique. The endoglycosidase H (endo H) sensitivity showed that overexpression of VAP-A or PRA2 engendered a delay in the trimming of $VSVG^{ts045}$ core *N*-linked carbohydrates, a post-translational modification added to the nascent protein in the ER (Fig.3.6). This trimming occurs at the Golgi compartment and confers resistance to endo H treatment, thus demonstrating $VSVG^{ts045}$ has reached the Golgi complex. This result confirmed that overexpression of PRA2 or VAP-A impedes the normal progress of $VSVG^{ts045}$ from the ER to the Golgi apparatus.

PRA2 and VAP-A do not affect proper folding of $VSVG^{ts045}$-GFP

Delay in proper folding of $VSVG^{ts045}$-GFP is a factor that could account for inhibition of ER exit observed upon overexpression of VAP-A or PRA2. To determine if PRA2 or VAP-A affected the folding of $VSVG^{ts045}$-GFP, I repeated the fluorescent time-

course and additionally stained the cells with an antibody specific to the properly folded state of $VSVG^{ts045}$. These results demonstrated that $VSVG^{ts045}$ is properly folded and that delay in ER exit in the cells overexpressing PRA2 or VAP-A was likely due to an inhibition in trafficking (Fig.3.5).

Co-expression of PRA2 and VAP-A does not rescue the $VSVG^{ts045}$ trafficking delay

In certain cases, the co-expression of two interacting inhibitory proteins can relieve the repression by essentially chelating each other. This has previously been demonstrated to be the case with VAP-A and VAMP2. Overexpression of VAP-A attenuated the insulin-dependent incorporation of GLUT4 into the plasma membrane, and the normal response was restored by co-expression of VAMP2 (Foster et al., 2000). Therefore, I performed the endo H assay from cells co-expressing VAP-A and PRA2, but found no rescue of $VSVG^{ts045}$ trafficking (Fig.3.6). This led me to hypothesize that the PRA2-VAP-A interaction might not prevent one or both proteins from having their effect on $VSVG^{ts045}$ trafficking, or that both proteins affect distinct transport steps.

The C- and N-termini of VAP-A are required for the $VSVG^{ts045}$ trafficking delay

I then overexpressed the VAP-A truncation mutants (previously used in the *in vitro* binding assay study) in the endo H assay to identify the domains involved in this inhibition. I found that deleting VAP-A's C-terminal transmembrane domain restored $VSVG^{ts045}$ transport to the Golgi compartment (Fig.3.6). This was expected because without its transmembrane domain, VAP-A is no longer anchored in the ER membrane and thus alters the interaction with its usual partners localized to this compartment.

Interestingly, deletion of the MSP domain-containing N-terminus also restored ER-to-Golgi trafficking of $VSVG^{ts045}$, suggesting that this domain, which is not required for PRA binding, is involved in VAP-A's delay of $VSVG^{ts045}$ trafficking (Fig.3.6). Although the MSP has been shown in nematodes to behave as a cytoskeleton protein involved in motility (Italiano et al., 1996), the VAP-A MSP domain is hypothesized to function in binding to microtubules (Pennetta et al., 2002). Even though these results demonstrated a role for PRA2 and VAP-A in ER-to-Golgi trafficking, they did not clarify the actual steps affected by these proteins.

VAP-A and PRA2 do not significantly localize to ER exit sites

One possible step regulated by these two proteins is vesicle formation and budding from the specialized ER exit sites. These sites are specialized subdomains of the ER enriched with the molecules involved in the formation and budding of COPII coated vesicles involved in anterograde ER-to-Golgi trafficking, as well as protein cargoes destined for trafficking out of the ER. However, through indirect immunofluorescence, I found limited co-localization between Sar1, a small Ras-like GTPase involved in formation of COPII vesicles at the ER, and either VAP-A or PRA2 (Fig.3.7). Although it is possible the small amount found at the ER budding sites could be the source of the trafficking inhibition, these results suggest an alternative site of action for PRA2 and VAP-A. It is possible that these two proteins segregate molecules involved in ER budding away from the ER exit sites, thereby affecting vesicle formation and/or budding. Examples of such affected molecules could be SNARE or Rab proteins that are known to function in the targeting and fusion of the resulting ER-derived vesicles. Their

recruitment to forming vesicles might be required for budding, in order to ensure the release of fusion-competent vesicles.

VAP-A, but not PRA2, affects the ER lateral movement of VSVG^{ts045}-GFP

Another possible explanation of the block in ER-to-Golgi transport is inhibition of VSVG^{ts045} lateral movement in the ER membrane. This would prevent it from reaching the ER exit sites and incorporate into COPII coated vesicles. To test this hypothesis, I performed a FRAP assay of VSVG^{ts045}-GFP in cells overexpressing PRA2 and VAP-A. VSVG^{ts045}-GFP ER lateral movement was slightly reduced in cells co-transfected with PRA2 with a total recovery period similar to control, suggesting a minimal role, if any, for PRA2 in this process (Fig.3.8 and 3.9). However, overexpression of VAP-A impeded the ER lateral movement of VSVG^{ts045}-GFP by at least 10-fold, because the fluorescent signal had not completely recovered even after 10 min (Fig.3.8 and 3.9). This indicates that VAP-A, by hindering VSVG^{ts045}-GFP ER lateral movement, would delay recruitment to ER exit sites and therefore overall rate of trafficking to the Golgi complex and beyond. Since I had found that deletion of VAP-A's N-terminus, which contains the MSP domain, rescued VSVG^{ts045} trafficking to the Golgi compartment, it was therefore logical to assume the N-terminus might be involved in this inhibition of ER lateral movement. Performing the FRAP assay on cells overexpressing the VAP-A deletion construct resulted in a strong rescue of VSVG^{ts045}-GFP ER lateral movement to levels similar to those associated with PRA2 overexpression (Fig.3.8 and 3.9). The diffusion coefficient obtained in control samples is roughly 10-fold lower than the one previously obtained by Nehls *et al.* (2000). The variation in cell line (CHO instead of COS-7) might underlie part

of the discrepancy. Since an increase in VAP-A expression can affect ER lateral movement of VSVG, then cell lines that differ in the level of expression of VAP-A or other proteins with similar effects could alter its ER membrane diffusion speed. In addition, as opposed to the 32 and 40 °C used by the other group, I performed the assay at 30 °C because the reduction in recovery speed I observed between 32 and 30 °C allowed me to perform the assay more consistently. Also, the assay Nehls *et al.* performed at 32 °C contained brefeldin A (BFA), which prevents ER exit and affects the ER compartment since the majority of the Golgi apparatus is dispersed and traffics back to the ER, thereby possibly affecting VSVG movement in the ER membrane. Although there is some inconsistency in VSVG diffusion in the ER membrane, this assay clearly demonstrates the effect overexpression of PRA2, VAP-A wild type or ΔN has on the ER lateral movement of VSVG. It is therefore clear that even though both PRA2 and VAP-A affect the ER-to-Golgi trafficking of $VSVG^{ts045}$-GFP, they achieve this through different mechanisms. Unlike PRA2, VAP-A seems to delay $VSVG^{ts045}$-GFP recruitment to nascent vesicles at the ER exit sites by hindering its lateral movement in the ER membrane. Also, VAP-A's N-terminus seems to be involved in this inhibition. The MSP domain contained in the N-terminus of VAP-A has been hypothesized to interact with the cytoskeleton. If such is the case, VAP-A could anchor subdomains of the ER to microtubules localized along the ER membrane through its MSP domain, thus creating static membrane domains that could, by means of specific interaction or simple physical obstruction, hinder the ER lateral movement of $VSVG^{ts045}$-GFP.

VAP-A interacts with microtubules

The mouse and *Drosophila* VAP-A orthologues have been previously shown to co-localize and interact *in vitro* with microtubules (Pennetta et al., 2002; Skehel et al., 2000). The only discordant information has been from Amarilio *et al.*'s publication, which has found that VAP-B did not seem to localize to microtubules (Amarilio et al., 2005). The microtubule association of VAP-A has been well documented and co-localization is supported by precise techniques such as electron microscopy, which suggests that the difference might be isoform specific. However, more work has to be done on VAP-B to clarify this divergence. Therefore, to test the hypothesis mentioned above, I had to confirm the ability of VAP-A to bind microtubules and examine the role of the MSP domain in this interaction. To achieve this, I performed an *in vitro* pulldown assay using commercially purified polymerized microtubules and extracts of cells transfected with VAP-A wild type or the N-terminal deletion construct. As was the case for the mouse and *Drosophila* VAP-A, the wild type protein sedimented with polymerized microtubules, but deletion of the N-terminus abrogated binding to microtubules, supporting the implication of this domain in microtubule binding (Fig.3.10). Difficulties in expression prevented me from testing if the N-terminus alone was sufficient for microtubules binding. Nevertheless, these results confirm VAP-A's previously observed microtubule-binding ability, and support the importance of the MSP domain in this interaction. It also concurs with the hypothesis previously mentioned and illustrated in Figure 4.2.1, where the ER membrane protein VAP-A anchors and stabilizes subdomains of the ER by interacting through its cytosolic N-terminus with microtubules. These properties then create, possibly with the help of homo or heterodimerization and

other interacting proteins, static ER membrane domains that hinder the ER lateral movement of VSVG through direct interactions or simply by acting as physical barriers. However, the process affected by PRA2, which results in the delay in VSVG^{ts045} trafficking, still remained unclear.

Microtubule depolymerization rescues VAP-A's delay in VSVG^{ts045} exit from the ER

Since PRA2 did not seem to greatly affect the ER lateral movement of VSVG^{ts045}-GFP or the initial folding of the protein, I turned my attention to an event located downstream in the normal trafficking of VSVG. Largely based on a technique developed by Dr. J.C. Hay (Univ. of Michigan) (Xu and Hay, 2004), I devised an experiment that allowed me to collect ER budded vesicles and thus calculate the percentage of myc-tagged VSVG^{ts045} that trafficked out of the ER onto these vesicles. This experiment allowed for a more precise analysis of a specific ER-to-Golgi trafficking step. First, overexpression of VAP-A was tested using that assay, and as expected due to the previous results, it produced a strong reduction in the amount of myc-VSVG^{ts045} on ER-derived vesicles compared to the control cells (Fig.3.11). This confirms that overexpression of VAP-A impedes VSVG recruitment to vesicles budding from the ER. Then, I performed part of the assay by chilling the cells on ice during collection and up to the actual budding portion of the assay. This treatment partly rescued the reduction in myc-VSVG^{ts045} budding caused by VAP-A overexpression (Fig.3.11). One consequence of cooling cells is depolymerization of microtubules (Mitchison and Kirschner, 1984), which following the model I have proposed would remove the anchor point for VAP-A, thereby allowing the ER lateral movement of myc-VSVG^{ts045} and its subsequent

incorporation into budding vesicles. However, depolymerization would not necessarily be complete with simple chilling because the budding portion of the assay is performed at 32 °C where repolymerization of microtubules could occur. This could explain why only partial recovery was seen with the ice treatment. This is in addition to the fact that microtubule depolymerization by chilling is not specific and a multitude of other cellular changes could contribute to increasing myc-VSVG^{ts045} budding from the ER. To target more directly microtubules and demonstrate their role in VAP-A inhibition of myc-VSVG^{ts045} trafficking, I added the drug nocodazole, which specifically induces microtubule depolymerization (Luduena and Roach, 1991). Addition of nocodazole rescued the reduction in myc-VSVG^{ts045} budding resulting from VAP-A overexpression, returning it to levels comparable to control cells (Fig.3.11). The reduction in control myc-VSVG^{ts045} budding observed under chilling or nocodazole treatment most likely relates to the yet undefined role microtubules play in vesicle budding. However, the fact that ER budding still occurs under microtubule depolymerization conditions demonstrates that even though microtubules facilitate budding, they are not an essential component. That is why it is important to compare myc-VSVG^{ts045} budding levels to the control cells that have undergone the same treatment. Nevertheless, the rescue of myc-VSVG^{ts045} trafficking, in the context of this specific microtubule depolymerization agent, strongly supports the model I have put forth in Figure 4.2.1.

Microtubule depolymerization rescues PRA2-dependant trafficking affect and increases VSVG^{ts045} exit from the ER

I then performed the assay using PRA2 overexpressing cells, to see if myc-VSVG^{ts045} budding would be diminished. Overexpression of PRA2 decreased myc-VSVG^{ts045} budding to a level similar to the one previously obtained from VAP-A overexpressing cells (Fig.3.11). Unexpectedly, depolymerization by chilling did not only rescue myc-VSVG^{ts045} budding in cells overexpressing PRA2, but increased it compared to control cells. This was confirmed by the addition of the more specific nocodazole, which resulted in an approximate doubling of myc-VSVG^{ts045} budding (Fig.3.11). Two conclusions can be extracted from these results. Overexpression of PRA2 causes an increase in myc-VSVG^{ts045} budding from the ER. However, overexpression of PRA2, through a mechanism that involves microtubules, either acts upstream of the first effect by preventing myc-VSVG^{ts045} budding or downstream by anchoring budded vesicles to microtubules and preventing their collection in the budding assay.

CONCLUSION

How does VAP-A affect VSVG^{ts045} trafficking?

The results I have obtained clarify the role of VAP-A in VSVG^{ts045} trafficking. I demonstrated that overexpression of VAP-A hinders the ER lateral movement of VSVG^{ts045}, thereby delaying its recruitment to COPII coated vesicles budding from the ER and consequently impeding its trafficking to the Golgi compartment. The N-terminus of VAP-A, which contains a MSP domain, is required for both this inhibition and association with polymerized microtubules. The MSP in nematode sperm is involved in signalling by activating the MAP kinase pathway thus promoting oocyte maturation and

sheath contraction (Kosinski et al., 2005; Miller et al., 2001). It is also involved in sperm motility, by what seems to be a push-pull mechanism based on the self-assembly mechanics of MSP (Stewart et al., 1994). The MSP protein, however, is only found in nematodes, whereas the MSP-like domain containing VAP-A is present in fungi, plants and animals. It is therefore possible that the self-assembling cytoskeleton properties of MSP were acquired through evolution of the microtubule binding ability of the ancestral VAP-A. It would also be interesting to know if the VAP-A MSP domain possesses a MAP kinase activating property or any other signalling characteristics. The fact that depolymerization of microtubules in cells overexpressing VAP-A rescues $VSVG^{ts045}$ delay in trafficking supports the idea of a causal relationship between VAP-A microtubule binding and $VSVG^{ts045}$ trafficking inhibition. VAP-A, by anchoring the ER membrane to microtubules, could create static subdomains that hinder the lateral diffusion of $VSVG^{ts045}$ and delay its recruitment to ER budding vesicles (Fig.4.2.1). It is likely that VAP-A would also affect the ER lateral movement of other membrane proteins, the identification of which could help us understand the scope of proteins affected and the implications of this property. The majority of $VSVG^{ts045}$ is located in the lumen of the ER (Hunt et al., 1978) whereas the opposite is true for VAP-A, implying that the hydrophobic domains are important. This suggests four possibilities as to the mechanism used by VAP-A to hinder $VSVG^{ts045}$'s lateral movement (Figure 4.2.1). Firstly, VAP-A could interact specifically with $VSVG^{ts045}$, which I was not able to assess due to the inability of my antibody to immunoprecipitate VAP-A. Under this assumption, only proteins capable of directly interacting with VAP-A would be affected. PRA1 has been shown to traffic from the ER to the Golgi complex and can interact *in vitro* with

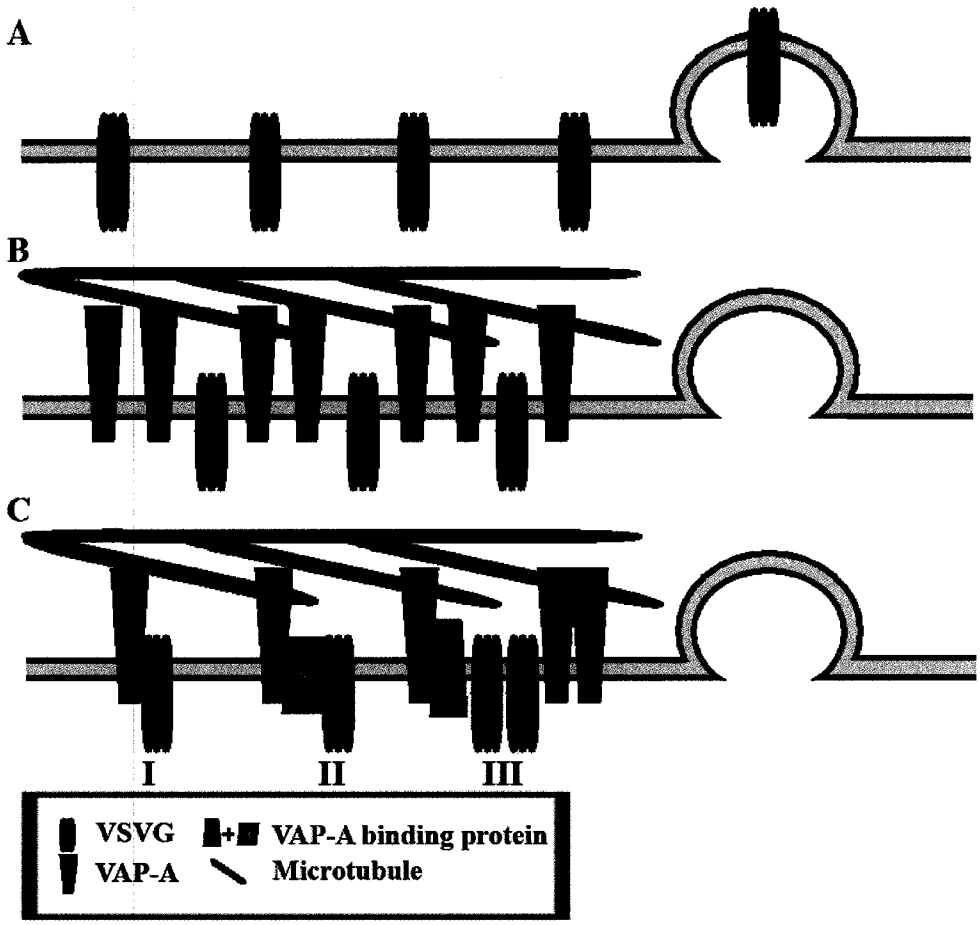

Figure 4.2.1. Model illustration of VAP-A's effect on VSVG^{ts045} trafficking. (A) Under normal conditions, VSVG moves laterally in the ER membrane to reach the ERES and is recruited onto budding vesicles. (B) Overexpressed VAP-A anchors ER subdomains to microtubules and prevents ER lateral movement of VSVG towards the ERES, and thus inhibits VSVG trafficking out of the ER. (C) Possible alternative modes of inhibition of VSVG ER lateral movement by VAP-A. *I.* VAP-A directly interacts specifically or non-specifically (hydrophobic interaction), with VSVG. *II.* VAP-A, as part of a complex, indirectly interacts with VSVG through a VAP-A and VSVG-binding protein. *III.* VAP-A, by itself or as part of a complex, inhibits lateral movement of VSVG by acting as a physical barrier.

VAP-A, thus under this hypothesis it would most likely be a target of VAP-A. When overexpressed with VAP-A, PRA1 properly localized to the Golgi compartment, suggesting that not all membrane proteins are inhibited by VAP-A. However, it is also possible that in this steady-state case, PRA1 has enough time to overcome the delay and exit the ER to reach the Golgi apparatus. It would be useful to examine in greater detail the effect of VAP-A overexpression on PRA1 and other known VAP-A-interacting proteins such as PRA2, VAMPs, syntaxin 1A, rbet1 and rsec22, to determine the range of VAP-A-interacting proteins affected by this inhibition of ER lateral movement. All of these proteins are involved in various vesicle trafficking steps, therefore delaying their exit from the ER would not only reduce the rate of ER-to-Golgi trafficking, but would also affect most trafficking steps. This could explain how overexpression of VAP-A attenuates the insulin-dependent translocation of GLUT4 to the plasma membrane. Secondly, the VAP-A-VSVG^{ts045} interaction could simply be due to non-specific hydrophobic interaction, in which case I would expect a great number of membrane proteins to be similarly affected. Under these two possibilities, PRA2 could simply be a ligand of VAP-A thereby explaining the *in vivo* interaction. Therefore, it would be interesting to see if overexpression of VAP-A affects the ER lateral movement of PRA2. Thirdly, VAP-A could be part of a static ER membrane protein complex, where another member binds directly VSVG^{ts045} and confers the specificity required. In this context, only a select number of proteins would be affected in their ER-to-Golgi trafficking, but this would provide greater flexibility than the first model. Fourthly, VAP-A could, through oligomerization or as part of a static protein complex, hinder the lateral movement of VSVG^{ts045} by acting as a physical barrier. In this case I would expect all

membrane proteins in the ER to be affected. Identifying which proteins have reduced ER lateral movement when VAP-A is overexpressed would greatly help to clarify which mechanism is used by VAP-A to hamper the ER lateral movement of $VSVG^{ts045}$.

Additional PRA-interacting proteins

The yeast two-hybrid screen I performed using PRA1 as bait produced an extensive number of positives. The most interesting positive was VAP-A due to its previously described interaction with VAMPs and possible function in trafficking. However, in the future it might be interesting to pursue some of the other positives. It is important to confirm *in vivo* the interaction between any of these positives and PRA1 or PRA2, because the yeast two-hybrid system is non-physiological. Bait and prey proteins may interact in this context even though they are never found in the same subcellular compartment of a mammalian cellular physiological environment. Also, membrane proteins such as PRA1 are not expressed in their normal membrane environment, which could result in false positives. However, the known properties of some of these proteins suggest it might be interesting to pursue the implication of these positives further. Firstly, ARL-6 interacting protein 1 is a membrane protein that interacts with Arf-like 6 (Ingley et al., 1999), a member along with Rabs of the Ras-like family of small GTPases (Ingley et al., 1999). Aside from its similarity to members of the Arf family, such as Arf1 which is involved in vesicle formation and trafficking at the Golgi compartment (Chavrier and Goud, 1999; Moss and Vaughan, 1998), little is known of the possible function of ARL-6 and even its subcellular localization is unclear. ARL-6 itself has been previously found by yeast two-hybrid to interact with PRA2 (Ingley et al., 1999), thereby suggesting a

possible implication of PRAs in the yet to be clarified function of the small GTPase ARL-6. Secondly, the yeast two-hybrid screen found sorting nexin 2 (SNX2) to be a PRA1 specific interacting protein. SNX2 and a second isoform SNX1, both contain a phospholipid-binding Phox homology domain (PX) are believed to be involved in protein trafficking and seem to be primarily localized to the endosome (Kurten et al., 2001; Nakamura et al., 2001; Teasdale et al., 2001; Zhong et al., 2002). Although the exact function of SNX2 has not been elucidated, its involvement in trafficking and protein sorting as well as its endosomal localization suggest an interaction with PRA1 might be relevant. Thirdly, Reticulon 1 is part of the Reticulon family believed to regulate the shape of the reticular ER (Voeltz et al., 2006). Elevated expression of this protein induced an increase in ER tubular shape. This function might come into play along with VAP-A to regulate the make-up and structure of the ER. Finally, the farnesyl diphosphate synthase seems to be able to interact with PRA1 and PRA2. This enzyme is involved in the synthesis of two molecules relevant in the hypotheses discussed in this thesis. Farnesyl diphosphate synthase regulates the synthesis of cholesterol as well as the prenyl moieties added to small Ras-like GTPases (reviewed by Goldstein and Brown, 1990). The implications of regulating both Ras-like small GTPase function through its prenylation and cholesterol synthesis by PRA1 and PRA2 would provide for additional regulation of vesicle/protein trafficking and ER membrane fluidity as discussed in this thesis. The known functions and properties of these putative PRA-interacting proteins suggest an implication along with PRA2 and VAP-A in vesicle/protein trafficking and the regulation of ER membrane fluidity.

Why does VAP-A affect VSVG^{ts045} trafficking?

The question remains as to how a cell would have a need to inhibit the ER lateral movement of VSVG^{ts045}? My hypothesis is that VAP-A acts as a sensor of ER membrane fluidity. In this model (Figure 4.2.2), the ER accumulation of overexpressed VSVG^{ts045} would be sensed by VAP-A using one of the methods mentioned earlier, which would then trigger two possible responses. First, after being retained in this static ER subdomain, the protein could be targeted for degradation, since membrane proteins that remain in the ER are usually translocated back to the cytosol and degraded (Bonifacino et al., 1989; Cheng et al., 1990). Second, VAP-A could respond to an increase in membrane protein density by triggering an increase of ER membranes. In fact, the mammalian VAP-A, as well as its yeast orthologue, has been shown to interact with a number of proteins involved in membrane and cholesterol regulation and transport (Table III). Interestingly, these cytosolic proteins share a VAP-A-binding motif termed FFAT, which interacts with the N-terminal MSP domain (Loewen et al., 2003). An increase in membrane protein density would be sensed by VAP-A, which in turn could recruit the FFAT motif containing protein to initiate an increase in membrane volume and fluidity to restore normal ER membrane conditions. These FFAT proteins might even compete with microtubules for the VAP-A MSP domain, thereby reducing the stable nature of this ER subdomain and facilitating phospholipid addition. It would be interesting to see if the addition of a FFAT motif-containing protein or simply a peptide, could rescue VAP-A's effect on VSVG^{ts045} ER lateral movement and trafficking. An increase in membrane protein load in the ER could also cause VAP-A to signal the activation of the Unfolded Protein Response (UPR). A number of biochemical and physiologic stimuli, such as

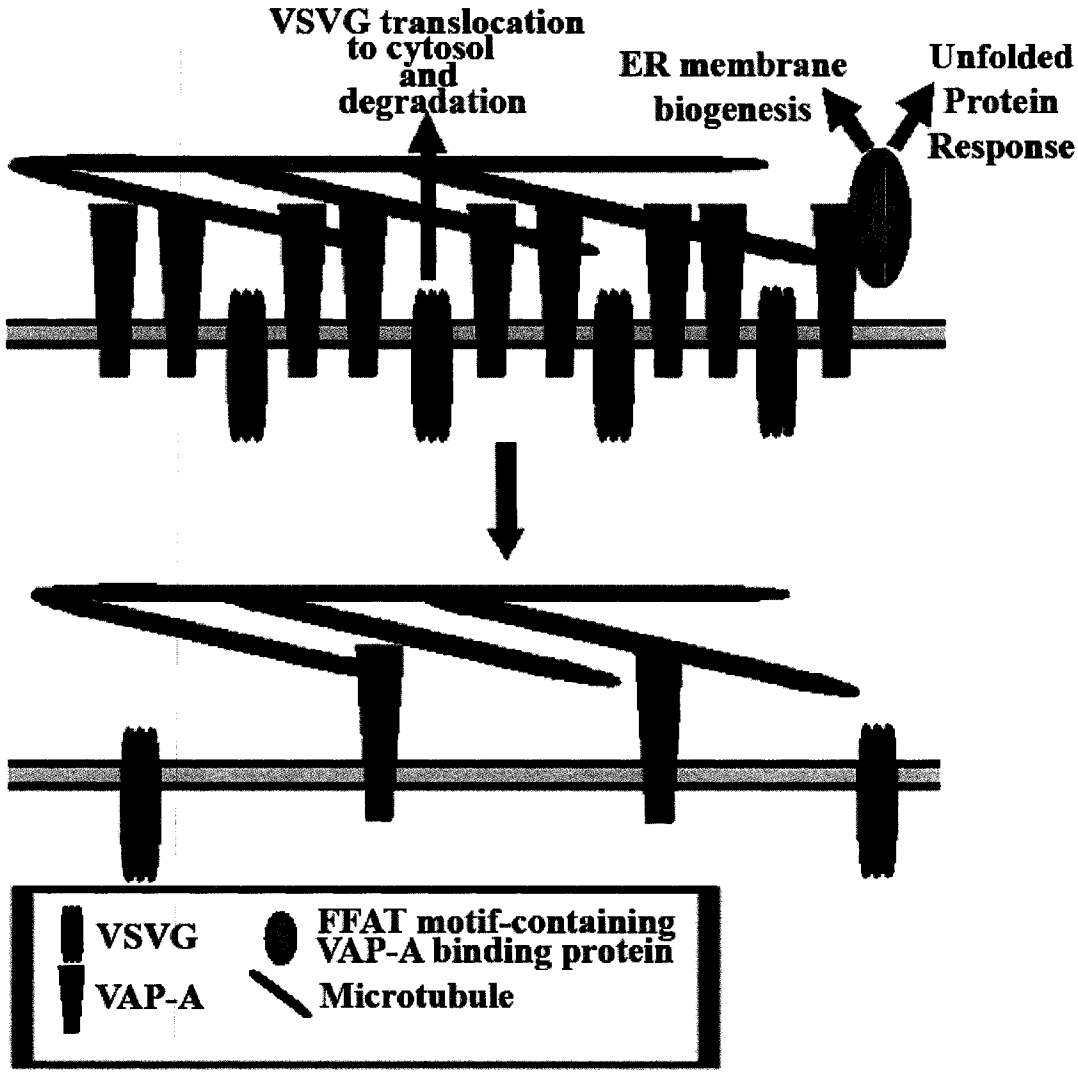

Figure 4.2.2. VAP-A signalling induced by accumulation of ER membrane proteins. VAP-A senses the ER accumulation of membrane proteins such as VSVG, and inhibits their lateral movement. The membrane protein is eventually translocated back to the cytosol and degraded. VAP-A can also trigger membrane biogenesis and the unfolded protein response (UPR) by signalling through the multiple FFAT domain containing proteins. This results in both lower levels of membrane proteins and an increase in ER membrane volume.

Homo sapiens VAP-A-interacting proteins that contain a FFAT domain	*S. cerevisiae* Scs2p interacting proteins that contain a FFAT domain
Oxysterol-Binding Protein (OSBP)	**OSBP Homologue (Osh) Isoforms 1,2 and 3**
OSBP-Related Protein (ORP) Isoforms 1,2,3,4,6,7 and 9	**Opi1p**
Ceramide Transporter (CERT)	
NIR Isoforms 1,2 and 3	

Table III. List of VAP-A-binding proteins that contain a FFAT motif. List of human and yeast proteins that contain a FFAT domain and interact with VAP-A and its yeast orthologue Scs2p.

perturbation in calcium homeostasis or redox status, expression of misfolded proteins, sugar/glucose deprivation, altered glycosylation, overloading of cholesterol, and elevated secretory protein synthesis can disrupt ER homeostasis, thus imposing stress to the ER (reviewed by Kaufman, 1999 and Mori, 2000). The UPR compensates primarily by augmenting the cell's folding capacity, but it is also believed to modulate the size of the ER in response to developmental demands and physiological changes (Iwakoshi et al., 2003; Wiest et al., 1990). If the perturbation remains for an extended period, then apoptosis will be initiated by the UPR and cell death will follow (Morishima et al., 2002; Nakagawa et al., 2000). Therefore, multiple facts seem to link VAP-A to the UPR. As I have mentioned, VAP-A could sense elevated ER levels of membrane proteins and recruit FFAT motif-containing proteins involved in membrane biogenesis to the ER, thereby allowing the cell to cope with this increase in membrane proteins. Scs2p, the yeast orthologue of VAP-A, has been shown to interact with the FFAT motif-containing Opi1p protein, a transcriptional regulator specific to phospholipid synthesis and believed to be involved in UPR response (Hancock et al., 2006). Overexpression of Scs2p rescues the inositol auxotrophy phenotype of the IRE1 or HAC1 mutants, which are part of the UPR pathway (Calfon et al., 2002; Kagiwada et al., 1998). In addition, a mutation in VAP-B has recently been shown to cause late-onset spinal muscular atrophy and amyotrophic lateral sclerosis (Nishimura et al., 2005; Nishimura et al., 2004). VAP-B can dimerize with VAP-A *in vitro* and also possesses the ability to bind FFAT motif containing proteins (Amarilio et al., 2005; Nishimura et al., 1999). The effect of the mutation on FFAT motif binding has not been tested but the VAP-B P56S substitution is localized near residues identified, by X-ray crystallography and *in vitro* binding assays,

as critical for FFAT motif binding (Kaiser et al., 2005). Not much is known about the abnormal cellular events responsible for the death of the affected neurons in this disease, but other mutations associated with ALS (amyotrophic lateral sclerosis) have been found in the SOD1 gene (ALS1) (Chiba et al., 2004; Gurney et al., 1994), which seems to affect the UPR (Atkin et al., 2006), and the alsin protein (ALS2) (Hadano et al., 2006), which has been shown to exert a neuroprotective function against neurotoxicity caused by SOD1 mutations *in vitro* (Hadano et al., 2006), therefore establishing another link between VAP and this cellular response. In addition, a recent study found that overexpression of VAP-B promotes the UPR (Kanekura et al., 2006). However, overexpression of the P56S mutant, a mutation in ALS8, actually reduces the UPR response. It seems this mutation renders the protein incapable of activating the UPR response and also increases homodimerization of VAP-B, thus preventing the endogenous wild type VAP-B from activating UPR. Interestingly, this VAP-B mutation does not increase binding to VAP-A, demonstrating important differences between the two proteins and suggesting the isoforms are not simple orthologs. Therefore, multiple lines of evidence seem to associate VAP-A with ER membrane expansion and the UPR, which is a logical complementary response to VAP-A's ability to sense ER membrane protein density.

Two alternative models of how PRA2 affects VSVG^{ts045} trafficking

Like PRA1, PRA2 also hinders VSVG^{ts045} trafficking. However the site of the inhibition correlates with the localization of the isoform, suggesting the use of a similar mechanism by both proteins to delay the trafficking of VSVG^{ts045}. As previously

mentioned, the S76A PRA1 mutation, which I have shown increases binding to Rab3A and VAMP2, amplified the delay caused by wild type PRA1. It produced a condensed Golgi complex morphology similar to that resulting from the expression of the dominant negative dynamin 2 that blocks vesicle formation from the *trans*-Golgi network. Overexpression of PRA1 wild type and even more so for the S76A mutant, could affect the recruitment of Rab and its effectors, as well as proteins such as VAMP2 that are required for subsequent vesicle docking and fusion, to vesicle forming sites. In fact, synaptic vesicle biogenesis from the endosome was shown to require the presence of VAMP2, most likely to ensure the formation of fusion-competent vesicles (Salem et al., 1998). Therefore, increasing the level of PRA1 and the strength of its interaction with Rab and VAMP2, as in the case of PRA1 S76A, could affect the segregation of these proteins to vesicle-forming domains, thereby reducing vesicle budding from the *trans*-Golgi network. Due to the similarities observed between the two PRA isoforms, I believe this hypothesis can be transferred to PRA2. As illustrated in Figure 4.2.3.I, overexpression of PRA2 would segregate from the ERES molecules such as Rab and ER-to-Golgi SNAREs. Since the sequestration of these molecules onto newly forming vesicles could be required for the formation of ER-derived fusion-competent vesicles, the overexpression of PRA2 would result in a reduction in vesicle budding from the ER and a delay in $VSVG^{ts045}$ trafficking. This would explain, why $VSVG^{ts045}$ ER lateral movement is not affected by PRA2 overexpression, and how PRA2, which seems to be localized predominantly outside the ER budding sites, can affect ER budding.

However, according to this hypothesis, PRA2 itself would have to be excluded from the ERES, otherwise it could recruit Rabs and ER-to-Golgi SNAREs to the vesicle

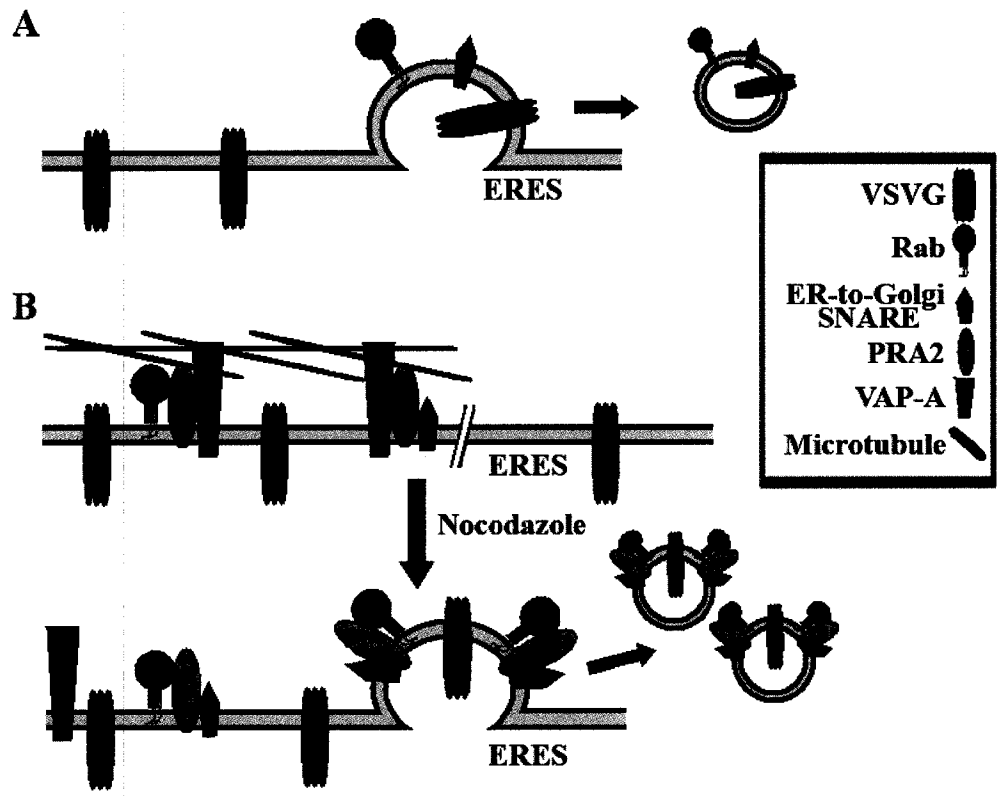

Figure 4.2.3.I. Model illustration of PRA2's effect on VSVG trafficking. Figure 4.2.3.I and II demonstrate two alternative models that describe PRA2's inhibition of VSVG trafficking. (A) In control conditions, VSVG moves laterally to the ERES, where proteins involved in vesicle formation are recruited. VSVG is sequestered onto the budding vesicle and traffics towards the Golgi. (B) Overexpressed PRA2 is localized outside the ERES and recruits proteins involved in vesicle budding. A direct or indirect interaction (possibly through VAP-A) with microtubules prevents ER lateral movement of PRA2 to the ERES, which reduces the availability of proteins involved in vesicle budding, thus decreasing the number of ER-derived vesicles. The addition of nocodazole disrupts the microtubules, which allows PRA2 to reach the ERES. This provides a greater number of proteins involved in vesicle budding, thereby increasing the number of vesicles formed.

forming domains, thereby increasing vesicle budding. The surprising increase in budding obtained by microtubule depolymerization suggested that PRA2 might be held static in the ER membrane, away from ERES, by a mechanism that requires microtubules. Because no evidence indicates a direct PRA2 interaction with microtubules, PRA2 complexes might interact with microtubule binding proteins, such as CLIMP-63, which are believed to be involved in the stabilization of the ER membrane through their interaction with microtubules (Klopfenstein et al., 1998; Schweizer et al., 1993). As described earlier, another obvious candidate could be VAP-A. Because of this microtubule anchor, I would expect PRA2 ER lateral movement to be hindered. With the addition of a depolymerizing agent such as nocodazole, PRA2 would be free to move towards the ER exit sites, thereby providing vesicle-forming subdomains of the ER with a larger supply of proteins required for vesicle budding, such as Rab and SNAREs. This would result in an increase in vesicle formation from the ER and thus an increase in the total amount of $VSVG^{ts045}$ on ER derived vesicles.

The reduction in $VSVG^{ts045}$ budded from the ER in control samples when nocodazole was added supports the belief that microtubules are involved in vesicle trafficking between the ER and Golgi compartments (Fig.3.11). In fact, it has been previously shown that ERES align along microtubules in certain cell types (Ralston et al., 2001) and the Sec23p component of the COPII complex directly interacts with the dynactin complex pathway (Watson et al., 2005). In addition, Golgi-directed VTCs were found to localize along a population of stable microtubules and translocate along microtubules towards the Golgi complex in a dynactin-dependent manner (Presley et al., 1997). However, little is known about how this coupling to microtubules regulates the

various trafficking events of the early secretory pathway. My results suggest that microtubules, although probably not necessary, increase the efficiency of ER vesicle budding.

Another explanation of the results I obtained is that overexpression of PRA2 recruits a greater amount of proteins, such as Rab and SNAREs, to newly forming ER-derived vesicles. As elaborated earlier, the increase in concentration at the ERES of proteins involved in ER-to-Golgi vesicle trafficking would increase the rate of vesicles formation and budding from the ER. This would allow for a greater amount of $VSVG^{ts045}$ to exit the ER (Figure 4.2.3.II). However, PRA2 recruited to vesicles, could stabilize the link between vesicles and microtubules, thus preventing them from trafficking towards the Golgi complex and from being collected by centrifugation in the ER budding assay. These vesicles would remain in the cell and the $VSVG^{ts045}$ they contain would be incorrectly believed to have stayed in the ER. The addition of nocodazole would release the vesicles thereby permitting their collection. As mentioned previously, a great amount of data supports the role of microtubules in vesicle trafficking between the ER and the Golgi complex. In addition, Rab6 has been shown to function as a tethering factor controlling the recruitment of dynactin to Golgi compartment membranes (Short et al., 2002), suggesting a possible direct interaction between other Rabs and the dynactin-dynein complex involved in motility along microtubules. It would therefore be possible for PRA2 to interact directly or indirectly with microtubules and prevent the normal progression of the vesicles. This model would predict an accumulation of ER-derived microtubule-associated vesicles that contain $VSVG^{ts045}$. Even though I did not observe

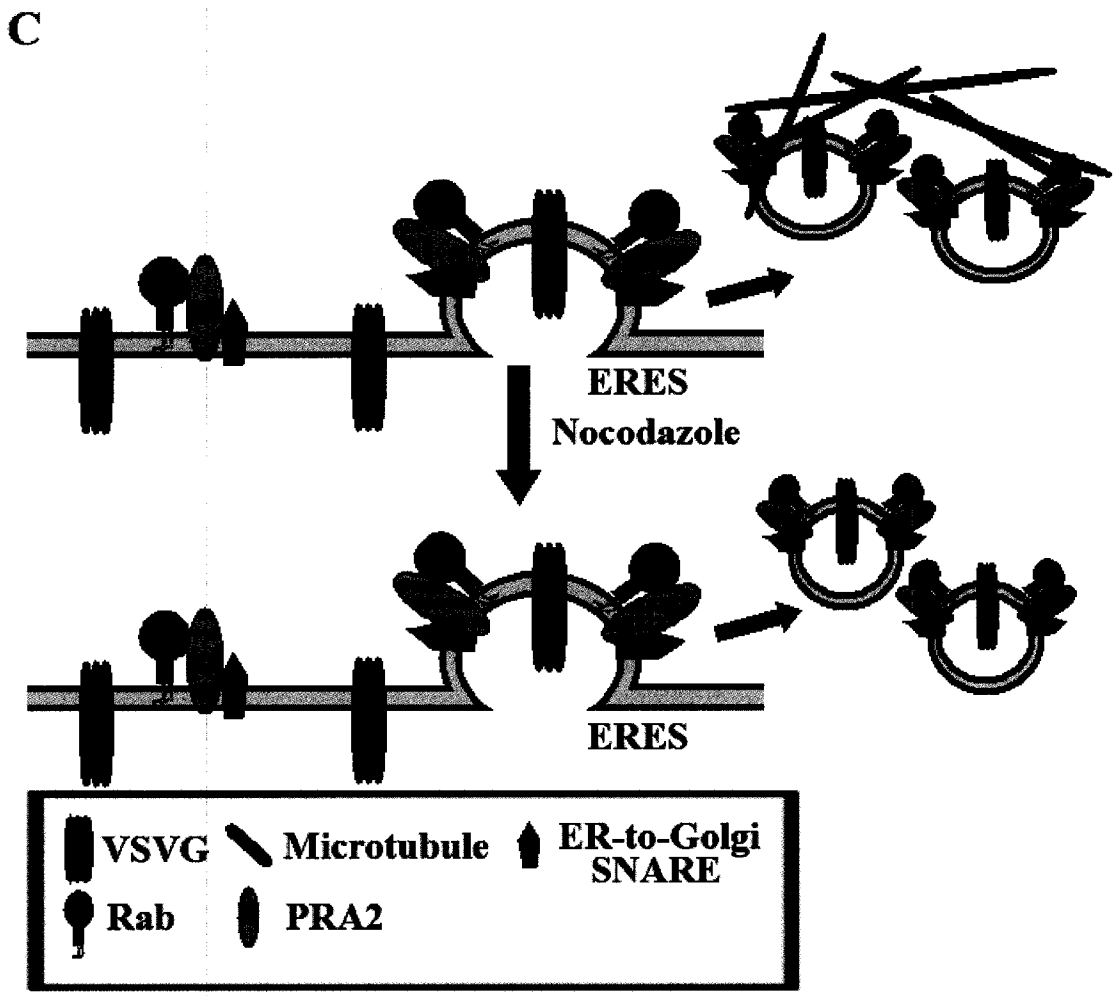

Figure 4.2.3.II. Model illustration of PRA2's effect on VSVG trafficking. (C) Overexpressed PRA2 recruits a greater number of proteins involved in vesicle budding to the ERES, thereby increasing the number of vesicles formed. However, PRA2 directly or indirectly anchors vesicles to microtubules, which prevents their collection. The addition of nocodazole eliminates this link to microtubules, thus allowing vesicle collection.

such a fluorescent distribution of $VSVG^{ts045}$-GFP when PRA2 was overexpressed, a more precise technique such as electron microscopy might reveal the presence of the vesicles. It would be interesting to study the ability of overexpressed PRA2 to move laterally in the ER membrane, because it represents a major difference between the two hypotheses.

Final remark

I set out trying to clarify the physical characteristics of PRAs and understand their function. The results I have obtained in the second chapter explained some of the characteristics of PRA's interaction with multiple proteins and in combination with results from the third chapter has helped clarify the possible role of PRA2 and VAP-A. My results support the idea that both proteins are involved in trafficking, but achieve this through different mechanisms. Although I am not able to identify which of the models I have proposed is correct, a number of experiments, using some of the techniques I have developed, could help identify the appropriate model. Understanding the function of PRAs and VAP-A would help further our knowledge of protein and vesicle trafficking, ER homeostasis and the UPR, but also could help understand and treat diseases like ALS or other diseases resulting from trafficking abnormality.

Chapter 5

References

Abdul-Ghani, M., P.Y. Gougeon, D.C. Prosser, L.F. Da-Silva, and J.K. Ngsee. 2001. PRA isoforms are targeted to distinct membrane compartments. *J. Biol. Chem.* 276:6225-33.

Albert, S., and D. Gallwitz. 1999. Two new members of a family of Ypt/Rab GTPase activating proteins. Promiscuity of substrate recognition. *J. Biol. Chem.* 274:33186-9.

Amarilio, R., S. Ramachandran, H. Sabanay, and S. Lev. 2005. Differential regulation of endoplasmic reticulum structure through VAP-Nir protein interaction. *J. Biol. Chem.* 280:5934-44.

Andres, D.A., M.C. Seabra, M.S. Brown, S.A. Armstrong, T.E. Smeland, F.P. Cremers, and J.L. Goldstein. 1993. cDNA cloning of component A of Rab geranylgeranyl transferase and demonstration of its role as a Rab escort protein. *Cell.* 73:1091-9.

Aoe, T., E. Cukierman, A. Lee, D. Cassel, P.J. Peters, and V.W. Hsu. 1997. The KDEL receptor, ERD2, regulates intracellular traffic by recruiting a GTPase-activating protein for ARF1. *Embo J.* 16:7305-16.

Aridor, M., S.I. Bannykh, T. Rowe, and W.E. Balch. 1995. Sequential coupling between COPII and COPI vesicle coats in endoplasmic reticulum to Golgi transport. *J. Cell Biol.* 131:875-93.

Aridor, M., J. Weissman, S. Bannykh, C. Nuoffer, and W.E. Balch. 1998. Cargo selection by the COPII budding machinery during export from the ER. *J. Cell Biol.* 141:61-70.

Aridor, M., and L.A. Hannan. 2000. Traffic jam: a compendium of human diseases that affect intracellular transport processes. *Traffic.* 1:836-51.

Aridor, M., K.N. Fish, S. Bannykh, J. Weissman, T.H. Roberts, J. Lippincott-Schwartz, and W.E. Balch. 2001. The Sar1 GTPase coordinates biosynthetic cargo selection with endoplasmic reticulum export site assembly. *J. Cell Biol.* 152:213-29.

Aridor, M., and L.A. Hannan. 2002. Traffic jams II: an update of diseases of intracellular transport. *Traffic.* 3:781-90.

Aridor, M., and L.M. Traub. 2002. Cargo selection in vesicular transport: the making and breaking of a coat. *Traffic.* 3:537-46.

Atkin, J.D., M.A. Farg, B.J. Turner, D. Tomas, J.A. Lysaght, J. Nunan, A. Rembach, P. Nagley, P.M. Beart, S.S. Cheema, and M.K. Horne. 2006. Induction of the unfolded protein response in familial amyotrophic lateral sclerosis and association of protein disulfide isomerase with superoxide dismutase 1. *J. Biol. Chem.*

Balch, W.E., J.M. McCaffery, H. Plutner, and M.G. Farquhar. 1994. Vesicular stomatitis virus glycoprotein is sorted and concentrated during export from the endoplasmic reticulum. *Cell.* 76:841-52.

Bannykh, S.I., T. Rowe, and W.E. Balch. 1996. The organization of endoplasmic

reticulum export complexes. *J. Cell Biol.* 135:19-35.

Barlowe, C., and R. Schekman. 1993. SEC12 encodes a guanine-nucleotide-exchange factor essential for transport vesicle budding from the ER. *Nature.* 365:347-9.

Barlowe, C., L. Orci, T. Yeung, M. Hosobuchi, S. Hamamoto, N. Salama, M.F. Rexach, M. Ravazzola, M. Amherdt, and R. Schekman. 1994. COPII: a membrane coat formed by Sec proteins that drive vesicle budding from the endoplasmic reticulum. *Cell.* 77:895-907.

Barlowe, C. 1998. COPII and selective export from the endoplasmic reticulum. *Biochim. Biophys. Acta.* 1404:67-76.

Barr, F.A., N. Nakamura, and G. Warren. 1998. Mapping the interaction between GRASP65 and GM130, components of a protein complex involved in the stacking of Golgi cisternae. *Embo J.* 17:3258-68.

Baumert, M., P.R. Maycox, F. Navone, P. De Camilli, and R. Jahn. 1989. Synaptobrevin: an integral membrane protein of 18,000 daltons present in small synaptic vesicles of rat brain. *Embo J.* 8:379-84.

Belden, W.J., and C. Barlowe. 2001. Role of Erv29p in collecting soluble secretory proteins into ER-derived transport vesicles. *Science.* 294:1528-31.

Benli, M., F. Doring, D.G. Robinson, X. Yang, and D. Gallwitz. 1996. Two GTPase isoforms, Ypt31p and Ypt32p, are essential for Golgi function in yeast. *Embo J.* 15:6460-75.

Bennett, M.K., N. Calakos, and R.H. Scheller. 1992. Syntaxin: a synaptic protein

implicated in docking of synaptic vesicles at presynaptic active zones. *Science.* 257:255-9.

Bergmann, J.E. 1989. Using temperature-sensitive mutants of VSV to study membrane protein biogenesis. *Methods Cell Biol.* 32:85-110.

Bi, X., R.A. Corpina, and J. Goldberg. 2002. Structure of the Sec23/24-Sar1 pre-budding complex of the COPII vesicle coat. *Nature.* 419:271-7.

Bigay, J., and B. Antonny. 2005. Real-time assays for the assembly-disassembly cycle of COP coats on liposomes of defined size. *Methods Enzymol.* 404:95-107.

Block, M.R., B.S. Glick, C.A. Wilcox, F.T. Wieland, and J.E. Rothman. 1988. Purification of an N-ethylmaleimide-sensitive protein catalyzing vesicular transport. *Proc. Natl. Acad. Sci. U S A.* 85:7852-6.

Bonifacino, J.S., C.K. Suzuki, J. Lippincott-Schwartz, A.M. Weissman, and R.D. Klausner. 1989. Pre-Golgi degradation of newly synthesized T-cell antigen receptor chains: intrinsic sensitivity and the role of subunit assembly. *J. Cell Biol.* 109:73-83.

Bourne, H.R. 1988. Do GTPases direct membrane traffic in secretion? *Cell.* 53:669-71.

Bourne, H.R., D.A. Sanders, and F. McCormick. 1991. The GTPase superfamily: conserved structure and molecular mechanism. *Nature.* 349:117-27.

Brennwald, P., B. Kearns, K. Champion, S. Keranen, V. Bankaitis, and P. Novick. 1994. Sec9 is a SNAP-25-like component of a yeast SNARE complex that

may be the effector of Sec4 function in exocytosis. *Cell.* 79:245-58.

Brigance, W.T., C. Barlowe, and T.R. Graham. 2000. Organization of the yeast Golgi complex into at least four functionally distinct compartments. *Mol. Biol. Cell.* 11:171-82.

Brosig, B., and D. Langosch. 1998. The dimerization motif of the glycophorin A transmembrane segment in membranes: importance of glycine residues. *Protein Sci.* 7:1052-6.

Bucci, C., M. Chiariello, D. Lattero, M. Maiorano, and C.B. Bruni. 1999. Interaction cloning and characterization of the cDNA encoding the human prenylated rab acceptor (PRA1). *Biochem. Biophys. Res. Commun.* 258:657-62.

Bullock, T.L., T.M. Roberts, and M. Stewart. 1996. 2.5 A resolution crystal structure of the motile major sperm protein (MSP) of Ascaris suum. *J. Mol. Biol.* 263:284-96.

Butchbach, M.E., L. Lai, and C.L. Lin. 2002. Molecular cloning, gene structure, expression profile and functional characterization of the mouse glutamate transporter (EAAT3) interacting protein GTRAP3-18. *Gene.* 292:81-90.

Calero, M., and R.N. Collins. 2002. Saccharomyces cerevisiae Pra1p/Yip3p interacts with Yip1p and Rab proteins. *Biochem. Biophys. Res. Commun.* 290:676-81.

Calero, M., C.Z. Chen, W. Zhu, N. Winand, K.A. Havas, P.M. Gilbert, C.G. Burd, and R.N. Collins. 2003. Dual prenylation is required for Rab protein localization and function. *Mol. Biol. Cell.* 14:1852-67.

Calfon, M., H. Zeng, F. Urano, J.H. Till, S.R. Hubbard, H.P. Harding, S.G. Clark, and

D. Ron. 2002. IRE1 couples endoplasmic reticulum load to secretory capacity by processing the XBP-1 mRNA. *Nature.* 415:92-6.

Campbell, J.L., and R. Schekman. 1997. Selective packaging of cargo molecules into endoplasmic reticulum-derived COPII vesicles. *Proc. Natl. Acad. Sci. U S A.* 94:837-42.

Cao, X., N. Ballew, and C. Barlowe. 1998. Initial docking of ER-derived vesicles requires Uso1p and Ypt1p but is independent of SNARE proteins. *Embo J.* 17:2156-65.

Cao, X., and C. Barlowe. 2000. Asymmetric requirements for a Rab GTPase and SNARE proteins in fusion of COPII vesicles with acceptor membranes. *J. Cell Biol.* 149:55-66.

Cao, H., H.M. Thompson, E.W. Krueger, and M.A. McNiven. 2000. Disruption of Golgi structure and function in mammalian cells expressing a mutant dynamin. *J. Cell Sci.* 113 (Pt 11):1993-2002.

Cassanelli, S., S. Bertolini, M. Rolleri, F. De Stefano, L. Casarino, N. Elicio, A. Naselli, and S. Calandra. 1998. A 'de novo' point mutation of the low-density lipoprotein receptor gene in an Italian subject with primary hypercholesterolemia. *Clin. Genet.* 53:391-5.

Castillo, P.E., R. Janz, T.C. Sudhof, T. Tzounopoulos, R.C. Malenka, and R.A. Nicoll. 1997. Rab3A is essential for mossy fibre long-term potentiation in the hippocampus. *Nature.* 388:590-3.

Chavrier, P., M. Vingron, C. Sander, K. Simons, and M. Zerial. 1990. Molecular

cloning of YPT1/SEC4-related cDNAs from an epithelial cell line. *Mol. Cell Biol.* 10:6578-85.

Chavrier, P., and B. Goud. 1999. The role of ARF and Rab GTPases in membrane transport. *Curr. Opin. Cell Biol.* 11:466-75.

Cheng, S.H., R.J. Gregory, J. Marshall, S. Paul, D.W. Souza, G.A. White, C.R. O'Riordan, and A.E. Smith. 1990. Defective intracellular transport and processing of CFTR is the molecular basis of most cystic fibrosis. *Cell.* 63:827-34.

Chiba, T., Y. Hashimoto, H. Tajima, M. Yamada, R. Kato, T. Niikura, K. Terashita, H. Schulman, S. Aiso, Y. Kita, M. Matsuoka, and I. Nishimoto. 2004. Neuroprotective effect of activity-dependent neurotrophic factor against toxicity from familial amyotrophic lateral sclerosis-linked mutant SOD1 in vitro and in vivo. *J. Neurosci. Res.* 78:542-52.

Christoforidis, S., H.M. McBride, R.D. Burgoyne, and M. Zerial. 1999. The Rab5 effector EEA1 is a core component of endosome docking. *Nature.* 397:621-5.

Clary, D.O., I.C. Griff, and J.E. Rothman. 1990. SNAPs, a family of NSF attachment proteins involved in intracellular membrane fusion in animals and yeast. *Cell.* 61:709-21.

Cole, N.B., N. Sciaky, A. Marotta, J. Song, and J. Lippincott-Schwartz. 1996. Golgi dispersal during microtubule disruption: regeneration of Golgi stacks at peripheral endoplasmic reticulum exit sites. *Mol. Biol. Cell.* 7:631-50.

Conchello, J.-A., J.J. Kim, and E.W. Hansen. 1994. Enhanced three-dimensional

reconstruction from confocal scanning microscope images. II. Depth discrimination versus signal-to-noise ratio in partically confocal images. *Appl. Opt.* 33:3740-3750.

Cosson, P., and F. Letourneur. 1994. Coatomer interaction with di-lysine endoplasmic reticulum retention motifs. *Science.* 263:1629-31.

de Silva, A., I. Braakman, and A. Helenius. 1993. Posttranslational folding of vesicular stomatitis virus G protein in the ER: involvement of noncovalent and covalent complexes. *J. Cell Biol.* 120:647-55.

DeBello, W.M., V. O'Connor, T. Dresbach, S.W. Whiteheart, S.S. Wang, F.E. Schweizer, H. Betz, J.E. Rothman, and G.J. Augustine. 1995. SNAP-mediated protein-protein interactions essential for neurotransmitter release. *Nature.* 373:626-30.

Deneka, M., M. Neeft, and P. van der Sluijs. 2003. Regulation of membrane transport by rab GTPases. *Crit. Rev. Biochem. Mol. Biol.* 38:121-42.

Dominguez, M., K. Dejgaard, J. Fullekrug, S. Dahan, A. Fazel, J.P. Paccaud, D.Y. Thomas, J.J. Bergeron, and T. Nilsson. 1998. gp25L/emp24/p24 protein family members of the cis-Golgi network bind both COP I and II coatomer. *J. Cell Biol.* 140:751-65.

Doms, R.W., A. Ruusala, C. Machamer, J. Helenius, A. Helenius, and J.K. Rose. 1988. Differential effects of mutations in three domains on folding, quaternary structure, and intracellular transport of vesicular stomatitis virus G protein. *J. Cell Biol.* 107:89-99.

Echard, A., F. Jollivet, O. Martinez, J.J. Lacapere, A. Rousselet, I. Janoueix-Lerosey, and B. Goud. 1998. Interaction of a Golgi-associated kinesin-like protein with Rab6. *Science*. 279:580-5.

Elferink, L.A., K. Anzai, and R.H. Scheller. 1992. rab15, a novel low molecular weight GTP-binding protein specifically expressed in rat brain. *J. Biol. Chem.* 267:5768-75.

Elkind, N.B., C. Walch-Solimena, and P.J. Novick. 2000. The role of the COOH terminus of Sec2p in the transport of post-Golgi vesicles. *J. Cell Biol.* 149:95-110.

Enouf, V., S. Chwetzoff, G. Trugnan, and J. Cohen. 2003. Interactions of rotavirus VP4 spike protein with the endosomal protein Rab5 and the prenylated Rab acceptor PRA1. *J. Virol.* 77:7041-7.

Ettayebi, K., and M.E. Hardy. 2003. Norwalk virus nonstructural protein p48 forms a complex with the SNARE regulator VAP-A and prevents cell surface expression of vesicular stomatitis virus G protein. *J. Virol.* 77:11790-7.

Evans, D.T., K.C. Tillman, and R.C. Desrosiers. 2002. Envelope glycoprotein cytoplasmic domains from diverse lentiviruses interact with the prenylated Rab acceptor. *J. Virol.* 76:327-37.

Fasshauer, D., W. Antonin, M. Margittai, S. Pabst, and R. Jahn. 1999. Mixed and non-cognate SNARE complexes. Characterization of assembly and biophysical properties. *J. Biol. Chem.* 274:15440-6.

Feiguin, F., A. Ferreira, K.S. Kosik, and A. Caceres. 1994. Kinesin-mediated

organelle translocation revealed by specific cellular manipulations. *J. Cell Biol.* 127:1021-39.

Fenster, S.D., W.J. Chung, R. Zhai, C. Cases-Langhoff, B. Voss, A.M. Garner, U. Kaempf, S. Kindler, E.D. Gundelfinger, and C.C. Garner. 2000. Piccolo, a presynaptic zinc finger protein structurally related to bassoon. *Neuron.* 25:203-14.

Figueroa, C., J. Taylor, and A.B. Vojtek. 2001. Prenylated Rab acceptor protein is a receptor for prenylated small GTPases. *J. Biol. Chem.* 276:28219-25.

Fischer von Mollard, G., G.A. Mignery, M. Baumert, M.S. Perin, T.J. Hanson, P.M. Burger, R. Jahn, and T.C. Sudhof. 1990. rab3 is a small GTP-binding protein exclusively localized to synaptic vesicles. *Proc. Natl. Acad. Sci. U S A.* 87:1988-92.

Foster, L.J., M.L. Weir, D.Y. Lim, Z. Liu, W.S. Trimble, and A. Klip. 2000. A functional role for VAP-33 in insulin-stimulated GLUT4 traffic. *Traffic.* 1:512-21.

Fukui, K., T. Sasaki, K. Imazumi, Y. Matsuura, H. Nakanishi, and Y. Takai. 1997. Isolation and characterization of a GTPase activating protein specific for the Rab3 subfamily of small G proteins. *J. Biol. Chem.* 272:4655-8.

Geppert, M., V.Y. Bolshakov, S.A. Siegelbaum, K. Takei, P. De Camilli, R.E. Hammer, and T.C. Sudhof. 1994. The role of Rab3A in neurotransmitter release. *Nature.* 369:493-7.

Geppert, M., Y. Goda, C.F. Stevens, and T.C. Sudhof. 1997. The small GTP-binding

protein Rab3A regulates a late step in synaptic vesicle fusion. *Nature*. 387:810-4.

Gibson, S.F., and F. Lanni. 1992. Experimental test of an analytical model of aberration in an oil-immersion objective lens used in three-dimensional light microscopy. *J. Opt. Soc.Am. A*. 9:154-66.

Goldstein, J.L., and M.S. Brown. 1990. Regulation of the mevalonate pathway. *Nature*. 343:425-30.

Gougeon, P.Y. and J.K. Ngsee. 2005. Purification and functional properties of prenylated Rab acceptor 2. *Methods Enzymol.* 403:799-807.

Gougeon, P.Y., D.C. Prosser, L.F. Da-Silva, and J.K. Ngsee. 2002. Disruption of Golgi morphology and trafficking in cells expressing mutant prenylated rab acceptor-1. *J. Biol. Chem.* 277:36408-14.

Guo, W., A. Grant, and P. Novick. 1999. Exo84p is an exocyst protein essential for secretion. *J. Biol. Chem.* 274:23558-64.

Guo, W., D. Roth, C. Walch-Solimena, and P. Novick. 1999. The exocyst is an effector for Sec4p, targeting secretory vesicles to sites of exocytosis. *Embo J.* 18:1071-80.

Gurney, M.E., H. Pu, A.Y. Chiu, M.C. Dal Canto, C.Y. Polchow, D.D. Alexander, J. Caliendo, A. Hentati, Y.W. Kwon, H.X. Deng, and et al. 1994. Motor neuron degeneration in mice that express a human Cu,Zn superoxide dismutase mutation. *Science*. 264:1772-5.

Haaf, A., P.J. Butler, H.M. Kent, I.M. Fearnley, T.M. Roberts, D. Neuhaus, and M.

Stewart. 1996. The motile major sperm protein (MSP) from Ascaris suum is a symmetric dimer in solution. *J. Mol. Biol.* 260:251-60.

Hadano, S., S.C. Benn, S. Kakuta, A. Otomo, K. Sudo, R. Kunita, K. Suzuki-Utsunomiya, H. Mizumura, J.M. Shefner, G.A. Cox, Y. Iwakura, R.H. Brown, Jr., and J.E. Ikeda. 2006. Mice deficient in the Rab5 guanine nucleotide exchange factor ALS2/alsin exhibit age-dependent neurological deficits and altered endosome trafficking. *Hum. Mol. Genet.* 15:233-50.

Hamamoto, I., Y. Nishimura, T. Okamoto, H. Aizaki, M. Liu, Y. Mori, T. Abe, T. Suzuki, M.M. Lai, T. Miyamura, K. Moriishi, and Y. Matsuura. 2005. Human VAP-B is involved in hepatitis C virus replication through interaction with NS5A and NS5B. *J. Virol.* 79:13473-82.

Hanada, K., K. Kumagai, S. Yasuda, Y. Miura, M. Kawano, M. Fukasawa, and M. Nishijima. 2003. Molecular machinery for non-vesicular trafficking of ceramide. *Nature.* 426:803-9.

Hancock, L.C., R.P. Behta, and J.M. Lopes. 2006. Genomic analysis of the Opi- phenotype. *Genetics.* 173:621-34.

Harter, C., J. Pavel, F. Coccia, E. Draken, S. Wegehingel, H. Tschochner, and F. Wieland. 1996. Nonclathrin coat protein gamma, a subunit of coatomer, binds to the cytoplasmic dilysine motif of membrane proteins of the early secretory pathway. *Proc. Natl. Acad. Sci. U S A.* 93:1902-6.

Hauri, H.P., F. Kappeler, H. Andersson, and C. Appenzeller. 2000. ERGIC-53 and traffic in the secretory pathway. *J. Cell Sci.* 113 (Pt 4):587-96.

Hay, J.C., J. Klumperman, V. Oorschot, M. Steegmaier, C.S. Kuo, and R.H. Scheller. 1998. Localization, dynamics, and protein interactions reveal distinct roles for ER and Golgi SNAREs. *J. Cell Biol.* 141:1489-502.

Hayashi, T., H. McMahon, S. Yamasaki, T. Binz, Y. Hata, T.C. Sudhof, and H. Niemann. 1994. Synaptic vesicle membrane fusion complex: action of clostridial neurotoxins on assembly. *Embo J.* 13:5051-61.

Hong, W. 1998. Protein transport from the endoplasmic reticulum to the Golgi apparatus. *J. Cell Sci.* 111 (Pt 19):2831-9.

Horiuchi, H., Lippe, R., McBride, H.M., Rubino, M., Woodman, P., Stenmark, H., Rybin, V., Wilm, M., Ashman, K., Mann, M., Zerial, M. 1997. A novel Rab5 GDP/GTP exchange factor complexed to Rabaptin-5 links nucleotide exchange to effector recruitment and function. *Cell.* 90:1149-59.

Huang, M., J.T. Weissman, S. Beraud-Dufour, P. Luan, C. Wang, W. Chen, M. Aridor, I.A. Wilson, and W.E. Balch. 2001. Crystal structure of Sar1-GDP at 1.7 A resolution and the role of the NH2 terminus in ER export. *J. Cell Biol.* 155:937-48.

Hughson, F.M. 1999. Membrane fusion: structure snared at last. *Curr. Biol.* 9:R49-52.

Hunt, L.A., J.R. Etchison, and D.F. Summers. 1978. Oligosaccharide chains are trimmed during synthesis of the envelope glycoprotein of vesicular stomatitis virus. *Proc. Natl. Acad. Sci. U S A.* 75:754-8.

Hunt, J.M., K. Bommert, M.P. Charlton, A. Kistner, E. Habermann, G.J. Augustine,

and H. Betz. 1994. A post-docking role for synaptobrevin in synaptic vesicle fusion. *Neuron.* 12:1269-79.

Hutt, D.M., L.F. Da-Silva, L.H. Chang, D.C. Prosser, and J.K. Ngsee. 2000. PRA1 inhibits the extraction of membrane-bound rab GTPase by GDI1. *J. Biol. Chem.* 275:18511-9.

Ingley, E., J.H. Williams, C.E. Walker, S. Tsai, S. Colley, M.S. Sayer, P.A. Tilbrook, M. Sarna, J.G. Beaumont, and S.P. Klinken. 1999. A novel ADP-ribosylation like factor (ARL-6), interacts with the protein-conducting channel SEC61beta subunit. *FEBS Lett.* 459:69-74.

Italiano, J.E., Jr., T.M. Roberts, M. Stewart, and C.A. Fontana. 1996. Reconstitution in vitro of the motile apparatus from the amoeboid sperm of Ascaris shows that filament assembly and bundling move membranes. *Cell.* 84:105-14.

Iwakoshi, N.N., A.H. Lee, P. Vallabhajosyula, K.L. Otipoby, K. Rajewsky, and L.H. Glimcher. 2003. Plasma cell differentiation and the unfolded protein response intersect at the transcription factor XBP-1. *Nat. Immunol.* 4:321-9.

Jamieson, J.D., and G.E. Palade. 1967. Intracellular transport of secretory proteins in the pancreatic exocrine cell. II. Transport to condensing vacuoles and zymogen granules. *J. Cell Biol.* 34:597-615.

Janoueix-Lerosey, I., F. Jollivet, J. Camonis, P.N. Marche, and B. Goud. 1995. Two-hybrid system screen with the small GTP-binding protein Rab6. Identification of a novel mouse GDP dissociation inhibitor isoform and two other potential partners of Rab6. *J. Biol. Chem.* 270:14801-8.

Johnston, P.A., B.T. Archer, 3rd, K. Robinson, G.A. Mignery, R. Jahn, and T.C. Sudhof. 1991. rab3A attachment to the synaptic vesicle membrane mediated by a conserved polyisoprenylated carboxy-terminal sequence. *Neuron.* 7:101-9.

Kadowaki, T., H. Kadowaki, D. Accili, Y. Yazaki, and S.I. Taylor. 1991. Substitution of arginine for histidine at position 209 in the alpha-subunit of the human insulin receptor. A mutation that impairs receptor dimerization and transport of receptors to the cell surface. *J. Biol. Chem.* 266:21224-31.

Kagiwada, S., K. Hosaka, M. Murata, J. Nikawa, and A. Takatsuki. 1998. The Saccharomyces cerevisiae SCS2 gene product, a homolog of a synaptobrevin-associated protein, is an integral membrane protein of the endoplasmic reticulum and is required for inositol metabolism. *J. Bacteriol.* 180:1700-8.

Kaiser, S.E., J.H. Brickner, A.R. Reilein, T.D. Fenn, P. Walter, and A.T. Brunger. 2005. Structural basis of FFAT motif-mediated ER targeting. *Structure.* 13:1035-45.

Kanekura, K., Y. Hashimoto, T. Niikura, S. Aiso, M. Matsuoka, and I. Nishimoto. 2004. Alsin, the product of ALS2 gene, suppresses SOD1 mutant neurotoxicity through RhoGEF domain by interacting with SOD1 mutants. *J. Biol. Chem.* 279:19247-56.

Kanekura, K., I. Nishimoto, S. Aiso, and M. Matsuoka. 2006. Characterization of amyotrophic lateral sclerosis-linked pro56ser mutation of vesicle-associated

membrane protein-associated protein B (VAPB/ALS8). *J. Biol. Chem.*

Kaufman, R.J. 1999. Stress signaling from the lumen of the endoplasmic reticulum: coordination of gene transcriptional and translational controls. *Genes Dev.* 13:1211-33.

Kaufman, R.J. 2002. Orchestrating the unfolded protein response in health and disease. *J. Clin. Invest.* 110:1389-98.

Khosravi-Far, R., R.J. Lutz, A.D. Cox, L. Conroy, J.R. Bourne, M. Sinensky, W.E. Balch, J.E. Buss, and C.J. Der. 1991. Isoprenoid modification of rab proteins terminating in CC or CXC motifs. *Proc. Natl. Acad. Sci. U S A.* 88:6264-8.

Khosravi-Far, R., G.J. Clark, K. Abe, A.D. Cox, T. McLain, R.J. Lutz, M. Sinensky, and C.J. Der. 1992. Ras (CXXX) and Rab (CC/CXC) prenylation signal sequences are unique and functionally distinct. *J. Biol. Chem.* 267:24363-8.

King, K.L., M. Stewart, T.M. Roberts, and M. Seavy. 1992. Structure and macromolecular assembly of two isoforms of the major sperm protein (MSP) from the amoeboid sperm of the nematode, Ascaris suum. *J. Cell Sci.* 101 (Pt 4):847-57.

Kinsella, B.T., and W.A. Maltese. 1992. rab GTP-binding proteins with three different carboxyl-terminal cysteine motifs are modified in vivo by 20-carbon isoprenoids. *J. Biol. Chem.* 267:3940-5.

Klopfenstein, D.R., F. Kappeler, and H.P. Hauri. 1998. A novel direct interaction of endoplasmic reticulum with microtubules. *Embo J.* 17:6168-77.

Klumperman, J. 2000. Transport between ER and Golgi. *Curr. Opin. Cell Biol.*

12:445-9.

Kopito, R.R. 1999. Biosynthesis and degradation of CFTR. *Physiol. Rev.* 79:S167-73.

Kosinski, M., K. McDonald, J. Schwartz, I. Yamamoto, and D. Greenstein. 2005. C. elegans sperm bud vesicles to deliver a meiotic maturation signal to distant oocytes. *Development.* 132:3357-69.

Kreis, T.E., and H.F. Lodish. 1986. Oligomerization is essential for transport of vesicular stomatitis viral glycoprotein to the cell surface. *Cell.* 46:929-37.

Kuehn, M.J., J.M. Herrmann, and R. Schekman. 1998. COPII-cargo interactions direct protein sorting into ER-derived transport vesicles. *Nature.* 391:187-90.

Kuge, O., C. Dascher, L. Orci, T. Rowe, M. Amherdt, H. Plutner, M. Ravazzola, G. Tanigawa, J.E. Rothman, and W.E. Balch. 1994. Sar1 promotes vesicle budding from the endoplasmic reticulum but not Golgi compartments. *J. Cell Biol.* 125:51-65.

Kurten, R.C., A.D. Eddington, P. Chowdhury, R.D. Smith, A.D. Davidson, and B.B. Shank. 2001. Self-assembly and binding of a sorting nexin to sorting endosomes. *J. Cell Sci.* 114:1743-56.

Lapierre, L.A., P.L. Tuma, J. Navarre, J.R. Goldenring, and J.M. Anderson. 1999. VAP-33 localizes to both an intracellular vesicle population and with occludin at the tight junction. *J. Cell Sci.* 112 (Pt 21):3723-32.

Laurent, F., G. Labesse, and P. de Wit. 2000. Molecular cloning and partial characterization of a plant VAP33 homologue with a major sperm protein

domain. *Biochem. Biophys. Res. Commun.* 270:286-92.

Lee, M.C., E.A. Miller, J. Goldberg, L. Orci, and R. Schekman. 2004. Bi-directional protein transport between the ER and Golgi. *Annu. Rev. Cell. Dev. Biol.* 20:87-123.

Lee, M.C., L. Orci, S. Hamamoto, E. Futai, M. Ravazzola, and R. Schekman. 2005. Sar1p N-terminal helix initiates membrane curvature and completes the fission of a COPII vesicle. *Cell.* 122:605-17.

Lefrancois, L., and D.S. Lyles. 1982. The interaction of antibody with the major surface glycoprotein of vesicular stomatitis virus. II. Monoclonal antibodies of nonneutralizing and cross-reactive epitopes of Indiana and New Jersey serotypes. *Virology.* 121:168-74.

Li, L.Y., H.M. Shih, M.Y. Liu, and J.Y. Chen. 2001. The cellular protein PRA1 modulates the anti-apoptotic activity of Epstein-Barr virus BHRF1, a homologue of Bcl-2, through direct interaction. *J. Biol. Chem.* 276:27354-62.

Lin, R.C., and R.H. Scheller. 1997. Structural organization of the synaptic exocytosis core complex. *Neuron.* 19:1087-94.

Lin, J., Z. Liang, Z. Zhang, and G. Li. 2001. Membrane topography and topogenesis of prenylated Rab acceptor (PRA1). *J. Biol. Chem.* 276:41733-41.

Lippincott-Schwartz, J., N.B. Cole, A. Marotta, P.A. Conrad, and G.S. Bloom. 1995. Kinesin is the motor for microtubule-mediated Golgi-to-ER membrane traffic. *J. Cell. Biol.* 128:293-306.

Loewen, C.J., A. Roy, and T.P. Levine. 2003. A conserved ER targeting motif in

three families of lipid binding proteins and in Opi1p binds VAP. *Embo J.* 22:2025-35.

Lotti, L.V., M.R. Torrisi, M.C. Pascale, and S. Bonatti. 1992. Immunocytochemical analysis of the transfer of vesicular stomatitis virus G glycoprotein from the intermediate compartment to the Golgi complex. *J. Cell Biol.* 118:43-50.

Luduena, R.F., and M.C. Roach. 1991. Tubulin sulfhydryl groups as probes and targets for antimitotic and antimicrotubule agents. *Pharmacol. Ther.* 49:133-52.

Ma, D., N. Zerangue, Y.F. Lin, A. Collins, M. Yu, Y.N. Jan, and L.Y. Jan. 2001. Role of ER export signals in controlling surface potassium channel numbers. *Science.* 291:316-9.

Ma, D., N. Zerangue, K. Raab-Graham, S.R. Fried, Y.N. Jan, and L.Y. Jan. 2002. Diverse trafficking patterns due to multiple traffic motifs in G protein-activated inwardly rectifying potassium channels from brain and heart. *Neuron.* 33:715-29.

Martincic, I., M.E. Peralta, and J.K. Ngsee. 1997. Isolation and characterization of a dual prenylated Rab and VAMP2 receptor. *J. Biol. Chem.* 272:26991-8.

Martinez-Menarguez, J.A., H.J. Geuze, J.W. Slot, and J. Klumperman. 1999. Vesicular tubular clusters between the ER and Golgi mediate concentration of soluble secretory proteins by exclusion from COPI-coated vesicles. *Cell.* 98:81-90.

Matteoli, M., K. Takei, R. Cameron, P. Hurlbut, P.A. Johnston, T.C. Sudhof, R. Jahn,

and P. De Camilli. 1991. Association of Rab3A with synaptic vesicles at late stages of the secretory pathway. *J. Cell Biol.* 115:625-33.

Mayer, A., W. Wickner, and A. Haas. 1996. Sec18p (NSF)-driven release of Sec17p (alpha-SNAP) can precede docking and fusion of yeast vacuoles. *Cell.* 85:83-94.

McAuliffe, M.J., F.M. Lalonde, D. McGarry, W. Gandler, K. Csaky, and B.L. Trus. 2001. Medical image processing, analysis & visualization in clinical research. *IEEE Computer-Based Medical Systems*:381-386.

McBride, H.M., V. Rybin, C. Murphy, A. Giner, R. Teasdale, and M. Zerial. 1999. Oligomeric complexes link Rab5 effectors with NSF and drive membrane fusion via interactions between EEA1 and syntaxin 13. *Cell.* 98:377-86.

McMahon, H.T., and I.G. Mills. 2004. COP and clathrin-coated vesicle budding: different pathways, common approaches. *Curr. Opin. Cell Biol.* 16:379-91.

Miller, M.A., V.Q. Nguyen, M.H. Lee, M. Kosinski, T. Schedl, R.M. Caprioli, and D. Greenstein. 2001. A sperm cytoskeletal protein that signals oocyte meiotic maturation and ovulation. *Science.* 291:2144-7.

Mitchison, T., and M. Kirschner. 1984. Dynamic instability of microtubule growth. *Nature.* 312:237-42.

Miyazaki, A., T. Sasaki, K. Araki, N. Ueno, K. Imazumi, F. Nagano, K. Takahashi, and Y. Takai. 1994. Comparison of kinetic properties between MSS4 and Rab3A GRF GDP/GTP exchange proteins. *FEBS Lett.* 350:333-6.

Montecucco, C., and G. Schiavo. 1993. Tetanus and botulism neurotoxins: a new

group of zinc proteases. *Trends. Biochem. Sci.* 18:324-7.

Mori, K. 2000. Tripartite management of unfolded proteins in the endoplasmic reticulum. *Cell.* 101:451-4.

Morishima, N., K. Nakanishi, H. Takenouchi, T. Shibata, and Y. Yasuhiko. 2002. An endoplasmic reticulum stress-specific caspase cascade in apoptosis. Cytochrome c-independent activation of caspase-9 by caspase-12. *J. Biol. Chem.* 277:34287-94.

Moss, J., and M. Vaughan. 1998. Molecules in the ARF orbit. *J. Biol. Chem.* 273:21431-4.

Mossessova, E., L.C. Bickford, and J. Goldberg. 2003. SNARE selectivity of the COPII coat. *Cell.* 114:483-95.

Murthy, V.N., and C.F. Stevens. 1999. Reversal of synaptic vesicle docking at central synapses. *Nat. Neurosci.* 2:503-7.

Nakagawa, T., H. Zhu, N. Morishima, E. Li, J. Xu, B.A. Yankner, and J. Yuan. 2000. Caspase-12 mediates endoplasmic-reticulum-specific apoptosis and cytotoxicity by amyloid-beta. *Nature.* 403:98-103.

Nakamura, N., M. Lowe, T.P. Levine, C. Rabouille, and G. Warren. 1997. The vesicle docking protein p115 binds GM130, a cis-Golgi matrix protein, in a mitotically regulated manner. *Cell.* 89:445-55.

Nakamura, N., G.H. Sun-Wada, A. Yamamoto, Y. Wada, and M. Futai. 2001. Association of mouse sorting nexin 1 with early endosomes. *J. Biochem. (Tokyo).* 130:765-71.

Nehls, S., E.L. Snapp, N.B. Cole, K.J. Zaal, A.K. Kenworthy, T.H. Roberts, J. Ellenberg, J.F. Presley, E. Siggia, and J. Lippincott-Schwartz. 2000. Dynamics and retention of misfolded proteins in native ER membranes. *Nat. Cell Biol.* 2:288-95.

Neu, M., V. Brachvogel, H. Oschkinat, M. Zerial, and P. Metcalf. 1997. Rab7: NMR and kinetics analysis of intact and C-terminal truncated constructs. *Proteins.* 27:204-9.

Ngsee, J.K., K. Miller, B. Wendland, and R.H. Scheller. 1990. Multiple GTP-binding proteins from cholinergic synaptic vesicles. *J. Neurosci.* 10:317-22.

Ngsee, J.K., A.M. Fleming, and R.H. Scheller. 1993. A rab protein regulates the localization of secretory granules in AtT-20 cells. *Mol. Biol. Cell.* 4:747-56.

Niemann, H., J. Blasi, and R. Jahn. 1994. Clostridial neurotoxins: new tools for dissecting exocytosis. *Trends Cell Biol.* 4:179-85.

Nishimura, N., and W.E. Balch. 1997. A di-acidic signal required for selective export from the endoplasmic reticulum. *Science.* 277:556-8.

Nishimura, Y., M. Hayashi, H. Inada, and T. Tanaka. 1999. Molecular cloning and characterization of mammalian homologues of vesicle-associated membrane protein-associated (VAMP-associated) proteins. *Biochem. Biophys. Res. Commun.* 254:21-6.

Nishimura, A.L., M. Mitne-Neto, H.C. Silva, A. Richieri-Costa, S. Middleton, D. Cascio, F. Kok, J.R. Oliveira, T. Gillingwater, J. Webb, P. Skehel, and M. Zatz. 2004. A mutation in the vesicle-trafficking protein VAPB causes late-

onset spinal muscular atrophy and amyotrophic lateral sclerosis. *Am. J. Hum. Genet.* 75:822-31.

Nishimura, A.L., A. Al-Chalabi, and M. Zatz. 2005. A common founder for amyotrophic lateral sclerosis type 8 (ALS8) in the Brazilian population. *Hum. Genet.* 118:499-500.

Nonet, M.L., J.E. Staunton, M.P. Kilgard, T. Fergestad, E. Hartwieg, H.R. Horvitz, E.M. Jorgensen, and B.J. Meyer. 1997. Caenorhabditis elegans rab-3 mutant synapses exhibit impaired function and are partially depleted of vesicles. *J. Neurosci.* 17:8061-73.

Nufer, O., S. Guldbrandsen, M. Degen, F. Kappeler, J.P. Paccaud, K. Tani, and H.P. Hauri. 2002. Role of cytoplasmic C-terminal amino acids of membrane proteins in ER export. *J. Cell Sci.* 115:619-28.

Nuoffer, C., S.K. Wu, C. Dascher, and W.E. Balch. 1997. Mss4 does not function as an exchange factor for Rab in endoplasmic reticulum to Golgi transport. *Mol. Biol. Cell.* 8:1305-16.

Orci, L., M. Tagaya, M. Amherdt, A. Perrelet, J.G. Donaldson, J. Lippincott-Schwartz, R.D. Klausner, and J.E. Rothman. 1991. Brefeldin A, a drug that blocks secretion, prevents the assembly of non-clathrin-coated buds on Golgi cisternae. *Cell.* 64:1183-95.

Ostermeier, C., and A.T. Brunger. 1999. Structural basis of Rab effector specificity: crystal structure of the small G protein Rab3A complexed with the effector domain of rabphilin-3A. *Cell.* 96:363-74.

Oyler, G.A., G.A. Higgins, R.A. Hart, E. Battenberg, M. Billingsley, F.E. Bloom, and M.C. Wilson. 1989. The identification of a novel synaptosomal-associated protein, SNAP-25, differentially expressed by neuronal subpopulations. *J. Cell Biol.* 109:3039-52.

Paccaud, J.P., W. Reith, J.L. Carpentier, M. Ravazzola, M. Amherdt, R. Schekman, and L. Orci. 1996. Cloning and functional characterization of mammalian homologues of the COPII component Sec23. *Mol. Biol. Cell.* 7:1535-46.

Palade, G. 1975. Intracellular aspects of the process of protein synthesis. *Science.* 189:347-58.

Pathak, R.K., R.K. Merkle, R.D. Cummings, J.L. Goldstein, M.S. Brown, and R.G. Anderson. 1988. Immunocytochemical localization of mutant low density lipoprotein receptors that fail to reach the Golgi complex. *J. Cell Biol.* 106:1831-41.

Patil, C., and P. Walter. 2001. Intracellular signaling from the endoplasmic reticulum to the nucleus: the unfolded protein response in yeast and mammals. *Curr. Opin. Cell Biol.* 13:349-55.

Peng, R., R. Grabowski, A. De Antoni, and D. Gallwitz. 1999. Specific interaction of the yeast cis-Golgi syntaxin Sed5p and the coat protein complex II component Sec24p of endoplasmic reticulum-derived transport vesicles. *Proc. Natl. Acad. Sci. U S A.* 96:3751-6.

Pennetta, G., P.R. Hiesinger, R. Fabian-Fine, I.A. Meinertzhagen, and H.J. Bellen. 2002. Drosophila VAP-33A directs bouton formation at neuromuscular

junctions in a dosage-dependent manner. *Neuron.* 35:291-306.

Peters, K.W., J. Qi, S.C. Watkins, and R.A. Frizzell. 2000. Mechanisms underlying regulated CFTR trafficking. *Med. Clin. North Am.* 84:633-40, ix-x.

Pfeffer, S.R., A.B. Dirac-Svejstrup, and T. Soldati. 1995. Rab GDP dissociation inhibitor: putting rab GTPases in the right place. *J. Biol. Chem.* 270:17057-9.

Pfeffer, S., and D. Aivazian. 2004. Targeting Rab GTPases to distinct membrane compartments. *Nat. Rev. Mol. Cell Biol.* 5:886-96.

Powers, J., and C. Barlowe. 2002. Erv14p directs a transmembrane secretory protein into COPII-coated transport vesicles. *Mol. Biol. Cell.* 13:880-91.

Prekeris, R., and D.M. Terrian. 1997. Brain myosin V is a synaptic vesicle-associated motor protein: evidence for a Ca2+-dependent interaction with the synaptobrevin-synaptophysin complex. *J. Cell Biol.* 137:1589-601.

Presley, J.F., N.B. Cole, T.A. Schroer, K. Hirschberg, K.J. Zaal, and J. Lippincott-Schwartz. 1997. ER-to-Golgi transport visualized in living cells. *Nature.* 389:81-5.

Pylypenko, O., A. Rak, T. Durek, S. Kushnir, B.E. Dursina, N.H. Thomae, A.T. Constantinescu, L. Brunsveld, A. Watzke, H. Waldmann, R.S. Goody, and K. Alexandrov. 2006. Structure of doubly prenylated Ypt1:GDI complex and the mechanism of GDI-mediated Rab recycling. *Embo J.* 25:13-23.

Rak, A., O. Pylypenko, T. Durek, A. Watzke, S. Kushnir, L. Brunsveld, H. Waldmann, R.S. Goody, and K. Alexandrov. 2003. Structure of Rab GDP-dissociation inhibitor in complex with prenylated YPT1 GTPase. *Science.* 302:646-50.

Rak, A., O. Pylypenko, A. Niculae, K. Pyatkov, R.S. Goody, and K. Alexandrov. 2004. Structure of the Rab7:REP-1 complex: insights into the mechanism of Rab prenylation and choroideremia disease. *Cell.* 117:749-60.

Ralston, E., T. Ploug, J. Kalhovde, and T. Lomo. 2001. Golgi complex, endoplasmic reticulum exit sites, and microtubules in skeletal muscle fibers are organized by patterned activity. *J. Neurosci.* 21:875-83.

Roberg, K.J., M. Crotwell, P. Espenshade, R. Gimeno, and C.A. Kaiser. 1999. LST1 is a SEC24 homologue used for selective export of the plasma membrane ATPase from the endoplasmic reticulum. *J. Cell Biol.* 145:659-72.

Rothman, J.E., and L. Orci. 1992. Molecular dissection of the secretory pathway. *Nature.* 355:409-15.

Rothman, J.E. 1994. Mechanisms of intracellular protein transport. *Nature.* 372:55-63.

Sacher, M., Y. Jiang, J. Barrowman, A. Scarpa, J. Burston, L. Zhang, D. Schieltz, J.R. Yates, 3rd, H. Abeliovich, and S. Ferro-Novick. 1998. TRAPP, a highly conserved novel complex on the cis-Golgi that mediates vesicle docking and fusion. *Embo J.* 17:2494-503.

Sacher, M., J. Barrowman, D. Schieltz, J.R. Yates, 3rd, and S. Ferro-Novick. 2000. Identification and characterization of five new subunits of TRAPP. *Eur. J. Cell Biol.* 79:71-80.

Salem, N., V. Faundez, J.T. Horng, and R.B. Kelly. 1998. A v-SNARE participates in synaptic vesicle formation mediated by the AP3 adaptor complex. *Nat.*

Neurosci. 1:551-6.

Saraste, J., and E. Kuismanen. 1984. Pre- and post-Golgi vacuoles operate in the transport of Semliki Forest virus membrane glycoproteins to the cell surface. *Cell.* 38:535-49.

Saraste, J., and K. Svensson. 1991. Distribution of the intermediate elements operating in ER to Golgi transport. *J. Cell Sci.* 100 (Pt 3):415-30.

Sasaki, T., A. Kikuchi, S. Araki, Y. Hata, M. Isomura, S. Kuroda, and Y. Takai. 1990. Purification and characterization from bovine brain cytosol of a protein that inhibits the dissociation of GDP from and the subsequent binding of GTP to smg p25A, a ras p21-like GTP-binding protein. *J. Biol. Chem.* 265:2333-7.

Scales, S.J., R. Pepperkok, and T.E. Kreis. 1997. Visualization of ER-to-Golgi transport in living cells reveals a sequential mode of action for COPII and COPI. *Cell.* 90:1137-48.

Scales, S.J., Y.A. Chen, B.Y. Yoo, S.M. Patel, Y.C. Doung, and R.H. Scheller. 2000. SNAREs contribute to the specificity of membrane fusion. *Neuron.* 26:457-64.

Schekman, R., and L. Orci. 1996. Coat proteins and vesicle budding. *Science.* 271:1526-33.

Schlichting, I., S.C. Almo, G. Rapp, K. Wilson, K. Petratos, A. Lentfer, A. Wittinghofer, W. Kabsch, E.F. Pai, G.A. Petsko, and et al. 1990. Time-resolved X-ray crystallographic study of the conformational change in Ha-Ras p21 protein on GTP hydrolysis. *Nature.* 345:309-15.

Schweizer, A., J.A. Fransen, K. Matter, T.E. Kreis, L. Ginsel, and H.P. Hauri. 1990.

Identification of an intermediate compartment involved in protein transport from endoplasmic reticulum to Golgi apparatus. *Eur. J. Cell Biol.* 53:185-96.

Schweizer, A., M. Ericsson, T. Bachi, G. Griffiths, and H.P. Hauri. 1993. Characterization of a novel 63 kDa membrane protein. Implications for the organization of the ER-to-Golgi pathway. *J. Cell Sci.* 104 (Pt 3):671-83.

Shaywitz, D.A., L. Orci, M. Ravazzola, A. Swaroop, and C.A. Kaiser. 1995. Human SEC13Rp functions in yeast and is located on transport vesicles budding from the endoplasmic reticulum. *J. Cell Biol.* 128:769-77.

Short, B., C. Preisinger, J. Schaletzky, R. Kopajtich, and F.A. Barr. 2002. The Rab6 GTPase regulates recruitment of the dynactin complex to Golgi membranes. *Curr. Biol.* 12:1792-5.

Sivars, U., D. Aivazian, and S.R. Pfeffer. 2003. Yip3 catalyses the dissociation of endosomal Rab-GDI complexes. *Nature.* 425:856-9.

Skehel, P.A., K.C. Martin, E.R. Kandel, and D. Bartsch. 1995. A VAMP-binding protein from Aplysia required for neurotransmitter release. *Science.* 269:1580-3.

Skehel, P.A., R. Fabian-Fine, and E.R. Kandel. 2000. Mouse VAP33 is associated with the endoplasmic reticulum and microtubules. *Proc. Natl. Acad. Sci. U S A.* 97:1101-6.

Slot, J.W., and J.J. Geuze. 1976. Synthesis and intracellular transport of proteins in the exocrine pancreas of the frog (Rana esculenta). II. An in vitro study of the transport process and the influence of temperature. *Cell Tissue Res.* 167:147-

65.

Sogaard, M., K. Tani, R.R. Ye, S. Geromanos, P. Tempst, T. Kirchhausen, J.E. Rothman, and T. Sollner. 1994. A rab protein is required for the assembly of SNARE complexes in the docking of transport vesicles. *Cell.* 78:937-48.

Sollner, T., S.W. Whiteheart, M. Brunner, H. Erdjument-Bromage, S. Geromanos, P. Tempst, and J.E. Rothman. 1993. SNAP receptors implicated in vesicle targeting and fusion. *Nature.* 362:318-24.

Soussan, L., D. Burakov, M.P. Daniels, M. Toister-Achituv, A. Porat, Y. Yarden, and Z. Elazar. 1999. ERG30, a VAP-33-related protein, functions in protein transport mediated by COPI vesicles. *J. Cell Biol.* 146:301-11.

Springer, S., and R. Schekman. 1998. Nucleation of COPII vesicular coat complex by endoplasmic reticulum to Golgi vesicle SNAREs. *Science.* 281:698-700.

Stenmark, H., and V.M. Olkkonen. 2001. The Rab GTPase family. *Genome Biol.* 2:REVIEWS3007.

Stewart, M., K.L. King, and T.M. Roberts. 1994. The motile major sperm protein (MSP) of Ascaris suum forms filaments constructed from two helical subfilaments. *J. Mol. Biol.* 243:60-71.

Strom, M., P. Vollmer, T.J. Tan, and D. Gallwitz. 1993. A yeast GTPase-activating protein that interacts specifically with a member of the Ypt/Rab family. *Nature.* 361:736-9.

Sutton, R.B., D. Fasshauer, R. Jahn, and A.T. Brunger. 1998. Crystal structure of a SNARE complex involved in synaptic exocytosis at 2.4 A resolution. *Nature.*

395:347-53.

Swaroop, A., T.L. Yang-Feng, W. Liu, L. Gieser, L.L. Barrow, K.C. Chen, N. Agarwal, M.H. Meisler, and D.I. Smith. 1994. Molecular characterization of a novel human gene, SEC13R, related to the yeast secretory pathway gene SEC13, and mapping to a conserved linkage group on human chromosome 3p24-p25 and mouse chromosome 6. *Hum. Mol. Genet.* 3:1281-6.

Tang, B.L., S.H. Low, H.P. Hauri, and W. Hong. 1995. Segregation of ERGIC53 and the mammalian KDEL receptor upon exit from the 15 degrees C compartment. *Eur. J. Cell Biol.* 68:398-410.

Taylor, S.I. 1992. Lilly Lecture: molecular mechanisms of insulin resistance. Lessons from patients with mutations in the insulin-receptor gene. *Diabetes.* 41:1473-90.

Teasdale, R.D., D. Loci, F. Houghton, L. Karlsson, and P.A. Gleeson. 2001. A large family of endosome-localized proteins related to sorting nexin 1. *Biochem. J.* 358:7-16.

Terasaki, M., J. Song, J.R. Wong, M.J. Weiss, and L.B. Chen. 1984. Localization of endoplasmic reticulum in living and glutaraldehyde-fixed cells with fluorescent dyes. *Cell.* 38:101-8.

Thyberg, J., and S. Moskalewski. 1985. Microtubules and the organization of the Golgi complex. *Exp. Cell Res.* 159:1-16.

Tolleshaug, H., K.K. Hobgood, M.S. Brown, and J.L. Goldstein. 1983. The LDL receptor locus in familial hypercholesterolemia: multiple mutations disrupt

transport and processing of a membrane receptor. *Cell.* 32:941-51.

Trimble, R.B., and F. Maley. 1984. Optimizing hydrolysis of N-linked high-mannose oligosaccharides by endo-beta-N-acetylglucosaminidase H. *Anal. Biochem.* 141:515-22.

Trimble, W.S., T.S. Gray, L.A. Elferink, M.C. Wilson, and R.H. Scheller. 1990. Distinct patterns of expression of two VAMP genes within the rat brain. *J. Neurosci.* 10:1380-7.

Van Der Sluijs, P., M. Hull, A. Zahraoui, A. Tavitian, B. Goud, and I. Mellman. 1991. The small GTP-binding protein rab4 is associated with early endosomes. *Proc. Natl. Acad. Sci. U S A.* 88:6313-7.

VanRheenen, S.M., X. Cao, S.K. Sapperstein, E.C. Chiang, V.V. Lupashin, C. Barlowe, and M.G. Waters. 1999. Sec34p, a protein required for vesicle tethering to the yeast Golgi apparatus, is in a complex with Sec35p. *J. Cell Biol.* 147:729-42.

Voeltz, G.K., W.A. Prinz, Y. Shibata, J.M. Rist, and T.A. Rapoport. 2006. A class of membrane proteins shaping the tubular endoplasmic reticulum. *Cell.* 124:573-86.

Wada, M., H. Nakanishi, A. Satoh, H. Hirano, H. Obaishi, Y. Matsuura, and Y. Takai. 1997. Isolation and characterization of a GDP/GTP exchange protein specific for the Rab3 subfamily small G proteins. *J. Biol. Chem.* 272:3875-8.

Walch-Solimena, C., R.N. Collins, and P.J. Novick. 1997. Sec2p mediates nucleotide exchange on Sec4p and is involved in polarized delivery of post-

Golgi vesicles. *J. Cell Biol.* 137:1495-509.

Waterman-Storer, C.M., and E.D. Salmon. 1998. Endoplasmic reticulum membrane tubules are distributed by microtubules in living cells using three distinct mechanisms. *Curr. Biol.* 8:798-806.

Watson, P., R. Forster, K.J. Palmer, R. Pepperkok, and D.J. Stephens. 2005. Coupling of ER exit to microtubules through direct interaction of COPII with dynactin. *Nat. Cell Biol.* 7:48-55.

Weber, T., B.V. Zemelman, J.A. McNew, B. Westermann, M. Gmachl, F. Parlati, T.H. Sollner, and J.E. Rothman. 1998. SNAREpins: minimal machinery for membrane fusion. *Cell.* 92:759-72.

Wei, C., R. Lutz, M. Sinensky, and I.G. Macara. 1992. p23rab2, a ras-like GTPase with a -GGGCC C-terminus, is isoprenylated but not detectably carboxymethylated in NIH3T3 cells. *Oncogene.* 7:467-73.

Weir, M.L., A. Klip, and W.S. Trimble. 1998. Identification of a human homologue of the vesicle-associated membrane protein (VAMP)-associated protein of 33 kDa (VAP-33): a broadly expressed protein that binds to VAMP. *Biochem. J.* 333 (Pt 2):247-51.

Weir, M.L., H. Xie, A. Klip, and W.S. Trimble. 2001. VAP-A binds promiscuously to both v- and tSNAREs. *Biochem. Biophys. Res. Commun.* 286:616-21.

White, M.J., J.P. Hirsch, and S.A. Henry. 1991. The OPI1 gene of Saccharomyces cerevisiae, a negative regulator of phospholipid biosynthesis, encodes a protein containing polyglutamine tracts and a leucine zipper. *J. Biol. Chem.*

266:863-72.

Wieland, F.T., M.L. Gleason, T.A. Serafini, and J.E. Rothman. 1987. The rate of bulk flow from the endoplasmic reticulum to the cell surface. *Cell.* 50:289-300.

Wiest, D.L., J.K. Burkhardt, S. Hester, M. Hortsch, D.I. Meyer, and Y. Argon. 1990. Membrane biogenesis during B cell differentiation: most endoplasmic reticulum proteins are expressed coordinately. *J. Cell Biol.* 110:1501-11.

Wojcik, J., M.A. Berg, N. Esposito, M.E. Geffner, N. Sakati, E.O. Reiter, S. Dower, U. Francke, M.C. Postel-Vinay, and J. Finidori. 1998. Four contiguous amino acid substitutions, identified in patients with Laron syndrome, differently affect the binding affinity and intracellular trafficking of the growth hormone receptor. *J. Clin. Endocrinol. Metab.* 83:4481-9.

Wyles, J.P., C.R. McMaster, and N.D. Ridgway. 2002. Vesicle-associated membrane protein-associated protein-A (VAP-A) interacts with the oxysterol-binding protein to modify export from the endoplasmic reticulum. *J. Biol. Chem.* 277:29908-18.

Xu, D., and J.C. Hay. 2004. Reconstitution of COPII vesicle fusion to generate a pre-Golgi intermediate compartment. *J. Cell Biol.* 167:997-1003.

Yang, B., L. Gonzalez, Jr., R. Prekeris, M. Steegmaier, R.J. Advani, and R.H. Scheller. 1999. SNARE interactions are not selective. Implications for membrane fusion specificity. *J. Biol. Chem.* 274:5649-53.

Yang, X., M. Rudolf, M.A. Carew, M. Yoshida, V. Nerreter, A.M. Riley, S.K. Chung, K.S. Bruzik, B.V. Potter, C. Schultz, and S.B. Shears. 1999. Inositol 1,3,4-

trisphosphate acts in vivo as a specific regulator of cellular signaling by inositol 3,4,5,6-tetrakisphosphate. *J. Biol. Chem.* 274:18973-80.

Zahraoui, A., N. Touchot, P. Chardin, and A. Tavitian. 1987. Complete coding sequences of the ras related rab 3 and 4 cDNAs. *Nucleic Acids Res.* 16:1204.

Zeuschner, D., W.J. Geerts, E. van Donselaar, B.M. Humbel, J.W. Slot, A.J. Koster, and J. Klumperman. 2006. Immuno-electron tomography of ER exit sites reveals the existence of free COPII-coated transport carriers. *Nat. Cell Biol.* 8:377-83.

Zhang, T., and W. Hong. 2001. Ykt6 forms a SNARE complex with syntaxin 5, GS28, and Bet1 and participates in a late stage in endoplasmic reticulum-Golgi transport. *J. Biol. Chem.* 276:27480-7.

Zhong, Q., C.S. Lazar, H. Tronchere, T. Sato, T. Meerloo, M. Yeo, Z. Songyang, S.D. Emr, and G.N. Gill. 2002. Endosomal localization and function of sorting nexin 1. *Proc. Natl. Acad. Sci. U. S. A.* 99:6767-72.

Annex

	Control	Control	Control	Control	Control	PRA2	PRA2	PRA2	PRA2	PRA2
Time (min)	G	R	T	Average	Std.Error	B	D	BB	Average	Std.Error
0.00	0.000	0.000	0.000	0.000	0.000	0.000	0.000	0.000	0.000	0.000
0.33	0.244	0.226	0.386	0.286	0.051	0.130	0.297	0.175	0.201	0.050
0.67	0.489	0.403	0.568	0.487	0.048	0.261	0.378	0.333	0.324	0.034
1.00	0.578	0.516	0.705	0.599	0.055	0.304	0.514	0.492	0.437	0.066
1.33	0.800	0.677	0.818	0.765	0.044	0.406	0.568	0.429	0.467	0.051
1.67	0.756	0.790	0.886	0.811	0.039	0.493	0.649	0.587	0.576	0.045
2.00	0.911	0.871	0.932	0.905	0.018	0.493	0.662	0.746	0.634	0.074
2.33	0.978	0.823	0.909	0.903	0.045	0.522	0.716	0.762	0.667	0.074
2.67	0.911	0.823	0.864	0.866	0.026	0.580	0.784	0.937	0.767	0.103
3.00	0.933	0.887	0.932	0.917	0.015	0.681	0.838	1.000	0.840	0.092
3.33	1.000	1.000	0.977	0.992	0.008	0.667	0.892	0.905	0.821	0.077
3.67	0.911	0.952	1.000	0.954	0.026	0.725	0.892	0.778	0.798	0.049
4.00	0.911	0.887	0.955	0.918	0.020	0.826	0.932	0.778	0.845	0.046
4.33	0.933	0.935	1.114	0.994	0.060	0.870	0.973	0.952	0.932	0.032
4.67	0.911	1.000	1.136	1.016	0.066	0.884	0.892	1.000	0.925	0.037
5.00	1.000	0.968	1.205	1.057	0.074	0.884	1.000	0.778	0.887	0.064
5.33	1.000	0.968	1.159	1.042	0.059	1.000	0.959	0.683	0.881	0.100
5.67	1.089	0.887	1.068	1.015	0.064	0.957	1.081	0.698	0.912	0.113
6.00	1.044	0.887	1.136	1.023	0.073	0.986	0.959	0.635	0.860	0.113
6.33	1.022	0.871	1.295	1.063	0.124	0.971	0.986	0.778	0.912	0.067
6.67	1.133	0.968	1.295	1.132	0.095	0.957	0.946	0.635	0.846	0.105
7.00	1.111	0.952	1.273	1.112	0.093	1.000	1.027	0.841	0.956	0.058
7.33	1.178	0.903	1.318	1.133	0.122	0.942	0.905	0.889	0.912	0.016
7.67	1.267	0.823	1.409	1.166	0.177	1.014	0.986	1.381	1.127	0.127
8.00	1.200	0.823	1.477	1.167	0.190	1.087	0.986	0.794	0.956	0.086
8.33	1.200	0.935	1.432	1.189	0.143	0.986	0.919	0.714	0.873	0.082
8.67	1.178	0.839	1.568	1.195	0.211	1.014	1.081	0.825	0.974	0.077
9.00	1.222	0.871	1.545	1.213	0.195	1.029	0.986	0.683	0.899	0.109
9.33	1.333	1.097	1.591	1.340	0.143	0.899	1.162	0.587	0.883	0.166
9.67	1.222	1.210	1.659	1.364	0.148	0.899	1.041	0.730	0.890	0.090
10.00	1.222	1.161	1.705	1.363	0.172	0.899	1.041	0.905	0.948	0.046
Width of Bleached Area (μm)	6.5	6.5	5.4			4.7	4.7	4.7		

Annex A.1. VSVG^{ts045}-GFP Fluorescent Recovery After Photobleaching values used for the calculation of the diffusion coefficient in control CHO cells or overexpressing PRA2. Table contains the photobleaching-adjusted and background-subtracted corrected values obtained by analysis with MIPAV software of the FRAP time course images.

	VAP-A	VAP-A	VAP-A	VAP-A	VAP-A	VAP-A ΔN	VAP-A ΔN	VAP-A ΔN	VAP-A ΔN	VAP-A ΔN
Time (min)	D	G	I	Average	Std.Error	I	J	S	Average	Std.Error
0.00	0.000	0.000	0.000	0.000	0.000	0.000	0.000	0.000	0.000	0.000
0.33	0.083	0.075	0.063	0.074	0.006	0.333	0.305	0.259	0.299	0.022
0.67	0.167	0.125	0.125	0.139	0.014	0.538	0.549	0.383	0.490	0.054
1.00	0.167	0.175	0.167	0.169	0.003	0.718	0.549	0.531	0.599	0.060
1.33	0.167	0.250	0.188	0.201	0.025	0.667	0.683	0.617	0.656	0.020
1.67	0.250	0.300	0.229	0.260	0.021	0.692	0.878	0.827	0.799	0.055
2.00	0.250	0.350	0.292	0.297	0.029	0.846	0.939	0.790	0.858	0.043
2.33	0.250	0.350	0.313	0.304	0.029	0.769	0.805	0.852	0.809	0.024
2.67	0.333	0.400	0.354	0.363	0.020	0.641	0.841	0.901	0.795	0.079
3.00	0.333	0.450	0.375	0.386	0.034	0.744	0.805	0.877	0.808	0.038
3.33	0.333	0.475	0.396	0.401	0.041	1.205	0.902	0.901	1.003	0.101
3.67	0.333	0.475	0.458	0.422	0.045	1.000	1.000	1.000	1.000	0.000
4.00	0.417	0.550	0.500	0.489	0.039	1.385	0.927	1.136	1.149	0.132
4.33	0.417	0.550	0.500	0.489	0.039	1.923	0.878	1.222	1.341	0.307
4.67	0.500	0.625	0.500	0.542	0.042	1.513	0.915	1.074	1.167	0.179
5.00	0.583	0.600	0.625	0.603	0.012	1.333	0.817	1.074	1.075	0.149
5.33	0.583	0.675	0.604	0.621	0.028	0.897	0.829	1.049	0.925	0.065
5.67	0.583	0.700	0.583	0.622	0.039	0.897	0.780	0.951	0.876	0.050
6.00	0.583	0.675	0.625	0.628	0.026	0.641	0.720	0.889	0.750	0.073
6.33	0.667	0.750	0.625	0.681	0.037	0.821	0.646	0.889	0.785	0.072
6.67	0.750	0.775	0.667	0.731	0.033	1.077	0.793	0.901	0.924	0.083
7.00	0.750	0.775	0.667	0.731	0.033	1.308	0.854	0.914	1.025	0.142
7.33	0.833	0.875	0.750	0.819	0.037	1.231	0.866	0.889	0.995	0.118
7.67	0.833	0.850	0.771	0.818	0.024	1.205	0.854	0.852	0.970	0.117
8.00	0.833	0.950	0.813	0.865	0.043	1.103	0.805	0.864	0.924	0.091
8.33	0.833	0.900	0.813	0.849	0.026	1.513	0.610	0.988	1.037	0.262
8.67	0.833	0.900	0.813	0.849	0.026	1.205	0.732	0.852	0.930	0.142
9.00	0.917	0.950	0.833	0.900	0.035	1.179	0.646	0.877	0.901	0.154
9.33	1.000	1.000	0.896	0.965	0.035	1.308	0.573	1.000	0.960	0.213
9.67	1.000	1.000	0.958	0.986	0.014	1.462	0.659	0.914	1.011	0.237
10.00	1.000	1.000	1.000	1.000	0.000	1.590	0.683	0.864	1.046	0.277
Width of Bleached Area (μm)	4.7	4.7	4.7			4.7	4.7	4.7		

Annex A.2. VSVG^{ts045}-GFP Fluorescent Recovery After Photobleaching values used for the calculation of the diffusion coefficient in CHO cells overexpressing VAP-A wild type or VAP-A ΔN. Table contains the photobleaching-adjusted and background-subtracted corrected values obtained by analysis with MIPAV software of the FRAP time course images.

A

	Control		VAP-A		PRA2	
Cell Treatment	Average	Std.Error	Average	Std.Error	Average	Std.Error
Normal	6.42	0.25	0.88	0.34	1.97	0.33
On Ice 1h	4.91	0.13	2.29	0.38	8.62	0.48
Nocodazole	2.47	0.59	2.20	0.41	4.94	1.04

B

	VAP-A		PRA2	
Cell Treatment	Average	Std.Error	Average	Std.Error
Normal	0.14	0.05	0.31	0.05
On Ice 1h	0.47	0.08	1.76	0.11
Nocodazole	0.89	0.27	2.00	0.64

Annex B. ER budding assay values. *A*) Percentage of total cellular $VSVG^{ts045}$-myc measured on ER-derived vesicles. *B*) Represents the budding assay results expressed as compared to the untransfected control of each experimental condition. The values were used to create the graphics of figure 3.11.